



Title	STUDIES ON CONSTRUCTION OF CHEMICAL STRUCTURE MODELS OF COAL AND THEIR EVALUATION BY COMPUTER SIMULATION
Author(s)	Murata, Satoru
Citation	大阪大学, 1996, 博士論文
Version Type	VoR
URL	https://doi.org/10.11501/3119653
rights	
Note	

The University of Osaka Institutional Knowledge Archive : OUKA

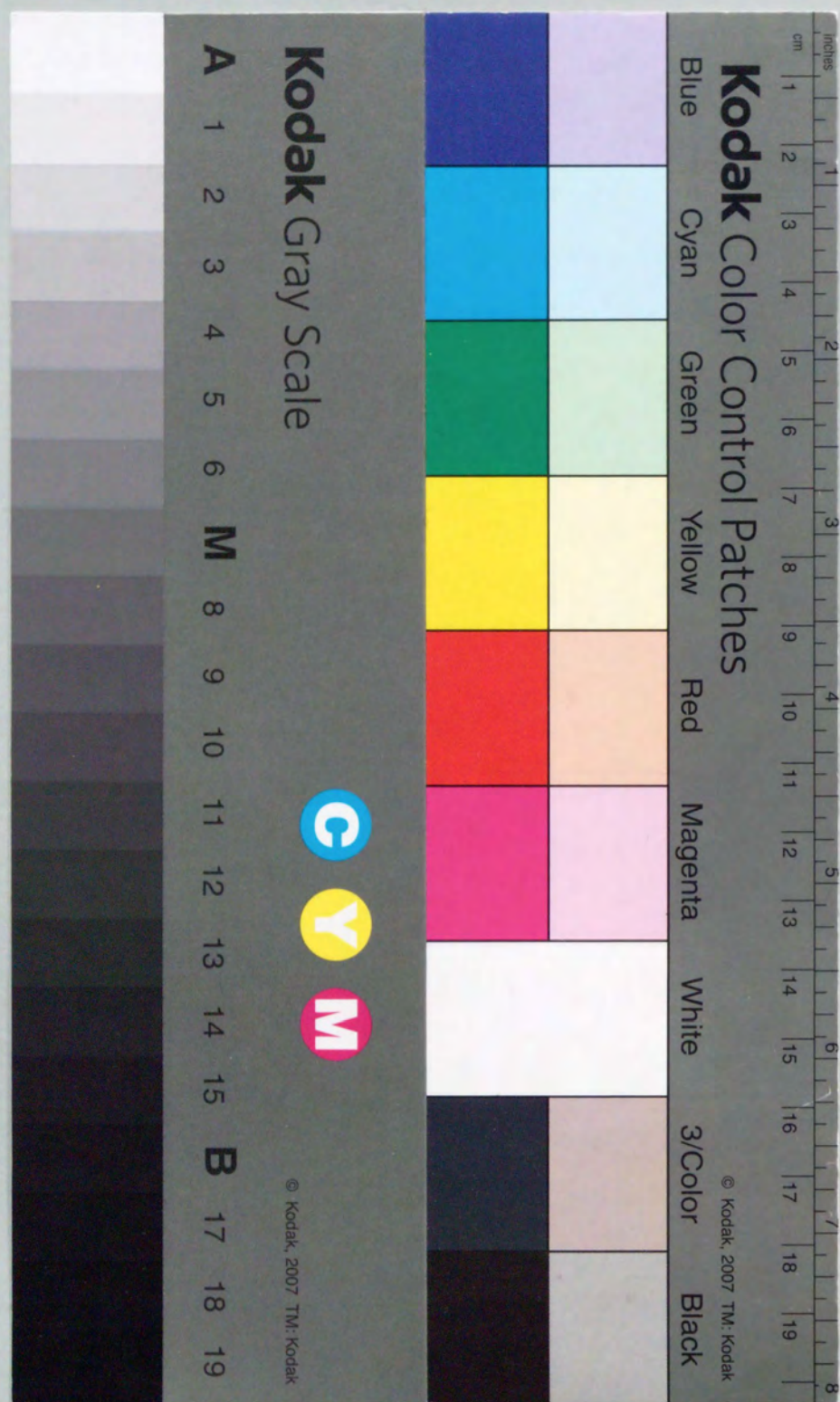
<https://ir.library.osaka-u.ac.jp/>

The University of Osaka

STUDIES ON CONSTRUCTION OF CHEMICAL STRUCTURE
MODELS OF COAL AND THEIR EVALUATION BY COMPUTER
SIMULATION

1996

SATORU MURATA



**STUDIES ON CONSTRUCTION OF CHEMICAL STRUCTURE
MODELS OF COAL AND THEIR EVALUATION BY COMPUTER
SIMULATION**

(石炭化学構造モデルの構築と計算機化学を
援用したモデルの評価に関する研究)

1996

SATORU MURATA

Preface

The work of this thesis has been carried out under the guidance of Professor Masakatsu Nomura of the Department of Molecular Chemistry, Faculty of Engineering, Osaka University.

The objective of this thesis is to obtain insight into the chemical structure of coal, which may be useful to comprehend its characteristics and helpful in undertaking its efficient utilization. The author hopes that the results obtained in this work can, to some extent, contribute to further development in the area of fuel chemistry.

Satoru Murata

Department of Molecular Chemistry,
Faculty of Engineering,
Osaka University,
2-1 Yamada-oka, Suita, Osaka 565, Japan
September, 1996

Contents

General Introduction	1
List of Publications	4
List of Supplementary Publications	5
 Chapter 1. Pyrolysis of Coal Model Compounds	
1.1. Introduction	6
1.2. Experimental Section	6
1.3. Results and Discussion	
1.3.1. Curie-Point Pyrolysis of Alkyl-Substituted Polycyclic Aromatic Compounds	8
1.3.2. Pyrolysis of Benzyl-Substituted Polycyclic Aromatic Hydrocarbons	15
1.4. References	22
 Chapter 2. Structural Analysis of Coal through Quinoline Extraction, Ruthenium-Ion Catalyzed Oxidation, and Liquefaction under Deuterium	
2.1. Introduction	23
2.2. Experimental Section	23
2.3. Results and Discussion	
2.3.1. Structural Studies on Illinois No.6 Coal through Quinoline Extraction	26
2.3.2. Ruthenium Ion-Catalyzed Oxidation of Coal	31
2.3.2. Liquefaction of Akabira coal catalyzed by molten salts under D ₂ atmosphere	36
2.4. References	42

Chapter 3. Construction of Chemical Structure Model for Chinese Bituminous Zao Zhuang Coal

3.1. Introduction	44
3.2. Experimental Section	44
3.3. Results and Discussion	46
3.4. References	53

Chapter 4. Computer-Aided Molecular Design Study of Coal Model Molecules

4.1. Introduction	54
4.2. Method	54
4.3. Results and Discussion	
4.3.1. Estimation of Physical Density of Coal Model Molecules	56
4.3.2. Density Simulation for Four Japanese Coals	60
4.3.3. Density Simulation for Model Structures of Bituminous Akabira Coal	63
4.4. References	70

Conclusion	71
------------	----

Acknowledgment	73
----------------	----

General Introduction

To comprehend the chemical structure of coal may be one of the essential propositions in undertaking the efficient conversion of coal to liquid fuels and chemicals. However, knowledge of the structure of coal at the level of molecule still remains meager, because its solid and insoluble properties make its analysis by conventional methods very difficult.

When drawing a structure of coal, we often use two types of structural models, *i.e.* (a) and (b) shown in Figure 1. As to the type (a) model, it is convenient to understand some properties of coal, including non-covalent bonding interactions. However, for the development of highly efficient coal conversion technologies it must involve detailed chemical structure, such as the type (b) model.

Shinn had proposed a comprehensive chemical model for a US bituminous coal in 1984¹ and thereafter, several researchers also described chemical structure models for a number of coals. In 1992 Nomura *et al.*

proposed an effective method for the construction of structural model for coal and applied it to Akabira coal, one of the representative Japanese bituminous coals (Figure 2).² They employed CP/MAS ¹³C NMR for determining the concentration of several carbon-functional groups and Curie-point pyrolysis-GC/MS for analyzing

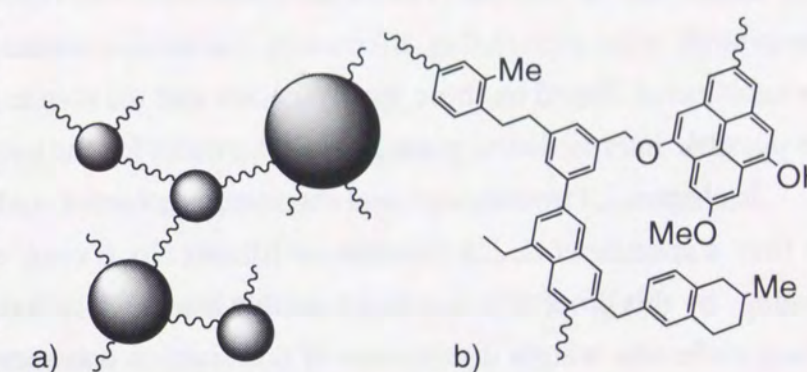


Figure 1. Representative models for coal

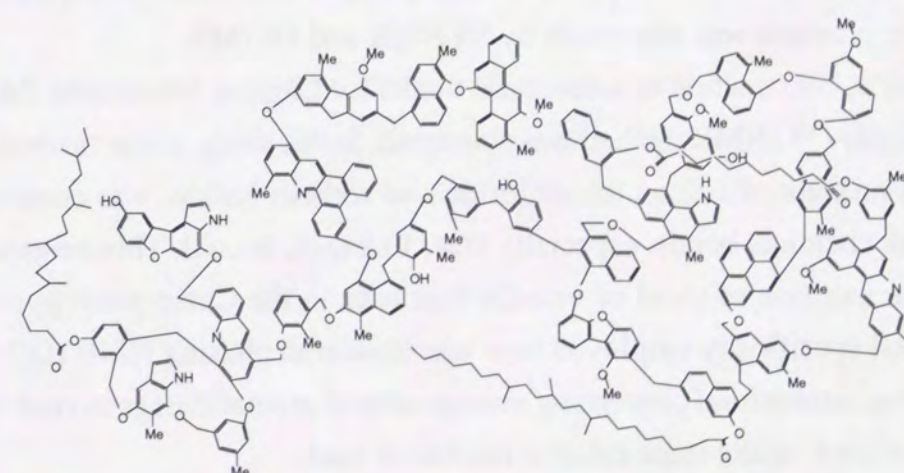


Figure 2. Chemical structural model for Japanese bituminous Akabira coal proposed by Nomura *et al.* (*Fuel Process. Technol.*, 1992, 31, 169).

the distribution of aromatic hydrocarbon skeletons. However, the method seems to contain several problematic points to be considered for its improvement; (1) molecular weight of coal or its solvent-soluble fractions, (2) quantitiveness of the data of CP/MAS ^{13}C NMR, (3) coke formation during pyrolysis, (4) pyrolytic behavior of coal molecules, and (5) quantification of non-bonding interactions between coal molecules. In this work, I have made some efforts to solve or improve these points.

In chapter 1, pyrolysis of two classes of coal model compounds were investigated to obtain fundamental information of the pyrolytic behavior of coal. In the Curie-point pyrolysis of the one class involving 14 aromatic hydrocarbons, each of which consists of one or two aromatic skeletons and a longer alkyl side chain or a longer alkylene bridge, alkanes and alkenes as well as aromatic fragments were appeared to be formed. One of the important parameters, molar ratio of alkanes to alkenes formed was found to vary depending on the aromatic skeletons and the bridge groups. Seven benzyl-substituted polycyclic aromatic hydrocarbons as the other class were also submitted to pyrolysis in the presence or absence of a hydrogen-donor solvent. The results indicated that reactivity and reaction mode of the compounds were remarkably affected by the mother aromatic skeletons and the position of the substituent. Based on these pyrolysis data and the results of molecular orbital calculations for possible intermediates, plausible mechanisms for the pyrolysis were proposed.

In chapter 2, I investigated coal chemical structure of coal by using three different methods. At first, a specific coal, US bituminous Illinois No. 6 coal, was treated with quinoline under heating. By this procedure, a solvent soluble fraction was found to be obtained in a high yield. Then, molecular weight distribution of this fraction was measured, so that association nature of the components of the coal could be discussed. Next, some coals were submitted to ruthenium ion-catalyzed oxidation reaction, which may give information about the distribution of alkyl side chain attached to aromatic rings in coal. Finally, Akabira coal was hydrolized using deuterium in the presence of tin(II) chloride and potassium chloride. Detailed analysis of the solvent soluble products was also made by ^2H NMR and GC/MS.

In chapter 3, construction of a structural model for Chinese bituminous Zao Zhuang coal using the pyrolysis / ^{13}C NMR method was attempted. In this study, a new method, pretreatment of coal with a mixture of silicon tetrachloride and sodium iodide, was employed to cleave relatively weak chemical bonds, especially ether linkages, in coal. This treatment was found to result in the increase of yield of volatile fractions in the Curie-point pyrolysis of coal. Another method specifically employed here was dipolar dephasing NMR (DD NMR) which may give precise information concerning average size of aromatic rings in coal. These devices appeared to enable to make more reliable models of coal.

In chapter 4, CAMD (computer-aided molecular design) technique was applied to coal model molecules. Among the parameters derived from CAMD study, physical density is

considered to be one of the most important ones. Consequently, a new method for calculation of physical density of coal model molecules was developed. This method was also applied to three types of coal model molecules, (1) simple models containing polycyclic aromatic hydrocarbons with polymethylene bridges, (2) four Japanese coal models which represent their elemental analyses, carbon aromaticities, and oxygen-functional groups, and (3) a relatively large model for Japanese bituminous Akabira coal proposed by Nomura *et al.*² On the basis of the calculated data, evaluation of reasonableness of the models was attempted.

References

- 1 Shinn, J. H. *Fuel* **1984**, *63*, 1187.
- 2 Nomura, M.; Matsubayashi, K.; Ida, T.; Murata, S. *Fuel Process. Technol.* **1992**, *31*, 169.

List of Publications

- 1) CAMD Study of Coal Model Molecules. 1. Estimation of Physical Density of Coal Model Molecule, K. Nakamura, S. Murata, and M. Nomura, *Energy Fuels*, **1993**, 7, 347.
- 2) CAMD Study of Coal Model Molecules. 2. Density Simulation for Four Japanese Coals, S. Murata, M. Nomura, K. Nakamura, H. Kumagai, and Y. Sanada, *Energy Fuels*, **1993**, 7, 469.
- 3) Computer-Aided Molecular Design Study of Coal Model Molecules. 3. Density Simulation for Model Structure of Bituminous Akabira Coal, T. Dong, S. Murata, M. Miura, M. Nomura, and K. Nakamura, *Energy Fuels*, **1993**, 7, 1123.
- 4) Effects of Pretreatment of Zao Zhuang and Akabira Bituminous Coals with SiCl_4 -NaI Reagents on Pyrolytic Behavior of Extracts, A. Yamamoto, S. Murata, and M. Nomura, *Chem. Lett.*, **1994**, 1387.
- 5) Scope and Limitations of Ruthenium Ion Catalyzed Oxidation of Coal as an Analytical Tool for an Aliphatic Portion of Coal Organic Materials, S. Murata, K. Uesaka, H. Inoue, and M. Nomura, *Prep. Pap.-Am. Chem. Soc., Div. Fuel Chem.*, **1994**, 39, 787.
- 6) Studies on Aliphatic Portion of Coal Organic Materials Based on Ruthenium Ion Catalyzed Oxidation, S. Murata, K. Uesaka, H. Inoue, and M. Nomura, *Energy Fuels*, **1994**, 8, 1379.
- 7) Studies on Curie-Point Pyrolysis of Coal Model Compounds, S. Murata, T. Mori, A. Murakami, M. Nomura, and K. Nakamura, *Energy Fuels*, **1995**, 9, 119.
- 8) Liquefaction of Japanese Bituminous Akabira Coal Catalyzed by Molten Salts under D_2 Atmosphere, M. Nomura, T. Muratani, Y. Tajima, and S. Murata, *Fuel Process. Technol.*, **1995**, 43, 213.
- 9) Pyrolysis of Coal Model Compounds. Thermal Behavior of Benzyl-Substituted Polyaromatic Compounds, S. Murata, M. Nakamura, M. Miura, and M. Nomura, *Energy Fuels*, **1995**, 9, 849.
- 10) Structural Studies on Illinois No. 6 Coal through Quinoline Extraction, S. Murata, E. Kawakami, and M. Nomura, *Energy Fuels*, **1996**, 10, 220.
- 11) Structural Study on Chinese Bituminous Zao Zhuang Coal, S. Murata, A. Yamamoto, K. Kidena, and M. Nomura, *in preparation*.

List of Supplementary Publications

- 1) A Study on Unit Chemical Structure of Bituminous Akabira Coal, M. Nomura, K. Matsubayashi, T. Ida, and S. Murata, *Fuel Process. Technol.*, **1992**, 31, 169.
- 2) Recent Advances in NMR Spectroscopy 1, M. Nomura and S. Murata, *J. Jpn. Inst. Energy*, **1992**, 71, 866.
- 3) Recent Advances in NMR Spectroscopy 2, M. Nomura and S. Murata, *J. Jpn. Inst. Energy*, **1992**, 71, 1133.
- 4) An Approach to Coal Chemical Structure, M. Nomura, S. Murata, M. Miyake, and M. Miura, *J. Jpn. Inst. Energy*, **1993**, 72, 321.
- 5) Studies on Chemical Structure of Coal (1) -Analysis of Chemical Constituents of Illinois No. 6 and Miike Coals with a Curie-point Pyrolyzer-, H. Hama, K. Matsubayashi, S. Murata, and M. Nomura, *J. Jpn. Inst. Energy*, **1993**, 72, 467.
- 6) Studies on Chemical Structure of Vacuum Residue of Illinois No. 6 Coal from a NEDOL Coal Liquefaction Process, T. Tanaka, S. Murata, and M. Nomura, *J. Jpn. Inst. Energy*, **1993**, 72, 935.
- 7) Studies on Chemical Structure of Coal (2) -Comparison of Carbon Distribution Based on Pyrolysis Data with Those from Solid State NMR Data-, H. Hama, S. Murata, and M. Nomura, *J. Jpn. Inst. Energy*, **1994**, 73, 177.
- 8) Structure and Property of Coal, S. Murata, M. Miura, and M. Nomura, *J. Jpn. Inst. Energy*, **1994**, 73, 446.
- 9) Application of Computer Chemistry to the Study of Coal Chemical Structure, S. Murata, M. Miura, M. Nomura, T. Takanohashi, M. Iino, H. Kumagai, Y. Sanada, and K. Nakamura, *J. Jpn. Inst. Energy*, **1995**, 74, 342.
- 10) Structure and Property of Coal, S. Murata, M. Miura, and M. Nomura, *J. Jpn. Inst. Energy*, **1995**, 74, 438.
- 11) Steam Gasification of Coal: The Effects of Acid- and Alkali-Leaching of Coal on Its Gasification Rate, S. Murata, A. Murakami, and M. Nomura, *Prep. Pap.-Am. Chem. Soc., Div. Fuel Chem.*, **1996**, 41, 237.
- 12) Solubilization of Meso-Carbon Materials by Butylation with Dibutylzinc and Butyl Iodide, Y. Zhang, K. Kidena, S. Murata, M. Nomura, Y. Yoneyama, and T. Kato, *Chem. Lett.*, **1996**, 491.
- 13) Quantitative Evaluation of Hydrogen Transfer Related to the Appearance of Coal Plasticity, M. Nomura, S. Murata, K. Kidena, and T. Chikada, *Tetsu To Hagane*, **1996**, 82, 361.
- 14) Studies on the Chemical Structural Change During Carbonization Process, K. Kidena, S. Murata, and M. Nomura, *Energy Fuels*, **1996**, 10, 672.

Chapter 1. Pyrolysis of Coal Model Compounds

1.1. Introduction

Of relevance to coal pyrolysis and liquefaction, there have been numerous studies on thermal behavior of coal model compounds in the presence or absence of hydrogen sources.¹ The results may also provide useful information in undertaking the efficient utilization of coal as fuel and chemicals by the processes. In light of these results, pyrolysis of two classes of coal model compounds (**1-4** and **5-8** in Scheme 1-1) was investigated in this chapter.

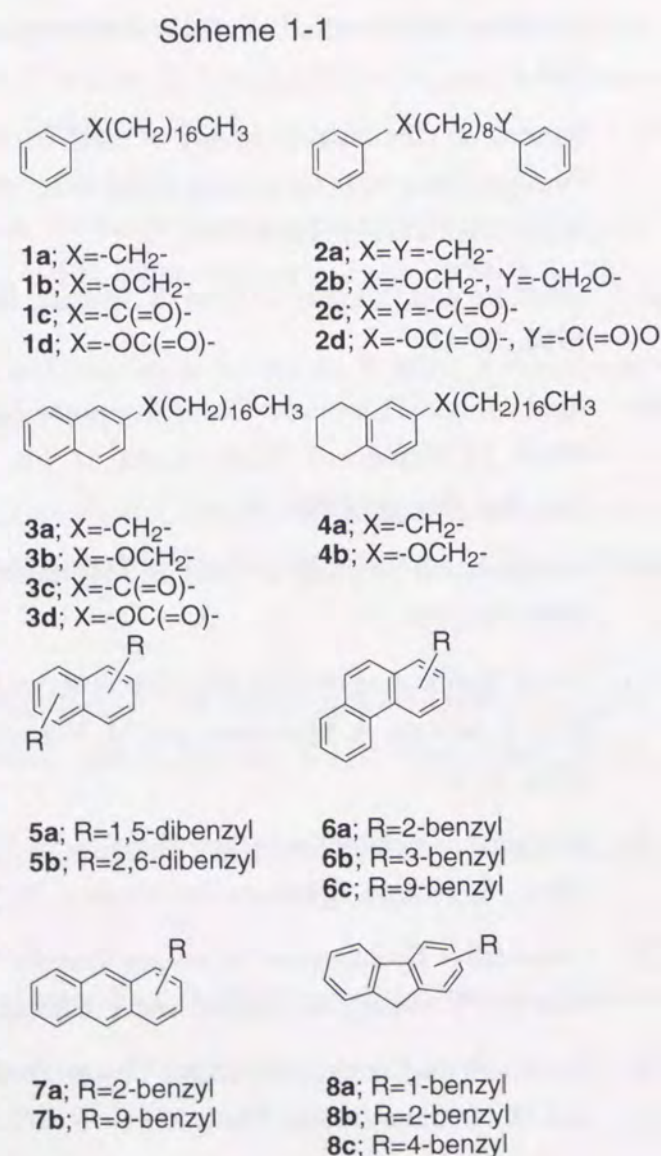
1.2. Experimental

Instrumental analysis

¹H NMR spectra were obtained with a JEOL JNM-GSX-400 spectrometer (400 MHz) for CDCl₃ solutions. GC-MS spectra were obtained with a Shimadzu QP-2000 spectrometer. FD-MS spectra were obtained with a JEOL JMS-DX-303 spectrometer. GC analysis was carried out on a Shimadzu GC-8APF gas chromatograph with a silicone OV-17 column (i.d. 2.6 mm x 1.5 m) and a Shimadzu GC-14A with a CBP-1 capillary column (i.d. 0.5 mm x 25m).

Preparation of model compounds

Octadecylbenzene (**1a**), 2-octadecylnaphthalene (**3a**), and 6-octadecyltetralin (**4a**) were obtained from reduction of the corresponding ketones **1c**, **3c**, and **4c** (33 mmol), with N₂H₄•H₂O (132 mmol) and potassium hydroxide (132 mmol) in triethyleneglycol (20 mL) at 120 °C for 2 h. After evaporation of hydrazine and water, the products were purified with silica gel column chromatography using hexane as eluant. Aryl octadecyl ethers, **1b**, **3b**, and **4b**, were prepared from 1-bromooctadecane (30 mmol) and sodium salt of phenol, 2-naphthol, or 6-hydroxytetralin (100 mmol) in dry DMF (100 mL) at room temperature and purified with silica gel column chromatography using hexane-benzene as eluant. Aryl heptadecyl ketones, **1c** and **3c**, were prepared from octanoyl chloride (30 mmol) and benzene (50 mL) or naphthalene (30 mmol in a 50 mL dry nitrobenzene) in the presence of aluminum trichloride (50 mmol) at



50 °C for 16 h and purified by silica gel column chromatography using hexane-benzene as eluant. Octanoic acid aryl esters, **1d** and **3d**, were prepared from octanoyl chloride (50 mmol) and phenol or 2-naphthol (50 mmol) in distilled ether (100 mL) in the presence of triethylamine (50 mmol) with magnetically stirring at room temperature for one night. These products were purified by recrystallization from hexane. Difunctional compounds **2a-d** were synthesized by the similar method to that for the mono-substituted compounds from 1,10-dibromodecane or 1,10-decandioyl chloride and benzene or phenol.

The benzyl-substituted polycyclic aromatic compounds (**5**, **6**, and **8**) were prepared from the corresponding benzoyl ketones, 1,5- and 2,6-dibenzoylnaphthalenes, 2-, 3-, and 9-benzoylphenanthrenes, 2-benzoylfluorene and 1- and 4-benzoylfluorenones. They were reduced by using triethylsilane in trifluoroacetic acid according to the reported method. In the case of the anthracene derivatives (**7**), 2- and 9-benzyl-9,10-dihydroanthracenes were formed by the reduction. Thus, the dihydro compounds were dehydrogenated by using a Pd/C catalyst in refluxing 1-hexanol for 16 h to produce the desired materials. The methods used for the preparation of the ketones were reported previously with the exception that for 2,6-dibenzoylnaphthalene. 2,6-Dibenzoylnaphthalene was obtained by chlorination of 2,6-naphthalenedicarboxylic acid with thionyl chloride followed by treatment with benzene in the presence of aluminum chloride. (1,2'-Dinaphthyl)phenylmethane was prepared by the reaction of 2-benzoylnaphthalene with 1-naphthylmagnesium bromide in ether followed by treatment with triethylsilane.

Each compound was purified by recrystallization and the purity was judged to be ≥ 95 % by GC and NMR analyses.

Curie-point pyrolysis of model compounds

Curie-point pyrolysis gas chromatographic (Py-GC) and -mass spectrometric (Py-GC-MS) analyses were carried out by using a Japan Analytical Industry JHP-3 type Curie-point pyrolyzer

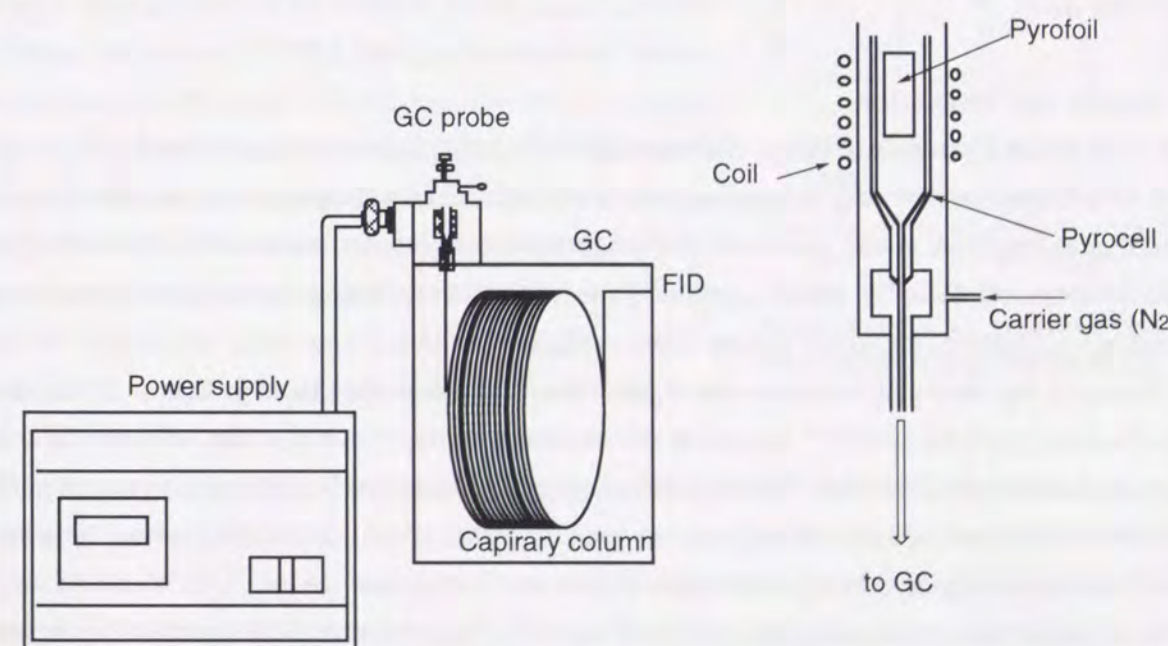


Figure 1-1. Schematic diagrams of Curie-point pyrolyzer

equipped with a Shimadzu GC-14BPFSC (CBP-1 capillary column, inner diameter 0.25 mm x length 25 m) and the same type of pyrolyzer equipped with a JEOL JMS-DX-303 GC-MS, respectively. Acquisition and analysis of MS data were carried out on a JEOL JMA-DA-5100 data station. Each model compound (*ca.* 0.5 mg) was pyrolyzed at 670 °C for 3 s at a heating rate of 2500 K/s under a nitrogen stream. Products remained on pyrocell and pyrofoil were defined as tar and coke, respectively (see Figure 1-1). Weight of these fractions was measured by a microbalance. Weight of volatile, which was introduced to GC, was calculated using following equation; weight of volatile = weight of sample - weight of tar - weight of coke.

Pyrolysis

The reaction was performed using a Pyrex glass tube (i.d. 6 mm x 100 mm). A benzyl-substituted polyaromatic compound *ca.* 20 mg (and an appropriate quantity of 9,10-dihydroanthracene) was added to the tube and the content was melted by heating. After cooling, the tube was evacuated and flame sealed. The sample tube was then heated for 1 h by inserting it into a thermostated electric furnace which was preheated at 430 °C. After cooling, it was opened and *ca.* 2 mL of dichloromethane containing an appropriate internal standard for GC analysis was added to the product mixture. Product identification and quantification were made by GC-MS and GC analysis.

Semiempirical MO calculations

All MO calculations were carried out on a Titan 750V workstation (Kubota Pacific Computer Co.) by using semiempirical molecular orbital calculation program, MOPAC (version 5.0). Bond dissociation energy of the reaction (DE), $R-R' \rightarrow R\cdot + R'\cdot$, was calculated by using following equation: $DE = DHfo(R\cdot) + DHfo(R'\cdot) - DHfo(R-R')$, where DHfo is an energy for standard heat of formation. For each calculation, AM1 method was used and, especially for radicals, AM1-UHF (Unrestricted Hartree-Fock) method was used. Titan version of this program was purchased from Simulation Technology Inc.

1.3. Results and Discussion

1.3.1. Curie-Point Pyrolysis of Alkyl-Substituted Polycyclic Aromatic Compounds

It is well known that coal organic materials (COM) contain a significant amount of aliphatic carbons. For example, Argonne premium coal samples were reported to contain 10 - 40 % of aliphatic carbons by referring their ^{13}C NMR spectra.² However, a detailed information about structure and distribution of aliphatic functional groups is not sufficient.

To clarify the chemical structures and distribution of aliphatic functional groups in COM, several studies such as pyrolytic study,³⁻¹³ oxidation of COM with RuO_4 ,¹⁴ or liquefaction under deuterium atmosphere have been carried out.¹⁵ These results suggested that aliphatic carbons are present in COM as a free form such as *n*-alkanes or terpanes trapped in COM, alkyl side chains attached to aromatic moieties, and polymethylene bridges between two aromatic moieties.

In recent studies, Nomura *et al.* have been investigating coal chemical structure by the use of CP/MAS ^{13}C NMR coupled with Curie-point pyrolysis GC-MS techniques.⁹⁻¹¹ Curie-point pyrolysis

of the coal or its extract afforded a series of *n*-alkanes and 1-alkenes, alkylbenzenes, alkylphenols, alkyl-naphthalenes, and so on. On the basis of these data we proposed a unit chemical structural model for Japanese bituminous Akabira coal.¹⁶ However, pyrolytic behavior of organic compounds in COM remains still unclear. Therefore, in order to get deeper understanding of pyrolytic behavior of organic compounds of COM, we prepared 14 coal model compounds having aliphatic functional groups *via* several functional groups (1-4, Figure 1-1) were prepared and their pyrolytic behavior was examined by using a Curie-point pyrolyzer.

Pyrolysis of model compounds 1 and 2

In our recent studies, Curie-point pyrolysis of some coals or their extracts was found to afford a series of *n*-alkanes having more than 30 carbon atoms along with the corresponding 1-alkenes.⁹⁻¹¹ However, their origins are still unclear. On the basis of the results reported previously, the possible origins of the aliphatic products are thought to be alkanes or terpanes trapped in COM, alkyl side chains attached to aromatic moieties in COM, and polymethylene bridges between two aromatic moieties. Subsequently, we have carried out pyrolysis of model compounds having aliphatic functional groups. We selected aromatic hydrocarbon connecting a longer alkyl side chain and two aromatic hydrocarbons having a polymethylene bridge between them as coal model compounds where we adopted an alkyl-aryl bond, an ether type bond, a ketone type bond and an ester type bond as a connecting group between aliphatic and aromatic moieties: the latter two functional groups, ketones and esters, are found to be rich in lower rank coals (Scheme 1-1).

Curie-point pyrolysis of benzene derivatives with a longer alkyl side chain (1a-d) and a polymethylene bridge (2a-d) was carried out at 670 °C for 3 s under a nitrogen stream. Yields of volatile, tar, and coke were summarized in Figure 1-2. Yield of coke, which is a major product in pyrolysis of macromolecules such as coal or its extract, was very low (less than 10 %). From this

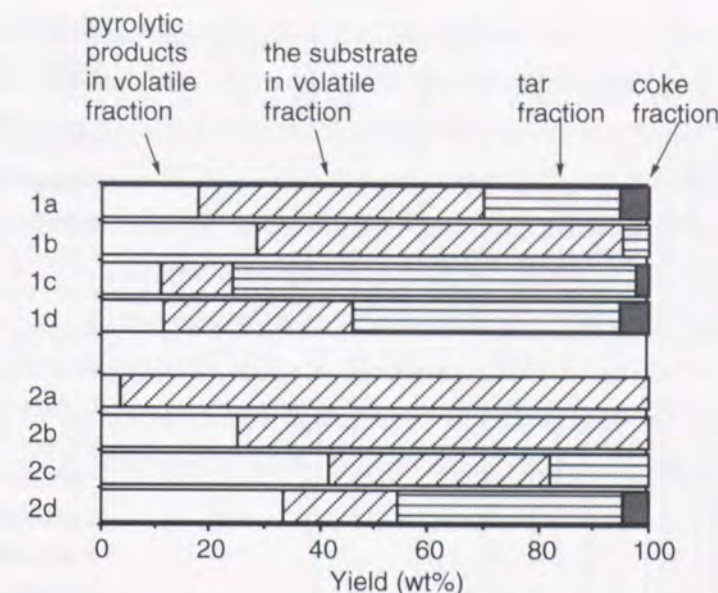


Figure 1-2. Yield of pyrolytic products from 1a-d and 2a-d.

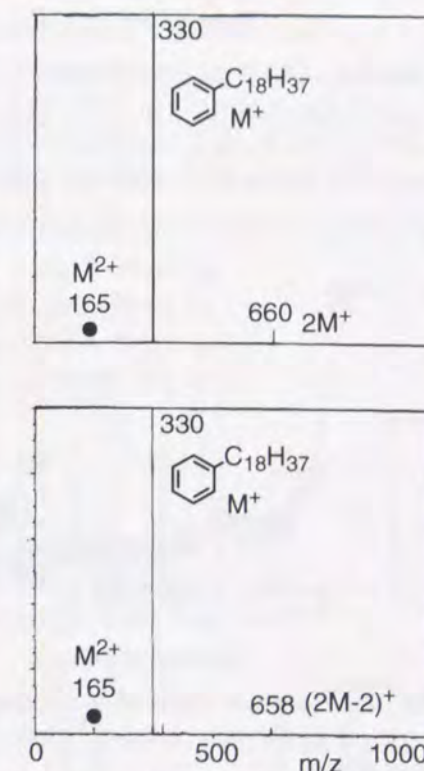


Figure 1-3. FD-MS spectra of 1a (top) and the tar fraction obtained from pyrolysis of 1a (bottom).

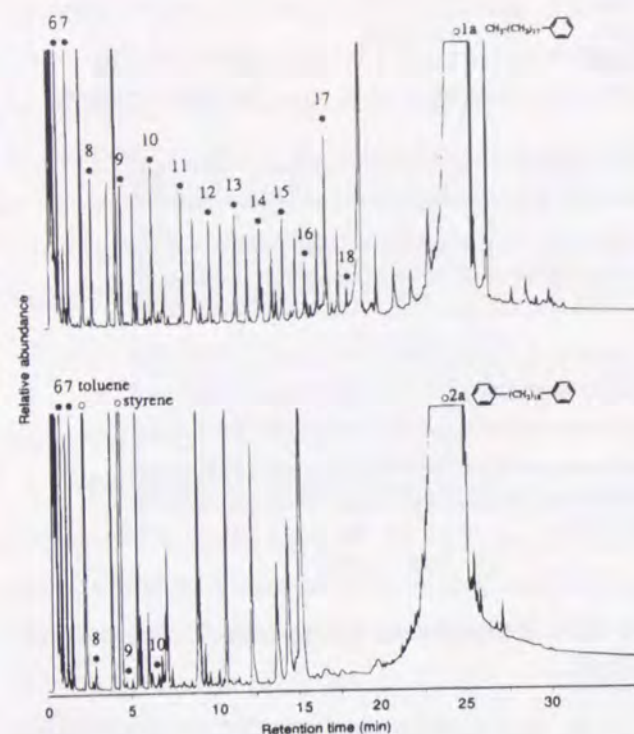


Figure 1-4. Curie-point pyrograms for **1a** (top) and **2a** (bottom) at 670 °C for 3 s under N₂; the Arabic numbers indicate the carbon numbers of 1-alkenes produced.

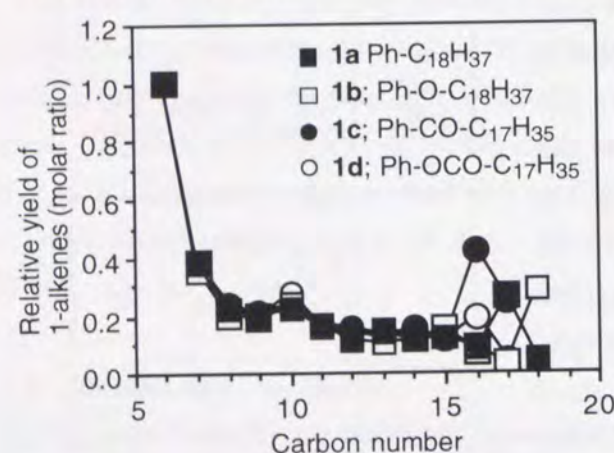


Figure 1-5. Relative yield of 1-alkene from Curie-point pyrolysis of **1a-d** (yield of hexene = 1, mol ratio)

Pyrograms of octadecylbenzene (**1a**) and 1,10-diphenyldecane (**2a**) were shown in Figure 1-4, these suggesting that very complicated reactions occurred. Major products from **1a** were a series of 1-alkenes and alkylbenzenes and from **2a** alkylbenzenes were mainly obtained along with small amount of 1-alkenes. These tendencies were also shown in pyrolysis of other model compounds, **1b-d** and **2b-d**. Major products and their yields (peak area) were shown in Tables 1-1. These results suggested that major origin of aliphatic compounds from pyrolysis of coal is alkyl side chain of COM.

Relative yields of alkenes from **1a-d** were shown in Figure 1-5 (yield of hexene=1.00, molar ratio). Distribution of C₆-C₁₅ alkenes from each compound was similar to each other, these results

Table 1-1. Main products from the Curie-point pyrolysis of **1a-d**^a

	1a	1b	1c	1d
hexene	3.48 ^b	5.39	3.84	3.51
heptene	1.54	2.64	1.75	1.53
octene	1.01	1.65	1.19	1.07
nonene	1.03	1.74	1.17	1.04
decene	1.29	2.38	1.49	1.53
undecene	1.03	1.78	1.16	1.06
dodecene	0.87	1.33	1.06	1.08
tridecene	1.02	1.25	1.01	0.92
tetradecene	0.90	1.45	1.20	1.21
pentadecene	1.02	2.19	1.00	0.91
hexadecene	0.74	0.96	4.40	1.72
heptadecene	2.14	0.60	2.56	0.48
octadecene	0.53	4.99		
benzene	0.46	1.97	4.54	0.86
toluene	3.56	0.42	0.74	1.29
ethylbenzene	1.01	0.46	0.36	0.75
styrene	6.95	0.88	1.32	2.17
propylbenzene	0.44	1.64	0.10	0.18
Ph-C ₃ H ₅			0.13	0.17
phenol		10.72	15.24	

total 29.02 44.43 29.03 36.71

^a Each compound was pyrolyzed at 670 °C for 3 s under a nitrogen stream. ^b Based on the area of total compounds excluding the area of the substrate.

figure, it was found that the compounds **2a-d** afforded less amounts of tar and coke fractions than that from the compounds **1a-d**, which might be due to their low molecular weight. FD-MS analysis of tar fraction from **1a** revealed that this fraction was composed of the substrate and small amount of its dimerized product (Figure 1-3).

Pyrograms of octadecylbenzene (**1a**) and 1,10-

suggesting that alkenes are produced from a common intermediate such as higher alkyl radicals.

The ratio of total aliphatic carbons to total aromatic carbons in the pyrolytic products from **1a** was calculated to be 3.11, this value agreeing well with that of original **1a** (3.0), where the molecular formula of the gaseous products were assumed to be (CH₂)_n. This is a most significant point of this reaction when this pyrolytic technique is applied to analysis of the components of COM. These results also suggest that although this pyrolysis proceeds in a complicated fashion along with several secondary reactions and formation of tar and coke fraction, the pyrolytic products obtained could reflect the chemical structure of original COM, if COM is structurally uniform. However, COM is now believed to be heterogeneous so it is important to treat carefully the pyrolytic results of COM. In this respect, the latest information that lighter fraction of COM is very close in constituents to heavier fraction of COM is very interesting.

Differences in pyrolytic products between from coal and from the model compounds

Pyrolysis of the model compounds afforded a series of 1-alkenes, while, as we had already reported, pyrolysis of coal or its extracts afforded a series of *n*-alkanes as main products along with minor amount of 1-alkenes.⁹⁻¹¹ This is a major difference between pyrolysis of coal and that of coal model compounds. We thought three possible reasons about these differences; (i) the presence of hydroaromatic compounds in coal, which might donate hydrogen atoms to alkyl radicals to give *n*-alkanes, (ii) the difference of degree of condensation of aromatic moieties, which could change the pyrolytic behavior of coal or model compounds, (iii) the presence of free *n*-alkanes in COM, which could become the origin of *n*-alkanes evolved during pyrolysis of coal. In order to obtain deep insight into these possibilities, we carried out the following two experiments; pyrolysis of the model compounds having more condensed aromatic ring such as naphthalene or hydroaromatic ring such as tetralin and pyrolysis of free *n*-alkanes.

Pyrolysis of naphthalene (**3a-d**) and tetralin (**4a-b**) derivatives were carried out. Figure 1-6 shows the pyrograms of **3a** and **4a**. Derivatives of naphthalene and tetralin and a series of aliphatic compounds were found in these pyrograms, these results suggesting that pyrolysis of these compounds proceeded in a similar fashion to those of **1a-d** (Tables 1-2 and 1-3). However, a series of *n*-alkanes was shown in the pyrograms (Figure 1-6). The order of the ratio of alkanes/alkenes (average of C₁₀-C₁₅ aliphatic compounds, mol ratio) increased as

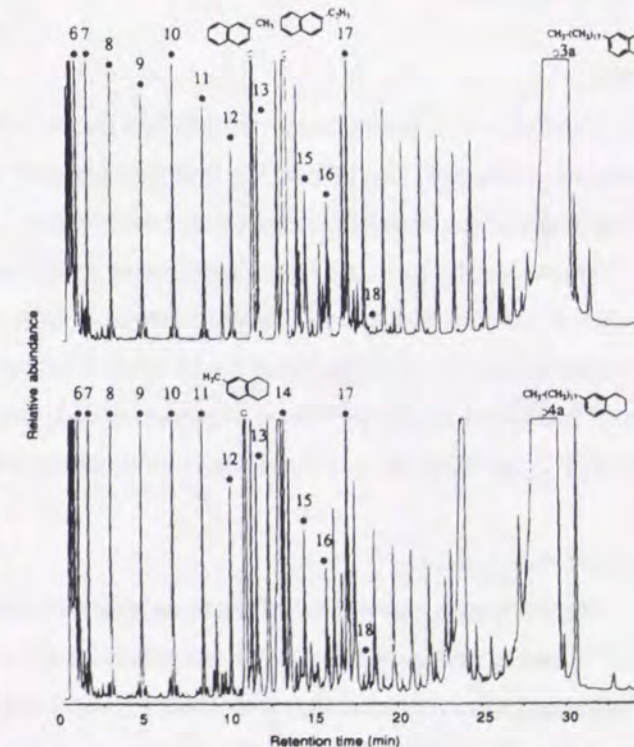


Figure 1-6. Curie-point pyrograms for **3a** (top) and **4a** (bottom) at 670 °C for 3 s under N₂; the Arabic numbers indicate the carbon numbers of 1-alkenes produced.

Table 1-2. Main products from the Curie-point pyrolysis of **3a-d**

	3a	3b	3c	3d
hexene	4.00	4.50	4.45	2.56
heptene	1.84	1.90	1.96	1.14
octene	1.18	1.27	1.35	0.84
nonene	1.21	1.34	1.33	0.85
decene	1.47	1.75	1.62	1.03
undecene	1.20	1.49	1.31	0.90
dodecene	1.05	1.15	1.17	0.91
tridecene	1.32	1.05	1.11	0.89
tetradecene	0.98	1.56	1.47	1.39
pentadecene	1.32	1.65	1.17	
hexadecene	1.45	0.93	2.75	3.08
heptadecene	2.82	1.87	1.29	1.38
octadecene	0.09	13.11		
Ar-H ^a	0.39	1.37	6.40	0.91
Ar-Me	6.32	0.28	1.43	0.55
Ae-Et	1.68	0.37	0.83	0.45
Ar-CH=CH ₂	11.41	0.93	2.49	1.54
Ar-C ₃ H ₇	1.59			
Ar-C ₃ H ₅		0.36		
ArOH		20.58		29.17
total	41.32	57.47	32.11	47.57

^a Ar=2-naphthyl

Table 1-3. Main products from the pyrolysis of **4a** and **4b**

	4a	4b
hexene	3.36	4.77
heptene	1.55	2.03
octene	0.98	1.22
nonene	0.97	1.29
decene	1.16	1.76
undecene	1.03	1.42
dodecene	0.78	1.04
tridecene	1.00	0.94
tetradecene	1.17	1.17
pentadecene	0.82	
hexadecene	0.60	1.36
heptadecene	2.20	0.64
octadecene	0.23	11.30
naphthalene	0.10	0.65
2-naphthol		3.05
tetralin	0.31	0.76
6-hydroxytetralin		10.25
total	16.24	43.65

follows; ~ 0 (**1a-d**) < 0.05 (**4a**) < 0.06 (**3c**) < 0.07 (**4b**) < 0.11 (**3a**) < 0.14 (**3b,d**). These results suggest that the more condensed aromatics and oxygen functional groups are some reasons of an evolution of *n*-alkanes in pyrolysis of coal or its

extracts.

Pyrolysis of *n*-hexacosane, which is a model compounds of free alkanes trapped in COM, gave a series of 1-alkenes, this indicating that free alkanes trapped in COM could be pyrolyzed to 1-alkenes having less carbon number under these conditions.

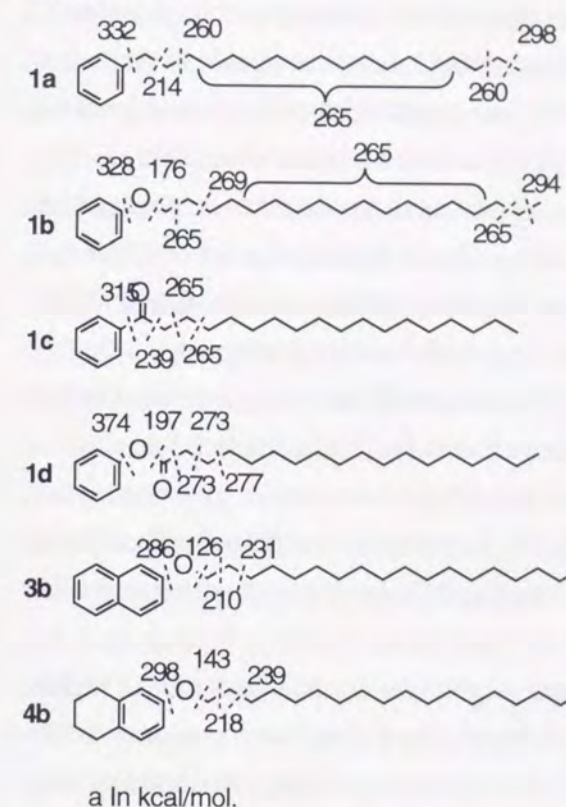
These results indicate that Curie-point pyrolysis of both the alkylaromatics and free *n*-alkanes afforded 1-alkenes along with varying amounts of *n*-alkanes, so we could not determine the origin of the alkanes formed during pyrolysis of coal. Calkins *et al.* had reported that the origin of the lower alkenes produced during pyrolysis of coal is (CH₂)_n groups,³⁻⁵ however, they had not determined whether these (CH₂)_n groups are in longer alkyl side chains attached to aromatic moieties or in free alkanes.

Pyrolytic mechanism

Mechanism for pyrolysis of these model compounds was investigated. Poustma *et al.*¹ and Savage *et al.*¹⁷⁻¹⁹ had investigated the pyrolysis mechanism and kinetics for many coal model compounds and the latter had also reported that pyrolysis of alkylaromatics (Ar-C_nH_{2n+1}) at relatively low temperature (around 400 °C) mainly affords methylarenes (Ar-CH₃), *n*-alkenes (C_{n-1}H_{2n-2}), vinylarenes (Ar-CH=CH₂), and *n*-alkanes (C_{n-2}H_{2n-2}), however, under the conditions employed in the present study, the pyrolysis temperature was higher, this resulting in production of more complicated mixture.

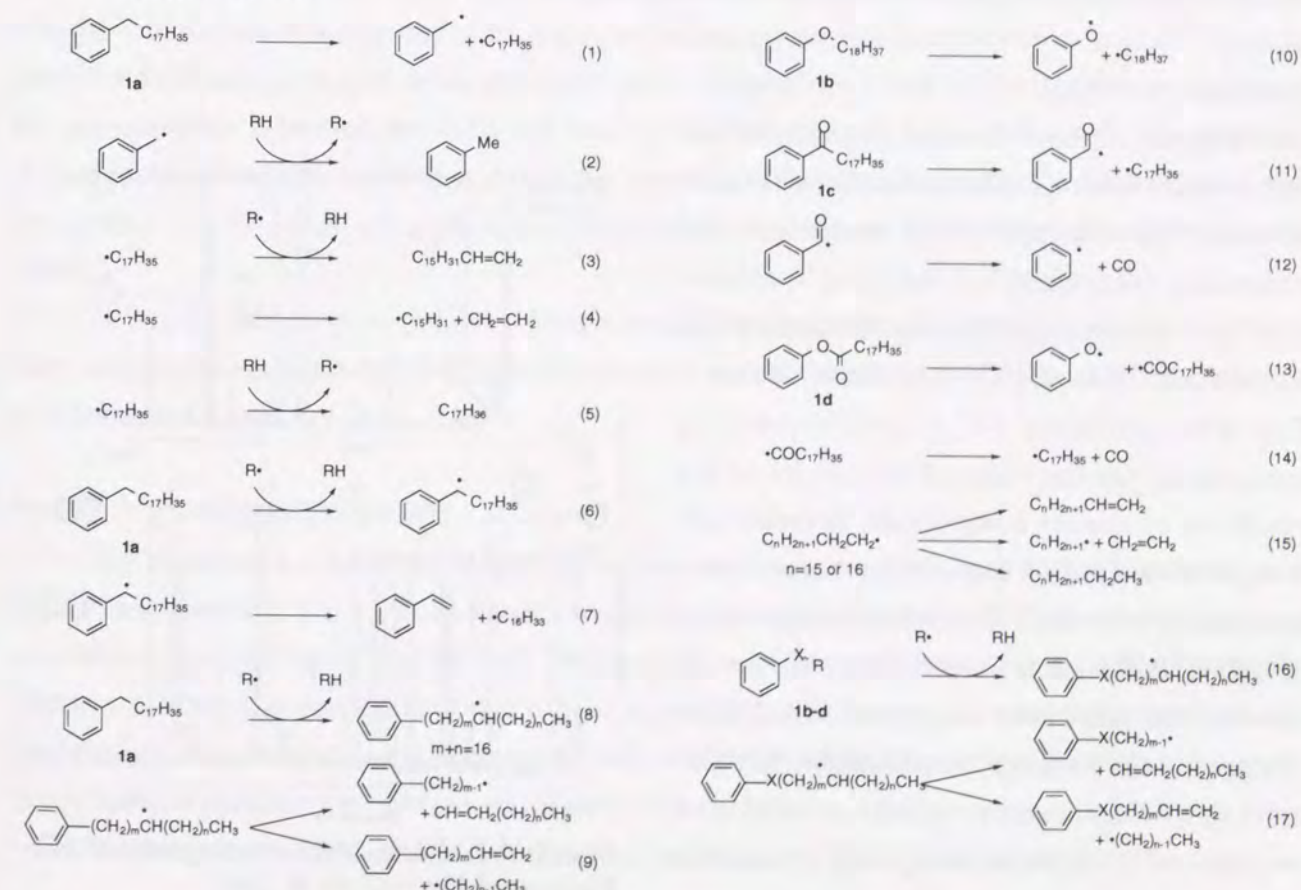
First stage of the pyrolysis is thought to be initiated by cleavage of the weakest bond in the

Scheme 1-2^a



a In kcal/mol.

Scheme 1-3



model in unimolecular fashion. Therefore, bond dissociation energies for each bond in the model compounds were very important. So we calculated these values by using semiempirical molecular orbital calculation program (MOPAC-AM1 method²⁰), the resulting energies being shown in Scheme 2. Calculated values were lower than the values obtained experimentally, for example, bond dissociation energies for PhCH₂-R → PhCH₂• + R• and PhO-R → PhO• + R• were calculated 51 and 42 kcal/mol (R = C₁₇H₃₅), respectively, these values being 28 - 33 % lower than the values obtained experimentally such as 70 (R = C₂H₅ or *n*-C₃H₇) and 63 kcal/mol (R = CH₃ or C₂H₅).²¹ Generally, it is well known that MO calculations of odd electron systems is very difficult, thus this being probably the source of errors. However, it was reported that AM1 method could reproduce the relative order of these values,²⁰ so I used these calculated values. We would like to note that these values in Scheme 1-2 are not exact bond dissociation

energies.

At first, mechanism of pyrolysis of **1a** was discussed. From pyrolysis of **1a**, toluene, styrene, and 1-alkenes were obtained as major products. First stage of the reaction is thought to be a fission of the bond between α - and β -position to the phenyl ring, giving benzyl and 1-heptadecyl radicals (initiation reaction, eq. 1). Benzyl radical extracts hydrogen to afford toluene (eq. 2). Fate of heptadecyl radical is very complicated; loss of hydrogen atom (eq. 3), releasing ethylene (eq. 4), or extraction of hydrogen atom (eq. 5) to give 1-heptadecene, 1-pentadecyl radical, or *n*-heptadecane, respectively. In propagation step, the radicals produced in situ attacks **1a** to give radicals (eqs. 6 and 8), which were converted to styrene, heptadecyl radical, ω -phenylalkyl radicals, 1-alkenes, ω -phenyl-1-alkenes, and alkyl radicals (eqs. 7 and 9). The alkyl radicals formed were thought to be degraded according to the eqs. 3-5.

As to **1b**, **1c**, and **1d**, first stage of the reaction is thought to be bond fission of the weakest bonds as shown in Scheme 1-2 and eqs. 10-14, to give phenoxy, phenyl, octadecyl, and heptadecyl radicals. Phenoxy and phenyl radicals abstract hydrogen from another radicals or substrates to give phenol and benzene, which were observed as major products in the pyrolysis of these compounds. The fate of these alkyl radicals were thought to be similar to those from **1a** (eq. 15). In propagation steps, similar degradation might take place (eqs 16 and 17).

As to **3** and **4**, pyrolysis proceeded in a similar fashion to give similar products, but in higher yields. This is partly due to more weaker bonds in **3** and **4** (Scheme 1-2). Difunctional compounds **2a-d** were pyrolyzed in a similar fashion to give benzene derivatives as major products. It is unclear why pyrolysis of the compounds having more condensed aromatic rings such as **3** or **4** afforded more amount of alkanes than that from **1**. Consequently, we have to investigate the pyrolytic behavior of the model compounds having more condensed aromatic rings or polyfunctionalized model compounds.

Pyrolysis of COM

Figure 1-7 shows the typical pyrogram for coal extracts (acetone soluble fraction of Illinois #6 coal).¹² In this pyrogram, more than 140 compounds were identified including, *n*-alkanes (C_3 - C_{28}), 1-alkenes (C_5 - C_{23}), alkylbenzenes ($-C_4$), styrene, alkylphenols ($-C_3$), alkyl naphthalenes ($-C_5$), dibenzofurans ($-C_3$), and three ring compounds. On the basis of the results of the pyrolysis of model compounds, styrene was thought to be formed from the pyrolysis of the compounds with alkyl side chains (propyl group or higher). Although aromatic compounds having several alkyl side chains ($-C_5$) were found in the pyrogram, these compounds could not be identified until now. However, the results of oxidation reaction of COM with RuO_4 told us that the

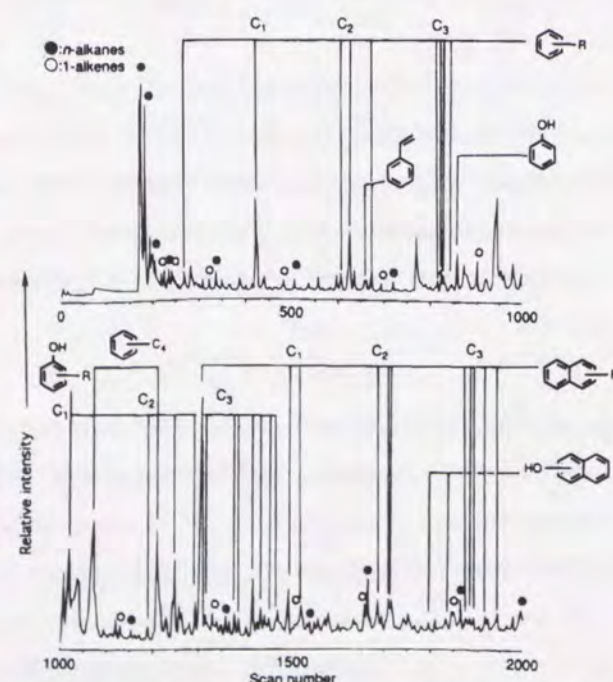


Figure 1-7. Curie-point pyrogram of AS fraction of Illinois No. 6 coal.

abundance of alkyl side chains or polymethylene bridges having more than three carbons were very low,¹⁴ this suggesting that these aromatic compounds might be polyalkylated one (preferentially polymethylated compounds). On the basis of the results of pyrolysis of the model compounds and coal extracts, it was suggested that COM was mainly composed of compounds of aromatic hydrocarbons and oxygen containing aromatic compounds with several alkyl side chains and bridges.

As to the aliphatic structure of COM, some researchers³⁻⁸ had reported that coal contain longer alkyl side chains attached to aromatic rings and/or linear alkanes which are located in the pores of the coals and are not chemically bound as described in introduction, however we could not confirm the ratio of free *n*-alkanes to alkyl side chains on the basis of the only pyrolytic results of coal itself and coal model compounds. To obtain these kind of information, we are now carrying out the further studies concerning more detailed analysis of the pyrolytic products of COM, quantitative and qualitative analysis of ^{13}C -NMR of COM, and deuterium incorporation during coal liquefaction.¹⁵

1.3.2. Pyrolysis of Benzyl-Substituted Polycyclic Aromatic Hydrocarbons

One of the model compound types extensively subjected to pyrolysis is diaryl methane,²²⁻²⁹ since the methylene bond is considered to be an important linkage connecting aromatic fragments in coal,³⁰⁻³² as well as ether, dimethylene, and polymethylene. The possible modes of cleavage of the relatively strong bond may involve ipso-hydrogen attack by free hydrogen addition, reverse radical disproportionation (RRD), and radical hydrogen transfer (RHT) mechanisms.^{1,22-29} In unsymmetrical diarylmethanes, there exit two possible cleavage directions. Futamura *et al.* described that 9-benzylphenanthrene undergoes hydrogenolysis in the presence of tetralin to give phenanthrene together with toluene.²⁸ Pyrolysis of 1-[4-phenylethyl]benzyl]naphthalene in the presence of 9,10-dihydroanthracene was reported to produce predominantly naphthalene by Farcaciu *et al.*²⁹ In such benzyl-substituted polycyclic aromatic compounds, the position of the substituent could also affect the reaction path. However, the influence has been little examined, while with a specific substrate, 1,2'-dinaphthylmethane, McMillen, Malhotra, and their co-workers have clearly demonstrated that the product ratio of 1-methylnaphthalene to the 2-isomer depends on the hydrogen donor compounds added.

In light of these results pyrolytic behavior of benzyl-substituted aromatic hydrocarbons have been investigated (compounds **5-8**, Scheme 1-1) with or without addition of 9,10-dihydroanthracene as a hydrogen source.

Pyrolysis of dibenzyl naphthalenes

The reaction of 1,5-dibenzyl naphthalene (**5a**) and 2,6-isomer (**5b**) was at first conducted in a sealed tube at 430 °C for 1 h without addition of 9,10-dihydroanthracene (DHA) and the resulting mixture was analyzed by GC and GC-MS. The conversions of **5a** and **5b** were 16 and 12 %, respectively (Table 1-4). The observed higher conversion of **5a** parallels with the general trend that a 1-substituted naphthalene compound is thermodynamically less stable than the corresponding 2-substituted isomer. From **5a** was produced a mixture of toluene and benzene in a ratio of 86:14 together with 1-benzyl naphthalene (1-BN) and 1-benzyl-5-methylnaphthalene (1,5-BMN). This suggest that *path a* in

Scheme 1-4 preferably occurs compared with *path b*. The yield of toluene and 2-BN were around 30%, suggesting that the hydrogen source of the cleavage reaction is the substrate itself and hence oligomeric products, which as derived from a free radical, possibly a benzylic radical, were also produced. In contrast to the reaction of **5a**, **5b** selectively gave benzene in a yield of 18%, only a negligible amount of toluene being detected. However, the corresponding fragment product, **5b** was very low (less than 2%). These results may

suggest that the major reaction path is different from that of **5a**. In the case of **5b**, oligomerization of the substrate may be the major reaction and benzene is formed after the process. It should be noted that 1-BN and 2-BN are stable under the conditions employed. This could be due to the fact that a large part of BN (bp ca 350 °C) exists in the vapor phase, whereas that of dibenzylanthracenes does as liquid under the reaction conditions employed.

Addition of 5 or 10 equiv of DHA to the reaction considerably increased both the conversion of **5a** and **5b**, indicating that hydrogen transfer from DHA to dibenzylanthracenes effectively takes place. In the reaction of **5b**, toluene was preferably formed along with 2-BN, in contrast to that without DHA. Thus, DHA appears to enhance *path a* in Scheme 1-4, while homo- and cross-coupling reactions of radicals formed from **5b** and DHA could also take place, since both the yields of toluene and 2-BN were around 30%.

Pyrolysis of Benzylphenanthrenes and Anthracenes

The results for the reaction of benzylphenanthrenes (**6**) and benzylanthracenes (**7**) are presented in Table 1-5. In the reaction of **6c** without DHA, toluene (40%) and phenanthrene (47%) were formed along with benzene (4.3%), the conversion of the substrate being 31%. By contrast, **6a** gave benzene (6.2%) as a sole measurable product. Similarly, a negligible amount of toluene was formed in the reaction **6b**, while phenanthrene (9.9%) was detected in a comparable amount with 3-methylphenanthrene (3-MP, 4.4%). These low product yields suggest that the reaction **6a** and **6b** produces a large amount of high molecular weight products. The conversions of **6a** and **6b** were 15 and 8.2% which are smaller than that of **6c**. These results may indicate that the reaction of **6c** parallels

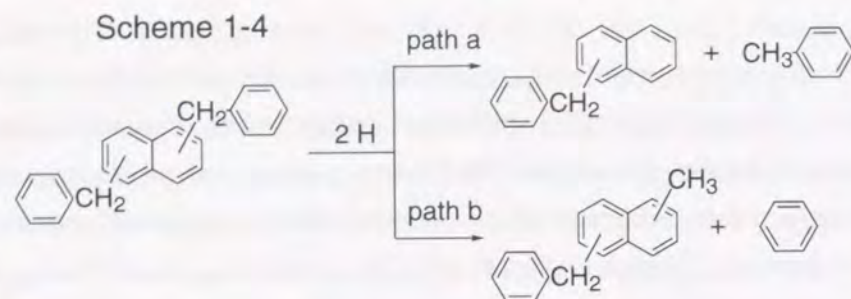


Table 1-4. Pyrolysis of **5a** and **5b**^a

substrate	DHA ^b (equiv)	Conv. (%) ^c	products (%) ^{c,d}				
			B ^e	T ^f	BN ^g	BMN ^h	B:T ⁱ
5a	none	15.9	5.6	35.7	28.5	1.3	14:86
5a	5	21.8	9.1	94.4	48.4	1.6	9:91
5a	10	28.0	7.3	67.7	38.1	1.2	9:91
5b	none	11.8	18.2	tr	tr	1.7	100:0
5b	5	15.8	27.4	38.9	26.1	3.6	41:59
5b	10	20.7	19.9	33.0	27.3	3.7	38:62

^a The reaction was carried out at 430 °C for 1 h. ^b 9,10-Dihydroanthracene.

^c Determined by GC analysis. ^d Based on substrate consumed.

^e Benzene. ^f Toluene. ^g Benzylnaphthalene. ^h Benzylmethylnaphthalene.

ⁱ Benzene / toluene ration.

with that of **5a** and the behavior of **6a** and **6b** is similar to **5b**.

Addition of 10 equiv of DHA to the reaction of **6c** enhanced toluene formation, which is similar to the reaction **5a**. In the case of **6a** and **6b**, the formation of toluene was induced, as for the reaction of **5b**. However, the increase in the substrate conversion of each benzylphenanthrene was relatively small compared with that of the corresponding naphthalene derivatives.

The reaction of 9-benzylanthracene (**7b**) without DHA gave a mixture of toluene (50%) and anthracene (67%) along with benzene (0.6%), as for the reaction of **6c**. It was

somewhat surprising that 2-benzylanthracene (**7a**) also gave a similar product mixture, although the yield of each product was relatively low. This is in contrast to the reaction of **6a** where benzene was the single measurable product. Addition of DHA to the reaction of **7a** and **7b** also enhanced the yield of toluene. The conversion of **7a** and **7b** were considerably higher than **6a** and **6c**, respectively, suggesting that the anthracene derivatives are relatively more reactive than the corresponding phenanthrene compounds.

The results for the reaction of 1-, 2-, and 4-benzylfluorenes (**8a**, **8b**, and **8c**) are summarized in Table 1-6. The reaction of **8a** and **8c** without DHA gave benzene and toluene in comparable amounts, while the yields of the corresponding fragments, fluorene, and methylfluorene were very low, suggesting formation of large amounts of oligomeric products. Interestingly, **8b** selectively gave benzene, no toluene being detected. Addition of DHA to each reaction increased the ratio of toluene to benzene as expected.

Reaction Scheme

The initial step of the reaction of **5a** to toluene and 1-BN and to benzene and 1,5-BMN (Scheme 1-4) may involve *ipso*-hydrogen addition. The hydrogen may be provided (a) from another substrate of DHA by a bimolecular process accompanied by formation of a benzylic radical formed by hydrogen abstraction of the substrate of DHA radical (9-hydroanthracenyl radical) (RRD mechanism) and/or (b) from DHA radical accompanied by formation of anthracene (RHT mechanism). A recent theoretical study has suggested that the RRD mechanism might be preferable. However, I do not argue the

Table 1-5. Pyrolysis of **6a-c** and **7a,b**

substrate	DHA (equiv)	conv. (%)	products (%)				
			B	T	P or A ^a	MP or MA ^b	B : T
6a	none	15.3	6.2	tr	tr	tr	100 : 0
6a	10	17.8	7.3	8.4	k	-	47 : 53
6b	none	8.2	4.6	tr	9.9	4.4	100 : 0
6b	10	9.4	4.4	21.2	-	-	17 : 83
6c	none	31.5	4.3	40.0	4.7	tr	10 : 90
6c	10	33.3	3.7	79.1	-	-	5 : 95
7a	none	53.0	0.4	19.4	13.9	1.5	2 : 98
7a	10	69.4	1.4	38.4	-	-	4 : 96
7b	none	98.3	0.6	49.5	66.9	tr	1 : 99
7b	10	98.6	0.6	98.9	-	-	1 : 99

^a P, phenanthrene; A, anthracene.

^b MP, methylphenanthrene; b, methylantracene.

Table 1-6. Pyrolysis of benzylfluorene **8a-c**

substrate	DHA (equiv)	conv. (%)	products (%)				
			B	T	F ^a	MF ^b	B:T
8a	none	9.0	13.3	17.0	4.8	0.9	44 : 56
8a	10	32.5	4.2	17.3	13.6	-	20 : 80
8b	none	7.8	21.5	tr	tr	tr	100 : 0
8b	10	24.2	10.2	8.1	14.3	-	56 : 44
8c	none	7.2	10.9	4.9	tr	tr	69 : 31
8c	10	15.6	6.3	4.5	4.0	-	58 : 42

^a Fluorene. ^b Methylfluorene.

precedence of the two reaction mechanisms, since detailed kinetic investigation has not been carried out. By considering the reaction conditions and the substrate employed, free hydrogen does not seem to participate significantly in the reaction, since hydrogen adducts to the substrates may be enough stable to form free hydrogen atom. Hydrogen transfer to a *non-ipso* position could also lead to the products. Its participation, if any, seems to be small, since no traces of dihydrogenated products could be detected even by careful analysis of the product mixture in the early stage of the reaction. Of the two possible sites of ipso-hydrogen addition, the results for the reaction indicate that the addition to the naphthalene ring predominantly occurs and that to the benzene ring is much less favorable process. This may be interpreted in terms of the relative stability of the two hydrogen adduct intermediates. Semiempirical MO calculation (by MOPAC-AM1 method, see experimental section) of these intermediates has also suggested that the hydrogen adduct at the naphthalene ring is relatively more stable as intuitively expected based on the resonance stabilization (Figure 1-8). As noted above, the reaction may also produce high molecular weight products derived from the substrate radical, while their formation is apparently suppressed in the presence of DHA. The reactions of **6c** and **7b** may proceed, as does that of **5a**. The selective formation of toluene from these substrates is in harmony with the results reported previously.

The MO calculation of two possible hydrogen adducts to **5b** has also suggested that the adduct at the naphthalene ring is relatively more stable (Figure 1-8). Therefore, from the substrate toluene along with 2-BN could also be formed. In the presence of DHA, it was indeed the preferable product. However, benzene was predominantly produced as the single major product in the absence of DHA. Thus, the major reaction path appears to be different from that of **5a**. It may be conceivable that in the case of **5b** alone, oligomerization of the substrate seems to be the major reaction and benzene may be formed from the oligomeric products as considered precedently.

Consequently, the product mixture from the reaction **5a** and **5b** without DHA was analyzed by FD-MS (Figure 1-9). Both the spectra show peaks in the *m/z* region more than 1200, suggesting that oligomeric products at least up to tetramers were formed. Among the peaks, those at *m/z* 614 and 920 are confidently assignable to the corresponding dimers and trimers. The existence of the other considerable peaks suggests that the oligomeric products underwent further reaction. The

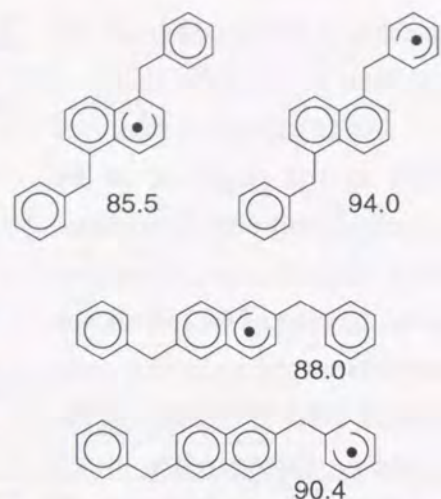


Figure 1-8. Heats of formation of ipso-hydrogen adducts of **5a** and **5b**.

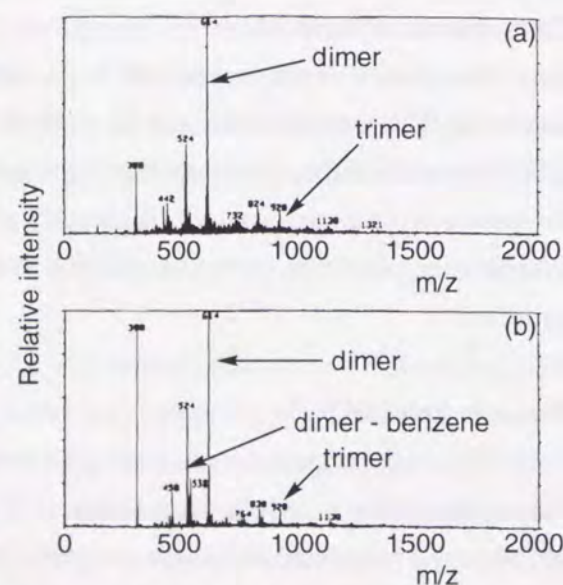


Figure 1-9. FD-MS spectra of the reaction mixture of (a) 1,5-dibenzyl-naphthalene (**5a**) and (b) 2,6-dibenzyl-naphthalene (**5b**).

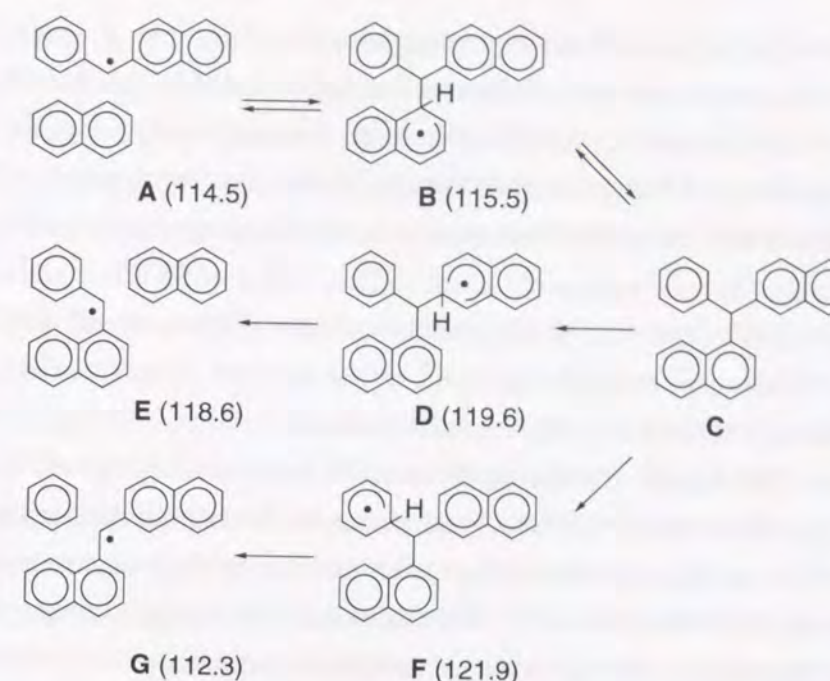


Figure 1-10. Possible mechanism for formation of benzene in the pyrolysis of **5b**. Value in parentheses indicates heat of formation (kcal/mol) calculated by the MOPAC-AM1 method.

significant peak at *m/z* 524 may be due to a compound(s) formed by cleavage of the dimer with liberation of toluene. The observed higher yield of toluene compared with 1-BN in the reaction of **5a** may be due to the contribution of such a secondary reaction. The fact that only a trace amount of toluene was detected in the reaction of **5b**, however, suggests that in this case, compound(s) having *m/z* 524 could not be formed from its dimer and come from higher oligomeric products, although the details are not clear. In the spectrum of the product mixture from **5b**, a considerable signal at *m/z* 538 which corresponds to compound(s) dimer - benzene is also observed. It should be noted that the corresponding peak in the spectrum that from **5a** was relatively small. Thus, formation of the compound(s) having *m/z* 538 may provide the clue for the origin of the selective formation of benzene from **5b**.

Based on the above results, a possible route which may lead to the formation of benzene from **5b** is illustrated in Figure 1-10. The heats of formation of the postulated radical intermediates were also calculated by the semiempirical MO method. To save calculation time the intermediates were represented by somewhat simplified compounds; **5b** and its dimerization pair were replaced by 2-BN and naphthalene, respectively. Reaction of benzylic radical formed from 2-BN reacts with naphthalene (pair A) gives radical B and the subsequent hydrogen loss (possibly by reaction with another radical species in the medium) affords a dinaphthylphenylmethane C which corresponds to a 2,6-dimer. Ipso-Hydrogen addition to C regenerates radical B or give two other possible radicals D and F. Radicals B, D, and F may afford pairs A, E, and G, respectively. The MO calculation suggests that G is the most stable pair, while the most stable hydrogen adduct radical is B. The observed selective formation of benzene from **5b** would imply equilibrium between C and E as well as C and A. While interconversion among radicals B, D, and F could occur without formation of C, it does not seem to be significant,

since the process had to involve a relatively high energy barrier.

In order to confirm which product, *i.e.*, benzene or naphthalene, is favorably formed from the dimer equivalent C, (1,2'-dinaphthyl)phenylmethane was prepared and pyrolyzed under the same conditions as those applied to **5b**. It was observed that the compound was consumed in 17% conversion to produce benzene selectively; the yields of benzene and naphthalene were 9.0 and 1.3%, respectively. This suggests that benzene may be selectively liberated from dimer of **5b** dimer and also from higher oligomeric products. It is noted that, in the reaction of the triarylmethane, formation of 1,2'-dinaphthylmethane was not observed. This may imply that the corresponding unsubstituted dinaphthylmethyl radical tends to form oligomerized products.

In the presence of DHA, *ipso*-hydrogen addition to **5b**, as for the reaction of **5a**, may also occur to give the product pair of toluene and 2-BN. Thus, it may be considered that, in the reaction of **5b** alone, dimerization is the energetically favorable process than the cleavage reaction *via ipso*-hydrogen addition at the early stage. It should be noted that analysis of the gas phase of the reaction mixture revealed evolution of hydrogen, although its quantification was not made.

The FD-MS spectrum of the product mixture from **6a** showed a characteristic signal *m/z* 458 (dimer - 76) which may corresponds a dipehnathrylmethane as well as that at 444 (dimer-90), this being similar to that for **5b** (Figure 1-11). The semiempirical MO calculation could also support that the reaction of **6a** without DHA proceeds by a similar way to that of **5b** (Figure 1-12). In the reaction of **6b**, formation of phenanthrene and 3-methyl-phenanthrene was also observed, while only a trace amount of toluene could be detected. These products could also be formed by secondary reaction of oligomeric materials.

The reaction of **7a** without DHA unexpectedly gave the product pair of toluene and anthracene, while

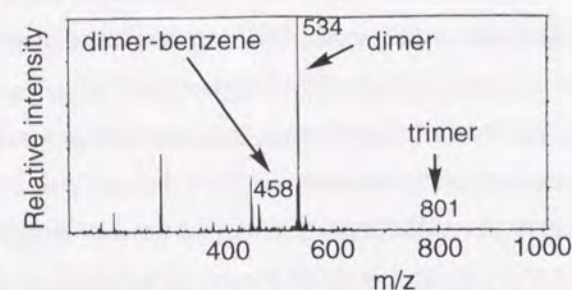


Figure 1-11. FD-MS spectrum of the reaction mixture of 2-benzylphenanthrene (**6a**).

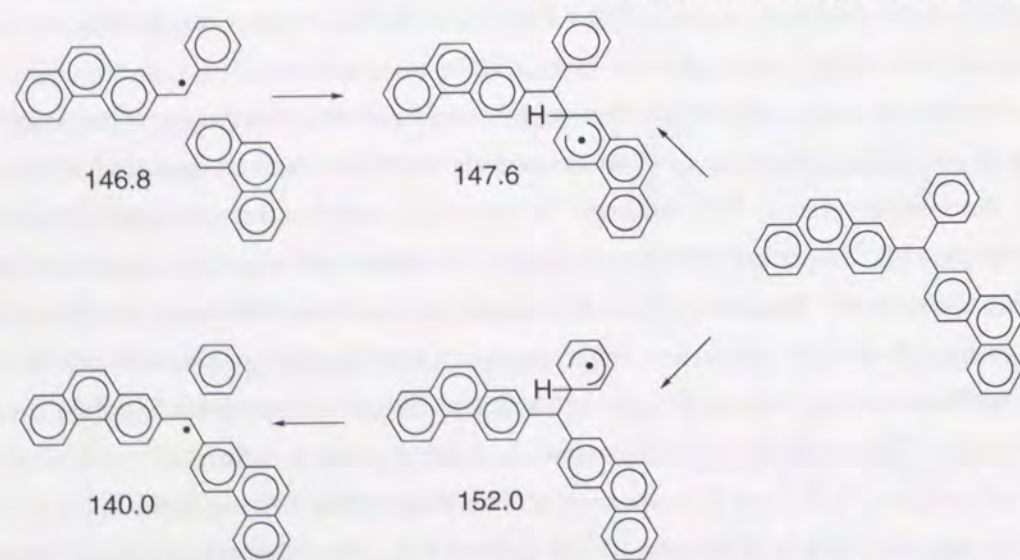


Figure 1-12. Possible mechanism for formation of benzene in the pyrolysis of 2-benzylphenanthrene (**6a**). The numbers indicate heat of formation (kcal/mol) calculated by the MOPAC-AM1 method.

the yields were rather low and hence a relatively large amount of oligomeric products is considered to be formed. This would imply that (a) oligomerization is the major reaction as for the case of **6a** and **5b**, but benzene liberation as in Figures 1-10 and 1-12 is an energetically less favorable process and (b) in this reaction, *ipso*-hydrogen addition can occur. There is a possibility that 9,10-dihydroanthracene derivatives are formed during the pyrolysis and they act as hydrogen donors as well as the substrate itself.

The substrates, **5a**, **6c**, and **7b**, may be considered to be α -benzyl-substituted type compounds, whereas **5b**, **6a**, **6b**, and **7a** may be classified to β -benzyl substituted compounds. The results of the pyrolysis of these compounds are summarized as follows: (a) the α -substituted type substrates selectively give toluene as the cleavage product along with the corresponding polyaromatic fragments accompanied by formation of oligomeric products. The cleavage reaction possibly proceeds by initial *ipso*-hydrogen addition, which can be enhanced by addition of the hydrogen source, DHA. (b) The major reaction of the β -substituted type compounds is oligomerization involving radical intermediates formed by hydrogen abstraction from the substrates and benzene may be selectively liberated from the oligomers, with the exception of the reaction of **7a**. In the presence of DHA, toluene can also be formed, as for the α -type substrates.

Although benzylfluorenes cannot be classified to the α - and β -types, the behavior of **8b** seems to be similar to that of the β -type compounds. **8a** and **8c** also gave benzene in considerable amounts and the yields of the detectable products were relatively low. Thus, the major thermal reaction may also be rather similar to the β -type compounds. Although from **8a** and **8c** toluene was produced considerable amounts, the yield of the corresponding fragment, fluorene, was relatively too small to be rationalized by the initial *ipso*-hydrogen addition mechanism. It was confirmed that fluorene is stable under the reaction conditions. Thus, in the reaction of **8a** and **8c**, toluene could be formed from oligomeric products. However, the reason for the different behavior between **8b** and **8a** and **8c** is not clear.

To obtain an insight into the different behavior between the α - and β -type compounds, the reaction energetics of *ipso*-hydrogen addition onto each substrate were calculated by MOAPC-AM1 method. The energy changes ($\Delta\Delta H_f$) by the addition to the polyaromatic rings of the substrates are summarized in Table 1-7. The data suggest that the reactions of the α -type compounds are relatively smaller energy change processes, whereas those for β -type substrates are relatively more endothermic with the exception of that for **7a**. The energy changes for the hydrogen additions to **8a**, **8b**, and **8c** are also large. Therefore, it may be considered that one of the major origins for the observed different pyrolytic results depending on the substrates examined is the ease of *ipso*-hydrogen addition.

Table 1-7. Difference of heats of formation between substrates and their *ipso*-hydrogen adducts estimated by semiempirical calculation using the MOPAC-AM1 method

$\Delta\Delta H_f$		$\Delta\Delta H_f$	
substrate	(kcal/mol)	substrate	(kcal/mol)
5a	0.4	7a	0.7
5b	7.0	7b	-0.7
6a	4.0	8a	8.4
6b	4.4	8b	5.2
6c	2.4	8c	5.8

1.4. References

- 1 Poutsma, M. L. *Energy Fuels* **1990**, 4, 114.
- 2 Franz, J. A.; Garcia, R.; Linehan, J. C.; Love, G. D.; Snape, C. E. *Energy Fuels* **1992**, 6, 598.
- 3 Calkins, W. H.; Hagaman, E.; Zeldes, H. *Fuel* **1984**, 63, 1113.
- 4 Calkins, W. H.; Tyler, R. J. *Fuel* **1984**, 63, 1119.
- 5 Calkins, W. H. *Fuel* **1984**, 63, 1125.
- 6 Snape, C. E.; Ladner, W. R.; Bartle, K. D. *Fuel* **1985**, 64, 1394.
- 7 Stock, L. M. *Acc. Chem. Res.* **1989**, 22, 427.
- 8 Stock, L. M.; Wang, S.-H. *Energy Fuels* **1989**, 4, 336.
- 9 Nomura, M.; Ida, T.; Miyake, M.; Kikukawa, T.; Shimono, T. *Chem. Lett.* **1989**, 645.
- 10 Matsubayashi, K.; Nomura, M.; Miyake, M. *Chem. Lett.* **1990**, 291.
- 11 Nomura, M.; Matsubayashi, K.; Miyake, M. *Chem. Lett.* **1990**, 1563.
- 12 Hama, H.; Matsubayashi, K.; Murata, S.; Nomura, M. *J. Jpn. Inst. Energy* **1993**, 72, 467.
- 13 Hama, H.; Murata, S.; Nomura, M.; *J. Jpn. Inst. Energy* **1994**, 73, 177.
- 14 See section 2.3.2 and its reference.
- 15 See section 2.3.3.
- 16 Nomura, M.; Matsubayashi, K.; Ida, T.; Murata, S. *Fuel Process. Technol.*, **1992**, 31, 169.
- 17 Savage, P. E.; Korotney, D. J. *Ind. Eng. Chem.* **1990**, 29, 499.
- 18 Smith, C. M.; Savage, P. E. *AIChE Journal* **1991**, 37, 1613.
- 19 Smith, C. M.; Savage, P. E. *Energy Fuels* **1991**, 5, 146.
- 20 Dewar, M. J. S.; Zebisch, E. G.; Healy, E. F.; Stewart, J. J. P. *J. Am. Chem. Soc.*, **1985**, 107, 3902.
- 21 McMillen, D. F.; Golden, D. M. *Ann. Rev. Phys. Chem.* **1982**, 33, 493.
- 22 Malhotra, R.; McMillen, D. F. *Energy Fuels* **1993**, 7, 227.
- 23 McMillen, D. F.; Malhotra, R.; Tse, D. S. *Energy Fuels* **1991**, 5, 179.
- 24 Malhotra, R.; McMillen, D. F. *Energy Fuels* **1990**, 4, 184.
- 25 McMillen, D. F.; Malhotra, R.; Hun, G. H.; Chang, S.-J. *Energy Fuels* **1987**, 1, 193.
- 26 McMillen, D. F.; Malhotra, R.; Chang, S.-J.; Ogier, W. C.; Nigenda, S. E.; Fleming, R. H. *Fuel* **1987**, 66, 1611.
- 27 Allen, D. T.; Gavalas, G. R. *Fuel* **1984**, 63, 586.
- 28 Futamura, S.; Koyanagi, S.; Kamiya, Y. *Fuel* **1988**, 67, 1436.
- 29 Farcasiu, M.; Smith, C. *Energy Fuels* **1991**, 5, 83.
- 30 Franz, J. A.; Ferris, K. F.; Camaioni, D. M.; Autrey, S. T. *Energy Fuels* **1994**, 8, 1016.
- 31 Heredy, L. A.; Kosto, A. E.; Neuworth, M. B. *Fuel* **1964**, 43, 414.
- 32 Heredy, L. A.; Kosto, A. E.; Neuworth, M. B. *Fuel* **1965**, 44, 125.

Chapter 2. Structural Analysis of Coal through Quinoline Extraction, Ruthenium-Ion Catalyzed Oxidation, and Liquefaction under Deuterium

2.1. Introduction

In the section of General Introduction, some further requisites for the construction of more precise coal structural models were pointed out; *e.g.* (a) information concerning non-covalent bonding interactions among coal molecules and (b) insight into the bridging groups between aromatic moieties. The former interactions have been of considerable interest, since they are significant factors in coal conversion reactions such as liquefaction and pyrolysis. Therefore, various studies have been carried out including solvent-swelling, extraction in the presence of electron-donor or acceptor reagents, and so on. In this chapter, some coals were submitted to heat treatment in quinoline and a large part of a specific coal could be solubilized by this treatment. Using the extract, I discussed non-bonding interactions through measurements of molecular weight and molecular size distributions of the extract. As to bridging groups, these are also important when we design coal conversion processes as I pointed out in Chapter 1. Therefore, two kinds of reactions, ruthenium ion-catalyzed oxidation and hydrolquefaction under deuterium atmosphere, were carried out to obtain information about the groups. These results may provide some insights into coal structure.

2.2. Experimental Section

Samples

Illinois No. 6 and Upper Freeport coals were purchased from Argonne National Laboratory, US. Other four coals such as Wandoan (Australian subbituminous coal), Akabira (Japanese bituminous coal), Miike (Japanese bituminous coal), and Zao Zhuang coals (Chinese bituminous coal), are our samples stored in glass vessels under a nitrogen atmosphere, respectively. Coals were pulverized under 100 mesh and dried at 40 °C *in vacuo* prior to use. All solvents were distilled before use. As to Illinois No. 6 coal, Argonne premium coal sample was employed. Whole coals used in this paper were pulverized under 100 mesh and dried at 100 °C *in vacuo* (5 mmHg) for 10 h prior to use. Solvents were distilled according to conventional methods. Other reagents were commercially available and used without further purification.

Extraction of Coals with Quinoline

The autoclave including 2 g of pulverized and dried coal and 10 mL of quinoline was pressurized with nitrogen up to 4.9 MPa, then being heated up to 350 °C at a heating rate of 8 K / min. The autoclave was kept at this temperature for 1 h with shaking. After 1 h passed, the autoclave was cooled to room temperature, gaseous products being collected and analyzed by a Shimadzu GC-8AIT (silica gel column). Solid and liquid products were recovered by washing the inside of the autoclave with

quinoline, being separated into quinoline-soluble (QS) and -insoluble (QI) fractions by centrifugation. After a removal of quinoline by evaporation at 80 °C under 5 mmHg, the resulting solid materials were washed three times with a mixture of methanol-water (8:2, v/v) under ultrasonic irradiation in order to remove small amounts of quinoline remained. The resulting QS and QI fractions were dried at 40 °C in vacuo, then the extract being submitted to the analysis by NMR, size exclusion chromatography, pyrolysis GC/MS, and so on.

Measurements of CP/MAS ^{13}C NMR

Measurement of CP/MAS ^{13}C NMR was carried out on a Chemmagetics CMX-300. Parameters were as follows: frequency 75.506 MHz, pulse width 90 °; pulse delay 7 s; contact time 2 s; pulse mode CP; scan number 2000.

Curie-point Pyrolytic Analysis

Curie-point pyrolysis gas chromatographic (Py-GC) and -mass spectrometric (Py-GC-MS) analyses were carried out by using a Japan Analytical Industry JHP-3 type Curie-point pyrolyzer equipped with a Shimadzu GC-14BPFSC (CBP-1 capillary column, inner diameter 0.25 mm x length 25 m) and the same type of pyrolyser equipped with a JEOL JMS-DX-303 GC-MS, respectively. Acquisition and analysis of MS data were carried out on a JEOL JMA-DA-5100 data station. Each sample (ca. 0.5 mg) was pyrolyzed at 670 °C for 3 s at a heating rate of 2100 K/s under a nitrogen stream. Products remained on pyrocell and pyrofoil were defined as tar and coke, respectively. Weight of these fractions was measured by a microbalance. Weight of volatile, which was introduced to GC, was calculated using following equation; weight of volatile = weight of sample - weight of tar - weight of coke. Details of the apparatus for the pyrolysis were described elsewhere (see also experimental section in chapter 1).

Measurement of Diffuse Reflectance FT/IR (DR/FT/IR)

Dried sample (50 mg) and KBr (450 mg) were mixed and ground by using an agate mortar. The resulting mixture was further dried at 90 °C for 10 h in vacuo. FT/IR spectrum of the sample was recorded on a JEOL JIR-AQS20M with diffuse reflectance method (128 scans). Data acquisition and analysis were also carried out on the computer equipped with the spectrometer.

Measurement of Particle Diameters by Light Scattering Method

Evaluation of particle diameter distribution was carried out by using an Otsuka Denshi DLS-700 dynamic light scattering meter with He-Ne laser ($\lambda=633$ nm). An extract was dissolved in *N,N*-dimethylformamide (4.4×10^{-2} g/L), the solution being filtered with membrane filter prior to measurement. Data collection and analysis were carried out on an NEC PC-9801 personal computer.

Measurement of Size Exclusion Chromatography

Analysis by size exclusion chromatography was conducted by using a Shimadzu LC-10AS system with Shodex KF-80M SEC column (30 cm, stationary phase: polystyrene gel) and a Yanaco M-315

ultraviolet detector ($\lambda=270$ nm). An extract (6.3 mg) was dissolved in 10 ml of DMF, 20 mL of which was injected to the LC system, where either DMF or DMF containing lithium bromide (0.01 mol/L) was used as eluant. Calibration of retention time - molecular weight relationships was conducted by using 14 kinds of standard polystyrene sample ($M_n=1.8 \times 10^3 - 3.16 \times 10^6$).

Procedure for RICO Reaction of Coal

RuCl_3 (40 mg) and coal (1 g) were added to a 100 mL flask containing MeCN (20 ml), CCl_4 (20 ml), and H_2O (30 ml), the mixture being stirred magnetically for 1 h. NaIO_4 (10 g) was added gradually, the resulting mixture being stirred at 40 °C for 24 h. After the end of the reaction, the mixture was filtered to remove an inorganic residue. The filtrate was analyzed with the following two methods; (i) For analysis of lower carboxylic acids ($\leq \text{C}_6$), aqueous NaOH solution (5 %, 100 ml) and ether (100 ml) were added to the filtrate and the resulting aqueous phase was separated. This aqueous solution was diluted to 1000 ml by using deionized water and 5 ml portion of this solution was analyzed by a DIONEX 2000i/sp ion chromatograph (HPICE-AS-1 column). (ii) For analysis of higher carboxylic acids ($\text{C}_7 \leq$), diluted hydrochloric acid (5 %, 100 ml) were added to the filtrate prepared from another run and the resulting solution was extracted twice with 100 ml of ether. The ethereal solution was dried over sodium sulfate. After evaporation of ether, carboxylic acids produced were esterified with diazomethane and analyzed with a Shimadzu GC-8APF (CBP-1 capillary column, ϕ 0.50 mm x 25 m) and a Shimadzu QP-2000A GC-MS (CBP-1 capillary column, ϕ 0.25 mm x 25 m).

Hydroliquefaction of Coal

The autoclave (50 ml) charged with 4 g of treated coal particles and deuterium (25 kg/cm^2) was agitated by a rocking motion. The heating regime was as follows: At first the autoclave was heated up to 200 °C at a rate of 12 °C/min. Shaking was started with 43 strokes/min at 200 °C, as the autoclave was further heated to 400 °C at a rate of 8 °C/min, and held at 400 °C for 1 h.

After the reaction, the contents of the autoclave was cooled as quickly as possible by air blow. Gaseous products were recovered in the gas bag, an aliquot of which was injected into a gas chromatograph for quantitative analysis. The contents of the autoclave were washed out into a beaker with a small portion of hexane followed by a small amount of tetrahydrofuran. After the evaporation of these solvents, resulting solid contents were transferred to a Soxhlet thimble and subjected to hexane extraction. The hexane soluble fraction was termed HS. Subsequent extraction with benzene gave a hexane insoluble and benzene soluble fraction (HI/BS). The pyridine soluble fraction of the thimble residue was washed with diluted HCl, deionized water, and then 6N HNO_3 in order to remove the salts.

The HS and HI/BS fractions were separated into 7 fractions (HS1-HS7, HI/BS1-HI/BS7), respectively, according to the improved USBM/API method.

Preparation of Coal Deposited with SnCl_2/KCl

Both SnCl_2 and KCl (3:2 molar ratio) were solubilized in methanol, being kept at 50 °C for 1 h with stirring. After evaporation of methanol from the resulting solution, the uniform mixture of $\text{SnCl}_2/$

KCl was dried at 160 °C under 2 mmHg for 2 h. Deposition of SnCl₂/KCl over coal particles was achieved by adding coal particles to the methanol solution of SnCl₂/KCl, followed by complete removal of methanol by evaporation. The coal with SnCl₂/KCl was dried at 100 °C for 12 h under 2 mmHg.

2.3. Results and Discussion

2.3.1. Structural Studies on Illinois No.6 Coal through Quinoline Extraction

Non-covalent bonding interactions among coal organic materials (COM) are thought to be one of the key factors to affect coal conversion technology.^{1,2} Larsen and Kovac had reported the importance of non-bonding interaction among the coal molecules and proposed the associated coal structure for the first time.³ Nishioka had investigated solvent-induced swelling of Illinois No. 6 coal and concluded that significant portion of the coal molecules are not a three-dimensional network, but are physically associated.⁴ Iino *et al.* had also pointed out that some coal extracts have a strong tendency to associate on the basis of the data from measurement of molecular size distribution by size exclusion chromatography, in which they found that anthracene, 1,1,2,2-tetracyanoethylene, 7,7,8,8-tetracyanoquinodimethane, and lithium bromide could cleave some non-bonding interactions between coal molecules.⁵ These studies seem to suggest the importance of non-bonding interactions among coal molecules.

The purpose of this work is to evaluate non-bonding interaction of coal molecules. I thought that effective solubilization was needed to accomplish this purpose. Several studies to solubilize coal in conventional solvents have been conducted extensively,¹ for example pyrolysis, hydrolysis, liquefaction, reductive alkylation, or depolymerization with superacids. Among these studies, I was interested in the treatment of coal with various solvents at around 350 °C reported by Larsen *et al.*⁶ and Ouchi *et al.*⁷ The treatment could make much amount of organic materials in coal soluble in conventional solvents without considerable change of chemical structure. Consequently, I applied this method to two subbituminous and four bituminous coals to obtain much amount of solvent soluble fraction and investigated its association nature using size exclusion chromatographic and light scattering methods by limiting the extract of Illinois No. 6 coal.

Extraction of Coal with Quinoline

Extraction of two subbituminous and four bituminous coals such as Illinois No. 6 (IL, C 77 wt%, daf), Wandoan (WN, C 78%), Akabira (AK, C 83%), Miike (MK, C 83%), Upper Freeport (UF, C 86%), and Zao Zhuang (ZZ, C 87%), with quinoline was conducted at 350 °C for 1 h under nitrogen pressure (4.9 MPa). This extraction afforded quinoline soluble fractions (QS) in 65-90% yields (Table 2-1) along with various amount of quinoline insoluble materials (QI). Summation of the yield of gas, QS and QI with each run was ranged from 94 wt% (in the lowest case, WN coal) to 99 wt% (in the highest case, AK coal). This suggests that loss of lighter fractions during processing of the products was rather small. Yield of the gaseous products was usually less than 2 wt%, in the case using IL coal, main gaseous products being H₂ (74 wt%), CO₂ (6 wt%), CH₄ (13 wt%), and C₂H₆ (4 wt%) according to GC analysis.

Ouchi *et al.* had also reported that extraction of Akabira coal with quinoline at around 350 °C

afforded a quinoline soluble fraction in 90% yield, however, only half amount of which was soluble in pyridine (about 50 wt% based on daf coal). The results as for solubility test indicated that only the QS from IL coal was completely soluble in pyridine or *N,N*-dimethylformamide, solubility of the QS fractions toward pyridine being also shown in Table 2-1. From this table, amounts of soluble part of QS fractions in pyridine except IL coal

were 36-44 %. The fact that only IL coal extract showed a complete solubilization to pyridine remains uncertain, however, this is probably due to specific structural features of IL coal: Under extraction conditions with IL coal, some retrogressive reactions seem to be prohibited.

The extraction of two Argonne premium coal samples, IL and UF coals, gave QS fraction in relatively high yields, 85 and 90 %, respectively. During extraction of IL coal, I have observed a decreasing yield of extract when used the coal sample being kept under nitrogen atmosphere for a long time after the opening of a sealed ampule. This might suggest that oxidation of IL coal retard extraction by somewhat oxygen participating-crosslinking.

Structural Analysis of IL Coal and Its QS Fraction

Larsen *et al.*⁶ had reported that the treatment of some coals including IL coal with pyridine or phenol at 350 °C resulted in the increase of solubility in pyridine and in the case using solvent system of pyridine and pyridine-d₅ (d₀:d₅=98:0, wt/wt), the considerable extents of H-D scrambling took place. On the basis of these results, they suggested the possibilities of solvent induced bond cleavage in this coal solubilization. On the other hand, Ouchi *et al.*⁷ conducted the pyridine extraction of treated coals (including the pretreatment with quinoline at 350 °C under N₂ pressure) and concluded that the pyridine extracts do not suffer from the thermal decomposition reaction, being the true extracts. The experimental conditions employed in this study seem to be similar to their conditions. Therefore, structural analysis of IL original coal and its extract was conducted by using ¹³C NMR, DR/FT/IR, and Py/GC/MS.

Elemental analyses of IL coal and its QS fraction are summarized in Table 2-2. From this table it was found that content of nitrogen in the QS increased, on the other hand, sulfur content decreased. This suggests that quinoline was incorporated into the extract during processing. As for the sulfur content, Huffman *et al.*, had reported that pyritic sulfur corresponds to 37% of total sulfur in the coal,⁸ thus contents of organic sulfur should be 3.0% (dry base), while sulfur contents of the QS fraction was 2.1 %. These suggest that some sulfur

Table 2-1. Extraction of six coals with quinoline at 350 °C for 1 h.

coal sample (location)	carbon contents (wt%, daf)	Yield		
		Gas	QS ^a (PS) ^b	QI ^c
Illinois No.6 (US)	77	1	85 (85) ^d	10 ^d
Wandoan (Australia)	78	<1	65 (40)	28
Akabira (Japan)	83	1	68 (37)	30
Miike (Japan)	83	<1	69 (36)	27
Upper Freeport (US)	86	1	90 (44)	7
Zao Zhuang (China)	87	1	83 (41)	13

^a Quinoline soluble fraction. ^b Fraction of pyridine soluble materials in QS (daf coal base). ^c Quinoline insoluble fraction.

^d Each experiments were carried out twice and reproducibility of the yield of QS and QI were ±5% and ±2%, respectively.

Table 2-2. Elemental analyses of the original IL coal and its QS fraction.

sample	elemental analysis (wt%, daf)					
	C	H	N	S	H/C	N/C
Original coal ^a	77.1	5.7	1.4	4.8 ^b	0.88	0.016
QS	77.7	5.4	2.1	2.1	0.83	0.023

^a Data from Argonne National Laboratory. ^b Dry base.

containing compounds were removed from the extract during the extraction. The residual sulfur may be concentrated in the QI fraction. I tried to carry out elemental analyses of the QI fraction, but reliable results were not obtained probably because of interference of inorganic matters in it.

Figure 2-1 shows CP/MAS ^{13}C NMR of IL original coal and its QS fraction, both giving similar spectra. These similarities suggest that chemical structures of original coal and QS fraction are very similar to each other. Their distributions of carbon functionalities based on CP/MAS ^{13}C NMR is shown in Table 2-3. Increase in carbon aromaticity (f_a) in the QS agrees well with decrease in H/C atomic ratio of the QS shown in Table 2-2. Major difference between these carbon distributions were observed with the concentration of aromatic carbons bearing alkyl group: %Ar-R in QS fraction is higher than that of the coal. I do not have any clear explanation about above observation (One possibility might be considered in the following: Extracts seem to suffer from degradation. This brings about some changes of peak shape around Ar-R resonance region. Deconvolution process of these peaks might cause some unusual results).

Figure 2-2 shows their diffuse reflectance FT/IR (DR/FT/IR) spectra. It is found that the intensity of the peaks at around 780-810 and 3000-3100 cm^{-1} in the spectrum

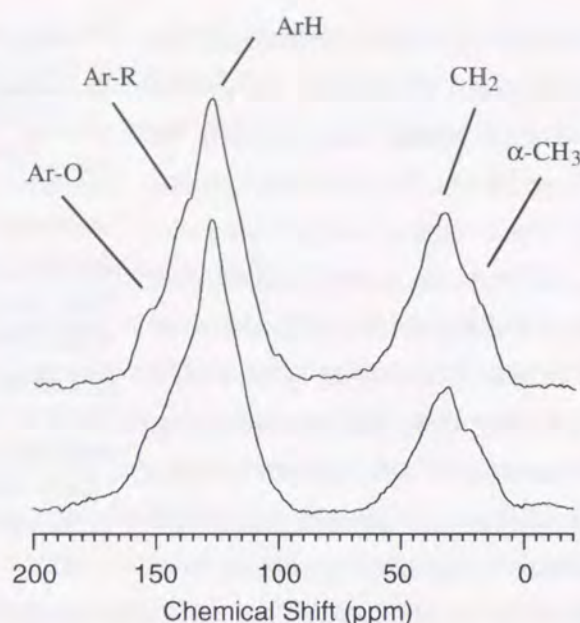


Figure 2-1. CP/MAS ^{13}C NMR for Illinois No. 6 virgin coal (upper) and its QS fraction (lower)

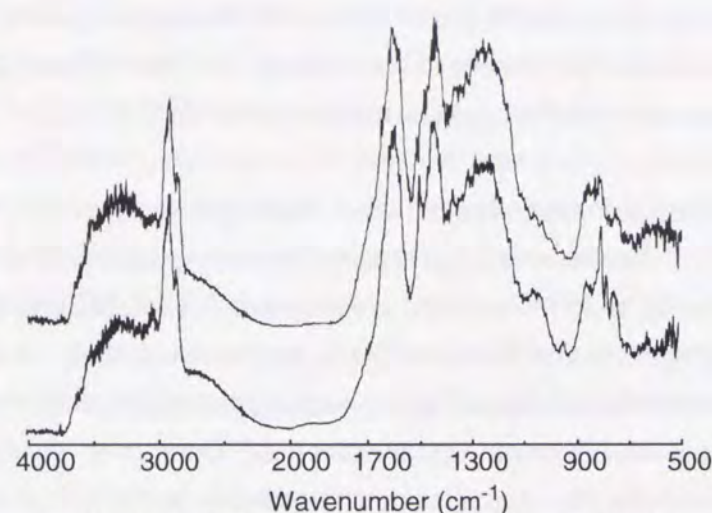


Figure 2-2. DR/FT/IR spectra of Illinois No. 6 virgin coal (upper) and its QS fraction (lower)

Table 2-3. Carbon Distribution of the original Coal and Its QS Fraction^a

sample	f_a	CO_2H	Ar-O	Ar-R	Ar-C,H	Ar-H	OCH_3	CH_2	CH_2	$\alpha\text{-CH}_3$	t- CH_3
Original coal	0.65	0	7	13	31	14	6	11	10	6	2
QS	0.70	1	7	20	28	15	2	8	12	4	3

^a CO_2H ; carbon in carboxyl group, Ar-O; aromatic carbon bearing oxygen atom, Ar-R; aromatic carbon bearing alkyl group, Ar-C,H; aromatic carbon bearing hydrogen atom (including quaternary aromatic carbon), Ar-H; aromatic carbon at ortho-position to substituted hydroxyl or ether group; OCH_3 , methoxy group; CH_2 ; methylene carbon attached to aromatic ring, CH_2 ; aliphatic methylene group, $\alpha\text{-CH}_3$; methyl group attached to aromatic rings, t- CH_3 ; terminal methyl group.

of QS fraction, these corresponding to out-of-plane bend of 2- and 4-neighboring aromatic C-H bonds and aromatic C-H stretching, respectively. These increasing peaks suggest that concentration of hydrogen bearing aromatic carbon in the QS is higher than that in original coal. The peak centered at 1376 cm^{-1} was also found to be increased in the spectrum of the QS, this corresponding to angle bend of methyl groups ($\delta\text{-CH}_3$). These results may indicate that the bond cleavage reaction occurs during extraction to form methyl groups and tertiary aromatic carbons. In order to compare the specimen of the QI fraction from extraction of IL coal with that of the QS, I also measured DR/FT/IR spectrum of the QI after removal of mineral matters by leaching with aqueous HF solution (46 %) at 90 $^\circ\text{C}$ for 7 h. However, reliable spectrum was not obtained because of small amounts of specimen and a lot of ash remained.

Curie-point pyrograms of the original coal and its QS fraction are shown in Figure 2-3, where the amounts of volatile fraction from the coal and QS were 28 and 29 wt%, respectively. These two chromatograms were also similar to each other. Major products from the both samples were derivatives of benzene, phenol, naphthalene, and naphthol. It should be noted that the concentration of β -methylnaphthalene in the latter pyrogram was higher than that of the former. β -Substituted naphthalene is known to give specific peak at 735-760, 805-835, and 835-862 cm^{-1} in IR spectrum,⁹ these peaks being shown in the DR/FT/IR spectrum of the QS fraction. This may indicate that poly-substituted naphthalenes in IL coal were cleaved during the extraction to afford β -substituted naphthalene favorably.

The results obtained in these analyses suggest that bond cleavage reaction occurs during extraction, this seeming to be responsible to solubilization of coal toward quinoline.

Evaluation of Association Structure of IL Coal Extract

In the previous context, I suggested that bond cleavage reaction could occur during extraction, but structure of aromatic cluster in QS fraction seems to be similar to those in the original coal on the basis of the results of Py/GC/MS. Due to the complete solubility of QS fraction in pyridine and DMF, I tried to evaluate the non-covalent bonding interactions between aromatic cluster in IL coal based on the QS fraction.

To evaluate particle size of QS, measurements of its

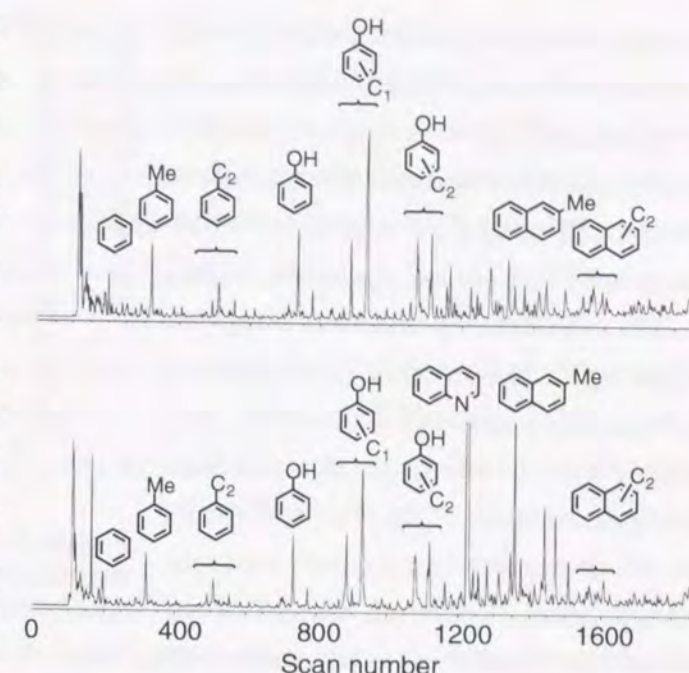


Figure 2-3. Curie-point pyrograms for Illinois No. 6 virgin coal (upper) and its QS fraction (lower) at 670 $^\circ\text{C}$ for 3 s.

Table 2-4. Particle Diameters of Standard Polystyrene Samples Determined by Light Scattering Method.

number average molecular weight (Da)	number average particle diameter (Å)
6.6×10^4	62
1.5×10^5	75
5.2×10^5	202
2.2×10^6	321
3.0×10^6	340

light scattering in DMF solution was conducted, the lowest limit of particle size-measurement of which is 30 Å. Figure 2-4 shows the particle size distribution of QS in DMF (4.4×10^{-2} g/L). The results indicate that QS molecules have particle diameters ranging from 100 to 140 Å, the number average of which was 122 Å. Cody *et al.*¹⁰ had reported that the pyridine soluble fraction of IL coal has 144 Å of number-average particle diameter on the basis of the results of small-angle neutron scattering measurements in pyridine solution. Both results showed a good accordance, however, these values correspond to that of the polystyrene molecules with molecular weight of 4×10^5 according to the relationship between number-average molecular weight and average diameter of polystyrene molecules determined by laser light scattering (Table 2-4). This result strongly suggests that these solvent soluble fractions still have associated structures even in a polar solvent such as DMF or pyridine. Cody *et al.* had also stated the presence of clustering and extended aggregation to be evident in the dilute solutions of pyridine extracts on the basis of their results.

In order to obtain an insight into molecular size distribution of the QS fraction, size exclusion chromatographic analysis was carried out by using DMF as mobile phase. A Shodex KF-80M size exclusion column (polystyrene gel) was used, where the exclusion limit was reported to be about 2×10^7 Da. Resulting molecular size distribution of QS fraction is shown in Figure 2-5, this suggesting that the major peak is located at an area of more than 10^7 Da. The value seems to be much higher than the value determined from light scattering method. Buchanan *et al.* reported that coal extracts and related model compounds are smaller retention volumes than polymer standards of the same molecular weight in their SEC experiments by using pyridine as mobile phase, while calculation of particle diameter from light scattering method contains some assumption. I think that these might be origin of large differences obtained in this study. These larger values of molecular weight for coal extracts are also reported on the basis of the data from size exclusion chromatographic measurement¹¹ and light scattering ones.^{12,13}

In order to reduce the interaction due

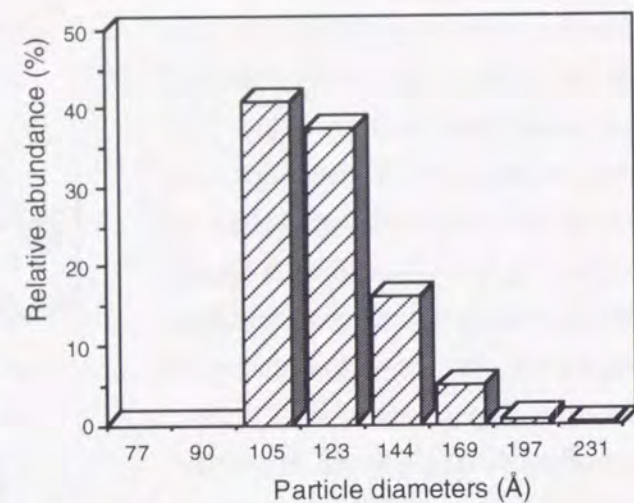


Figure 2-4. Distribution of particle diameters of QS fraction of Illinois No. 6 coal

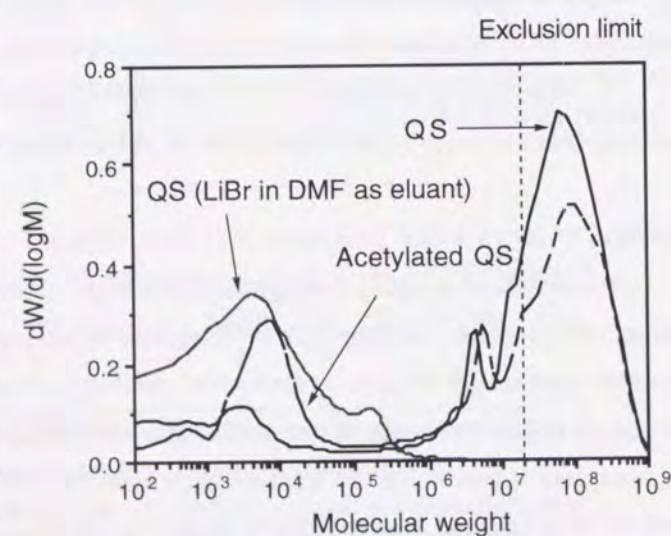


Figure 2-5. Molecular size distribution of QS and acetylated QS determined by size exclusion chromatography

to hydrogen bondings, among the extract the QS was treated with acetic anhydride in refluxing pyridine for 20 h to convert phenolic hydroxyl groups to their acetyl esters. The size exclusion chromatogram of the resulting acetylated QS is also shown in Figure 2-5. In the region around 10^4 Da, a relatively large peak appeared, this suggesting that acetylation could reduce some hydrogen bonding interactions. Surprisingly, addition of LiBr (0.01M) to the mobile phase (DMF) resulted in a complete disappearance of the broad peak at high molecular weight region. This result strongly suggests that QS fraction has a strong tendency to associate each other even in DMF solvent while LiBr in DMF can eliminate intermolecular interactions of these kinds of hydrogen bondings to an extreme extent. In polymer science, this kind of phenomena caused by lithium ion is reported in the case of polyesters or polyamides.¹⁴ These results found in the present paper are expected to play a valuable role in elucidating physical and chemical properties of IL coal.

2.3.2. Ruthenium Ion-Catalyzed Oxidation of Coal

Ruthenium ion catalyzed oxidation (RICO) reaction was introduced to the field of fuel chemistry by Stock *et al.*¹⁵ This reagent is well known to have a property to attack selectively sp^2 carbons in organic substrates: for example, using this reagent arylalkanes and diarylalkanes could be converted to aliphatic monocarboxylic and dicarboxylic acids, respectively. Stock *et al.* employed this technique to analyze an aliphatic portion of COM. According to their results, a distribution of alkyl side chains and polymethylene bridges involved in Illinois No. 6 and Pocahontas No. 3 coals was reported.¹⁵⁻¹⁹ They proposed a plausible chemical structure of Pocahontas No. 3 coal on the basis of the results of RICO reaction along with the average aromatic cluster size determined by dipolar dephasing ^{13}C NMR method.^{20,21} Aliphatic portions of coal,²²⁻²⁴ kerogen,²⁵ maceral concentrates,²⁶ and Athabasca oil sand bitumen^{27,28} were also analyzed using this technique by several researchers.

One of the most problematic points of this reaction is believed to be a difficulty of quantitative analyses of lower carboxylic acids (main products of the reaction of COM) because of their high volatility. Stock *et al.* and Strausz *et al.* had applied the isotope dilution method¹⁶ and esterification with phenacyl bromide²⁷ for this problem, respectively. The former, however, needs preparation of deuterium-labeled carboxylic acids and the latter has problem of conversion rate of the carboxylic acids produced to their phenacyl esters.

In this study, I have investigated the quantitateness and reproducibility of this RICO reaction of coal as an analytical tool for aliphatic parts of COM (aliphatic chains of aromatics and bridge polymethylene between aromatics). The results of RICO reaction of Illinois No. 6 (US subbituminous), Akabira (Japanese bituminous), and Zao Zhuang (Chinese bituminous) coals are reported.

Problems in RICO Reaction of Coal

At first, an analytical potential of ion chromatography was examined to analyze a mixture of lower carboxylic acids prepared from RICO reaction. Figure 2-6 shows ion chromatograms of a model mixture containing succinic, formic, acetic, propionic, butyric, and valeric acids and RICO products of Akabira coal, these suggesting that a peak separation is relatively good and analysis of these carboxylic acids is not disturbed by the presence of I^- and IO_3^- ions contained in the reaction mixture. I also

confirmed the quantitiveness of this analysis using aqueous solution containing these acids in various concentrations (10-50 mg/L).

The following factors affecting the results of RICO reaction were examined; (i) evolution of acetic acid from hydrolysis of MeCN, one component of mixed solvents for RICO, (ii) rate of RICO reaction of COM, and (iii) further decomposition of carboxylic acids produced with $\text{RuCl}_3\text{-NaIO}_4$. As to the first possibility, Strausz *et al.* had pointed out that EtCN should be employed in place of MeCN when analyzing methyl groups attached to aromatic moieties. In fact, a treatment of mixed solvent of MeCN, CCl_4 , and H_2O with $\text{RuCl}_3\text{-NaIO}_4$ at 40 °C for 24 h was found to afford 3.7 mmol of acetic acid along with 1.2 mmol of formic acid by the analysis with ion chromatography. These results suggest that, in this solvent system, reliable yields of carboxylic acids having more than two carbons (propionic acid or higher) could be obtained without interference of C_2 and C_1 acids from MeCN, however, analysis of acetic acid becomes uncertain because of contamination of the decomposition product from the solvent system. Hence, at first I tried $\text{CCl}_4\text{-H}_2\text{O}$ binary solvent system instead of the ternary system, however, effective mixing of this system could not be attained, because MeCN was found to play an important role in this RICO reaction to attain uniform reaction. Subsequently, EtCN was employed instead of MeCN in the way that Strausz *et al.* pointed out. Treatment of a mixture of EtCN, CCl_4 , and H_2O with $\text{RuCl}_3\text{-NaIO}_4$ afforded formic, acetic, propionic, and butyric acids, however, yield of acetic acid from EtCN was a small amount compared with that from MeCN, this suggesting that the use of EtCN is preferable to the use of MeCN for analysis of acetic acid from RICO reaction of coal.

Table 2-5 summarizes the results of treatment of a mixture of lower carboxylic acids with $\text{RuCl}_3\text{-NaIO}_4$ in the two solvent systems (MeCN or EtCN with $\text{CCl}_4\text{-H}_2\text{O}$). In the case of RCN being MeCN, 1.37 mmol excess of acetic acid was observed along with 0.74 mmol of formic acid. On the other hands, in the case using EtCN as RCN, excess amounts of acetic acid observed reduced to 0.77 mmol. On the basis of these results, I decided to use both the solvent system containing EtCN for analysis of acetic acid from α -methyl groups of aromatic moieties and the solvent system containing MeCN for analysis of carboxylic acids with more than two carbons (propionic acid or higher).

RICO reaction of methylarenes as some constituents of coal model compounds was carried out in the solvent system containing EtCN. The reaction of p-cresol and p-methylanisole proceeded almost

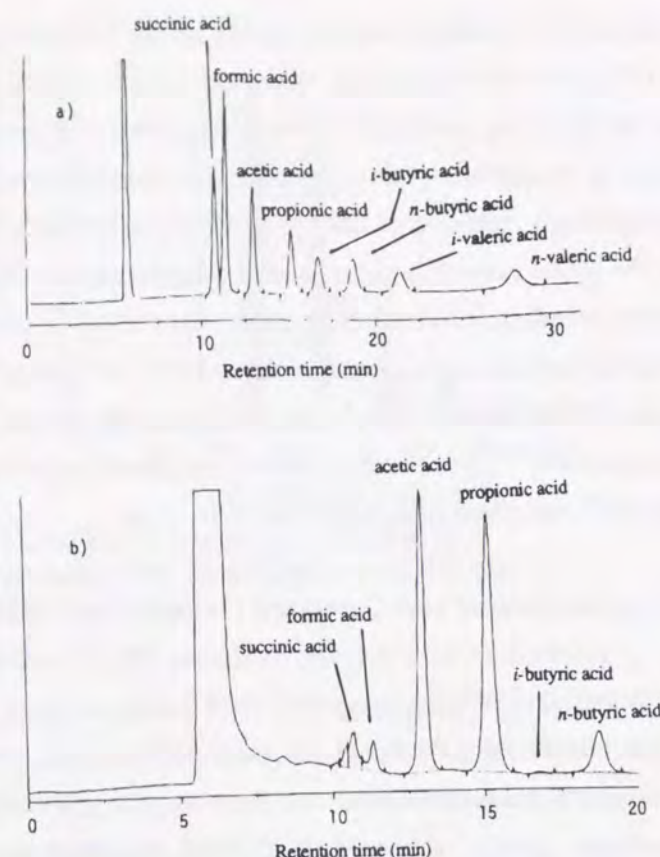


Figure 2-6. Ion chromatograms for model mixture of lower carboxylic acids (a) and the reaction products from the oxidation of Akabira coal (b).

Table 2-5. Treatment of Lower Carboxylic Acids with $\text{RuCl}_3\text{-NaIO}_4$ in $\text{RCN-CCl}_4\text{-H}_2\text{O}$ Mixed Solvent^a

	MeCN			EtCN		
	Amount used (mmol)	Amount observed (mmol) ^b	Difference (mmol)	Amount used (mmol)	Amount observed (mmol) ^b	Difference (mmol)
Formic acid	0.00	0.74	+0.74	0.00	0.08	+0.08
Acetic acid	1.74	3.11	+1.37	0.87	1.64	+0.77
Propionic acid	0.64	0.50	-0.14	0.68	0.92	+0.24
n-Butyric acid	0.49	0.48	-0.01	0.59	1.31	+0.72
n-Valeric acid	0.19	0.16	-0.03	0.50	0.47	-0.03

^a Treatment of carboxylic acids with RuCl_3 (40 mg) and NaIO_4 were carried out in the solvent system containing RCN (20 mL), CCl_4 (20 mL), and H_2O (30 mL) at 40 °C for 24 h.

^b Determined by ion chromatograph.

completely, while production of excess acetic acid (1.1 and 0.6 mmol) was observed. These results suggest that production of acetic acid from hydrolysis of EtCN was 0.85 ± 0.25 mmol, this value showing good agreement with the value in Table 2-5 (0.74 mmol). These results also suggested a reactivity of oxygen containing compounds is relatively high. Since coal usually has these functional groups, it is supposed that the reactivity of coal should be high.

In order to get more precise information about the conversion rate of coal under above reaction conditions, I have carried out the following experiments; after the end of RICO reaction of Akabira coal, the resulting reaction mixture was filtered, the filter cake being washed thoroughly with water and CH_2Cl_2 . All the residue was found to dissolve in water and CH_2Cl_2 , this suggesting that the coal was converted to soluble products almost completely.

Table 2-6. Elemental Analyses and Contents of Aliphatic Carbon for Illinois No. 6, Akabira, and Zao Zhuang Coals

coal sample	elemental analysis (wt%, daf)					aliphatic carbon content (%) ^b
	C	H	N	S+O ^a	H/C	
Illinois No.6 coal	76.6	5.3	1.4	16.7	0.84	37
Akabira coal	82.3	6.2	2.3	9.2	0.90	32
Zao Zhuang coal	86.6	5.1	1.3	7.0	0.71	24

^a By difference. ^b Determined by CP/MAS ^{13}C NMR.

RICO Reaction of Three Coals

Elemental analyses and aliphatic carbon contents of Illinois No. 6, Akabira, and Zao Zhuang coals are summarized in Table 2-6. As described in the experimental section, the ion chromatograph was used for analysis of lower carboxylic acids ($\leq \text{C}_6$) and GC and GC-MS were used for higher carboxylic acids ($\text{C}_7 \leq$) after esterification with diazomethane. Lower carboxylic acids were identified by comparison of their retention time with those of authentic samples. In the case of the analysis of acetic

Table 2-7. Yields of Lower Carboxylic Acids from Oxidation of the Coals with RuO_4

Coal	Yield (mmol/100 mmol C) ^a		
	Zao Zhuang	Akabira	Illinois No. 6
Acetic acid ^b	1.1 ^c	1.6	1.1
Propionic acid	0.56	0.18	0.16
i-Butyric acid	0.015	0.039	0.015
n-Butyric acid	0.046	0.037	0.052
2-Methylbutyric acid	0.017	0.015	0.0099
i-Valeric acid	0.025	0.017	0.011
n-Valeric acid	0.0065	0.0074	0.0041
Succinic acid	0.11	0.11	0.1

^a Determined by ion chromatography. ^b Instead of MeCN, EtCN was used as a co-solvent. ^c The yield of acetic acid was corrected on the basis of the results of oxidation reaction of the coal model compounds.

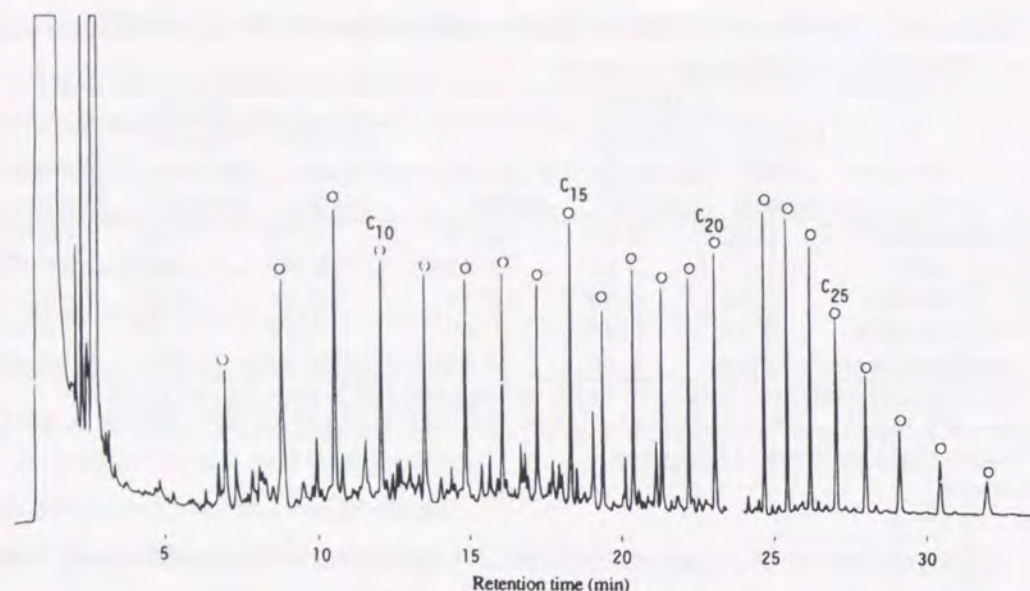


Figure 2-7. Gas chromatogram for carboxylic acid methyl esters (O) from the RICO reaction of Akabira coal.

acid produced, EtCN was used as a co-solvent.

Figure 2-6 shows a gas chromatogram for RICO reaction products of Akabira coal, this indicating that Akabira coal has a wide range of alkyl side chains from C_7 to C_{30} . Yields of lower carboxylic acids obtained from oxidation of the coals were summarized in Table 2-

7. Figure 2-7 shows the plots of yield of whole monocarboxylic acids against carbon numbers. From this figure, it is clear that yields of carboxylic acids decreased monotonically from acetic acid to valeric acid, this suggesting that methyl group is dominant substituents of aromatic moieties. This is parallel with the findings reported so far. As to yields of lower carboxylic acids, three coals showed very similar distribution of carboxylic acids, indicating distributions of aliphatic substitution of aromatic moieties ranging from methyl to butyl groups are very similar to each other. These results showed a good agreement with the results reported by Stock *et al.* On the other hands, yields of higher carboxylic acids are different among three coals: a lower rank coal has longer alkyl side chains attached to aromatic moieties than those of higher rank coal.

Yield of succinic acid, which derived from dimethylene bridges between two aromatic moieties, is almost 0.1 mmol per 100 mmol of carbons in COM. As to Akabira coal, the presence of higher aliphatic dicarboxylic acids could be detected according to the experiments (Figure 2-9), however, quantitative information about their yields could not be obtained because of their poor abundance in the RICO products. Although malonic acid, which might be derived from methylene bridges, was

Table 2-8. Carbon distribution of Illinois No. 6, Akabira and Zao Zhuang coals^a

	aromatic carbons (%)	aliphatic carbons (%)				
		CH ₃ O	CH ₂ ¹	CH ₂	α -CH ₃	t-CH ₃
Illinois No. 6	63	5	10	12	6	4
Akabira	68	4	4	13	8	3
Zao Zhuang	76	4	7	4	6	3

^a Determined by CP/MAS ^{13}C NMR followed by a curve deconvolution method. ^b OCH₃, methoxy group; CH₂¹, ring-joining methylene group, CH₂; aliphatic methylene group, α -CH₃; methyl group attached to aromatic rings, t-CH₃; terminal methyl group.

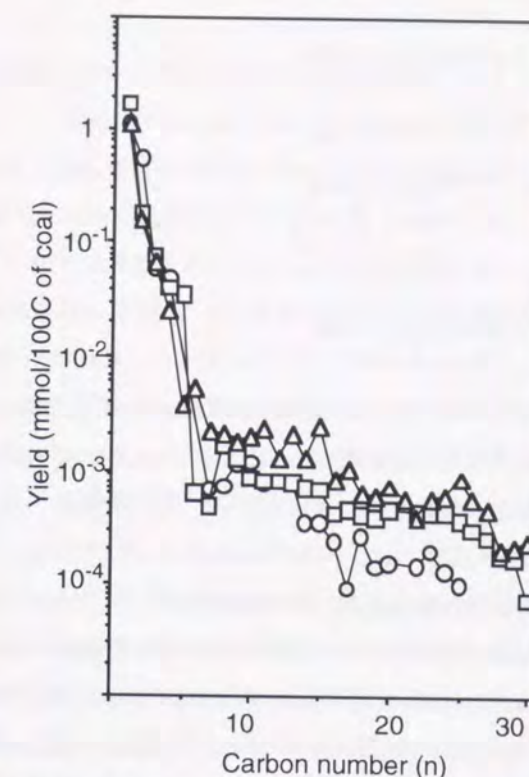


Figure 2-8. Yield of carboxylic acids, $C_nH_{2n+1}CO_2H$, from the oxidation reaction of Illinois No. 6 (Δ), Akabira (\square), and Zao Zhuang coals (\circ)

found to be unstable under these reaction conditions. The presence of methylene bridges is estimated by the measurements of CP/MAS ^{13}C NMR (Table 2-8). These results indicate that the main aliphatic linkages between two aromatic moieties in COM are mono- and dimethylene bridges. This kind of information seems to be very valuable when I estimate chemical structure of coal and develop more advanced utilization technology of coal.

Evaluation of RICO Reaction as an Analytical Tool for an Aliphatic Portion of COM

The total amounts of carbons detected in this oxidation reaction were 2.3 % for Illinois No. 6 coal, 2.9 % for Akabira coal, and 2.9 % for Zao Zhuang coal based on the total carbons in COM. These values were significantly smaller than those detected by ^{13}C NMR (37 % for Illinois No. 6 coal, 32 % for Akabira coal, and 24 % for Zao Zhuang coal, Table 2-6). Especially, yields of acetic acid (1.1~1.6 % based on the total carbons in COM) are considerably lower than the concentration of α -methyl groups determined by ^{13}C NMR (6~8 %). This is attributed to a limitation of this RICO reaction: for example, RuO_4 can oxidize β -methylnaphthalene to afford phthalic and acetic acids almost quantitatively according to the eq. 1, while, α -methylnaphthalene can give a mixture of phthalic, 3-methylphthalic, and acetic acids (eq. 2). According to the pyrogram of extracts from Illinois No. 6, Akabira, and Zao Zhuang coals α -methylnaphthalene could be observed along with β -methylnaphthalene. These α -methylnaphthalene derivatives could not be converted to quantitative amounts of acetic acid by RICO reaction based on above equation. Presence of methylated phthalic acid esters in Figure 2-9 also supports this explanation.

Since this RICO reaction has such limitation as described above, a detailed and complete

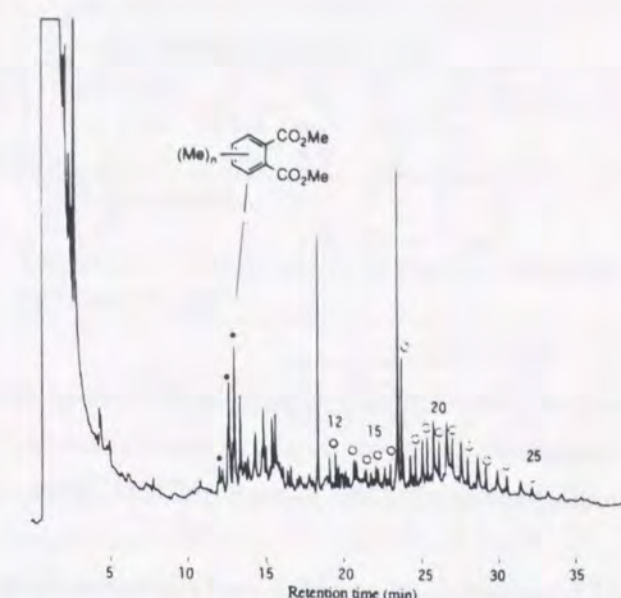
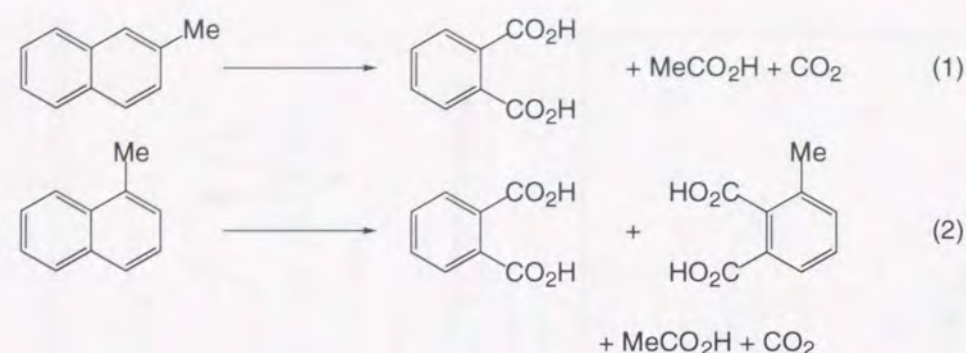


Figure 2-9. Gas chromatogram for dicarboxylic acid dimethyl esters (\circ) and alkyl-substituted phthalic acid dimethyl esters (\bullet) from the RICO reaction of Akabira coal.



information about all parts of aliphatic functional groups in COM can be hardly obtained only based on this reaction. However, I believe that the results of this RICO reaction can afford us more reliable information about aliphatic portion of COM by the combination use with solid state ^{13}C NMR.

2.3.3. Liquefaction of Akabira coal catalyzed by molten salts under D_2 atmosphere

Studies on coal liquefaction catalyzed by molten salts have been undertaken by many coal chemists. Zielke *et al.*²⁹⁻³¹ concentrated much attention on the development of a coal liquefaction process using massive amounts of molten salts with much stress on the use of ZnCl_2 . Berg *et al.*³² indicated the preferable characteristics of ZnCl_2/KCl melts over ZnCl_2 for coal liquefaction. Bell *et al.*³³⁻³⁶ have published several papers concerning kinetic aspects of molten salt-catalyzed liquefaction of coal. Nomura *et al.* have published a wide range of papers³⁷⁻⁴² on this topic of coal liquefaction in the presence of molten salts media.

The aim of this study is to carry out coal liquefaction experiments in the presence of massive amounts of molten salts under a deuterium atmosphere and to obtain a detailed analyses of the degree and the distribution of deuterium uptake of the products so as to derive closer understanding of coal liquefaction chemistry and coal structure.

Hydroliquefaction of Akabira Coal

Table 2-9 lists the hydroliquefaction of Akabira coal in the presence of molten salts under H_2 or D_2 atmospheres. Since D uptake in liquefied products is considered very informative in evaluating coal structure and the liquefaction mechanisms of coal organic materials, liquefaction under a H_2 atmosphere was also carried out to provide supportive analytical data. The yields of gaseous products were estimated according to the results of liquefaction under H_2 atmosphere. Table 2-8 indicates that conversion ranges from 89 to 98 % were achieved. Under these reaction conditions, gaseous products were as follows; (under H_2) methane 26 %, ethane 16 %, propane 19 %, *n*-butane 9 %, *i*-butane 9 %, CO_2 21 %; (under D_2) methane 22 %, ethane 17 %, propane 17 %, *n*-butane 8 %, *i*-butane 8 %, CO_2 28 %.

Table 2-9. Results of hydroliquefaction of Akabira coal (wt%, daf)

Atmosphere	Gas	HS	HI/BS	BI/PS	Conversion
H_2	13	20	16	49	98
D_2	13	23	18	35	89

Characterization of HS and HI/BS

Elemental analyses of HS and HI/BS fractions are listed in Table 2-9. Due to the incorporation of D atoms into liquefied products, products under D_2 atmosphere were not submitted for elemental analysis. Table 2-10 suggests that the H/C atomic ratio of HS is 1.21 while that of HI/BS is 0.95. These fractions were submitted to Curie-point pyrolysis. Volatile matter of HS (H_2) and HS (D_2) were 64 % (H_2) and 63 % (D_2) respectively, tar matter and coke being 25 % (H_2) and 23 % (D_2), 11 % (H_2) and 14 % (D_2) respectively.

Since volatile matter is the fraction injected into the gas chromatograph, about 2/3 of the mass of these samples could be analyzed instrumentally. However, in the case of the HI/BS fraction, volatiles were only 35 % (H_2 , D_2), tar being 29 % (H_2) and 21 % (D_2), and coke being 36 % (H_2) and 44 % (D_2).

This higher tendency of the HI/BS fraction to form coke during pyrolysis can be understood due to its high contents of heteroatoms like nitrogen, sulfur and oxygen, and its lower H/C value. The lower H/C value suggests the HI/BS fraction is more aromatic, and the degree of condensation of aromatic compounds should be higher than the HS fraction.

Table 2-11 shows the distribution of seven fractions of HS. From this table, HS1 to HS3 contains about 90 % of the whole sample. The distribution of the HI/BS fraction also indicates that the HI/BS4 to HI/BS7 fractions account for almost 80 % of the injected product.

Structural Features of HS1 Fraction

The FD/MS spectrum of HS1 (H_2) is shown in Figure 2-10a along with that of HS1 (D_2) (Figure 2-10b). Clear peaks appearing at regular interval of m/z 14 are considered to be alkanes of $\text{C}_n\text{H}_{2n+2}$ while these peaks disappear in the FD/MS of HS1 (D_2). These findings suggest that deuterium atoms are incorporated into alkane derivatives. The HS1 fraction is evaluated as a saturate fraction by referring to the definition of the improved

Table 2-10. Elemental analysis of HS and HI/BS fraction (wt%)

fraction	C	H	N	S	O (diff.)	H/C ^a
HS	86.3	8.7	0.9	0.2	3.9	1.21
HI/BS	85	6.7	1.3	1.2	5.8	0.95

^a Atomic ratio.

Table 3-11. Distribution of seven fractions of HS and HI/BS

atmosphere	fraction (wt%)						
	1	2	3	4	5	6	7
HS	H_2	34	17	34	4	2	7
	D_2	32	19	35	2	1	9
HI/BS	H_2	2	8	7	20	9	29
	D_2	2	8	8	17	11	29

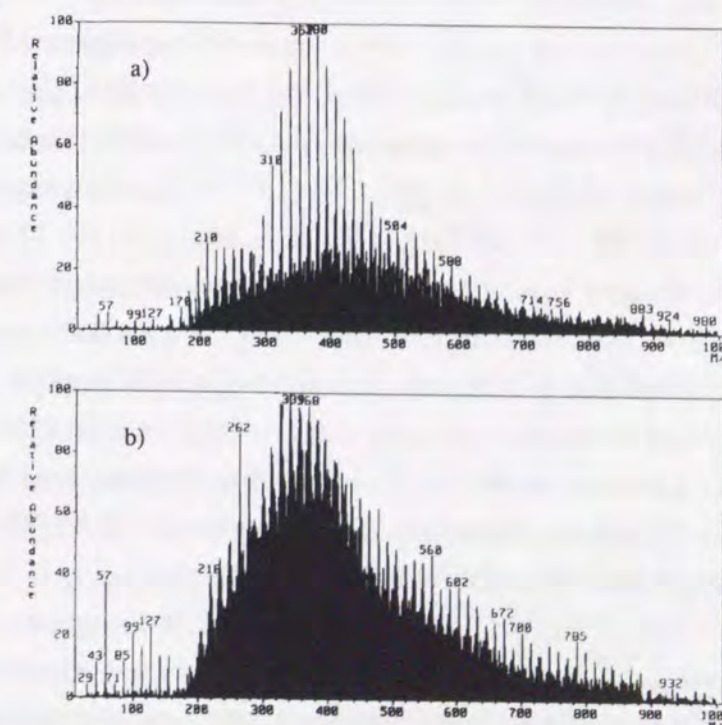


Figure 2-10. FD/MS spectra of HS1 from the liquefaction product under H_2 (a) and D_2 (b).

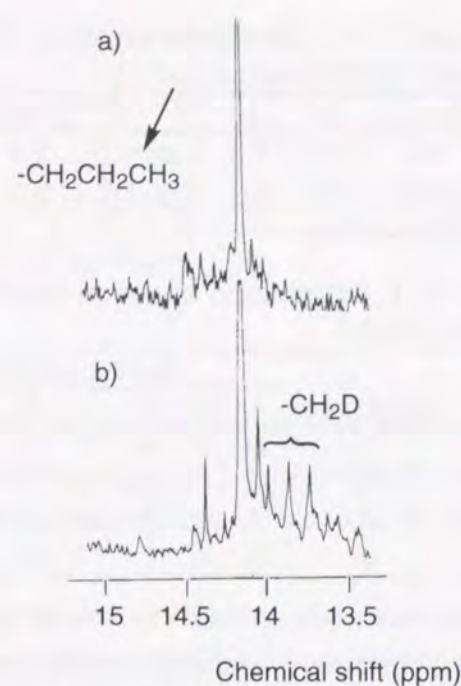


Figure 2-11. ^{13}C NMR spectra of HS1 fraction from the liquefaction product under H_2 (a) and D_2 (b).

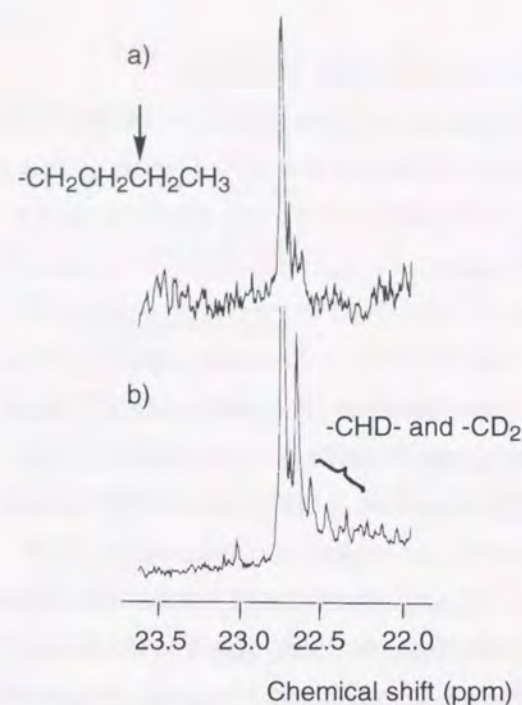


Figure 2-12. ^{13}C NMR spectra of HS1 fraction from liquefaction under H_2 (a) and D_2 (b).

USBM/API method. However, the H/C ratio of HS1 (H_2) was found to be 1.45, which suggests contamination with small amounts of aromatic compounds. GC/MS analysis of HS1 (H_2) indicated the presence of alkylbenzene, alkyl-naphthalene and tetralin derivatives. As for the separation of a saturate fraction from HS according to the improved USBM/API method, our separation was found not to be sufficient. I will discuss this point later.

Coal derived liquid is very complicated as suggested by the appearance of its FD/MS spectra so the ^1H and ^2H NMR spectra of these two fractions [HS1 (H_2) and HS1 (D_2)] were measured. According to the Brown-Ladner assignments, the distribution of four protons; Har (9.00-6.00 ppm), H α (5.00-2.00 ppm), H β (2.00-1.05 ppm), H γ (1.05-0.20 ppm) were estimated: HS1 (H_2) Har 16 %; H α 27 %; H β 43 %; H γ 14 %; HS1 (D_2) Har 25 %; H α 36 %; H β 30 %; H γ 9 %. These values are only relative ratios because I could not quantify the exact amount of deuterium incorporated in the HS1 fraction. However, the comparison of these values reveals the very interesting features of the resulting HS1 fraction: in that D atoms are incorporated into Har and H α preferentially. These tendencies are very important to our interpretation of the mechanism of incorporation of deuterium atoms.

Complete separation of saturate from HS was made by fractionating 50 mL of pentane elute in place of 250 mL of pentane. The measurement of ^2H -NMR of the resulting fraction indicates the disappearance of peaks around 9.00-2.00 ppm.

Partial regions (15-13.5 ppm) of ^{13}C NMR spectra of HS1 (H_2) and HS1 (D_2) are shown in Figure 2-11. In Figure 2-11b, I can observe clear triplet due to the presence of $-\text{CH}_2\text{D}$ while this spectra cannot be observed in Figure 2-11a. Another partial regions (23.5-22 ppm) of ^{13}C NMR spectra of HS1 (H_2) and HS1 (D_2) are indicated in Figure 2-12. The presence of $-\text{CHD}-$ and $-\text{CD}_2-$ is strongly

suggested by the appearance of peaks around 22.5 ppm in Figure 2-12b. From these considerations, deuterium atoms incorporated in alkane fraction exist at terminal methyl and methylene adjacent to terminal methyl group.

Straight chain alkane is known to show the strongest peak at m/z 57 in its mass spectrum. As expected, the GC/MS of HS (H_2) fraction shows the mass spectra of many alkane derivatives that have peaks at m/z 57 of C_4H_9^+ with a small isotope peak of m/z 58. However, each alkane of HS1 (D_2) shows C_4^+ fragments with m/z 57, 58, 59 and 60 (minor), this indicating each fragment contains from zero to three deuterium atoms. However, relative intensity of the peak with m/z 60 is negligible, so being omitted. Table 2-12 lists isotope distributions of alkanes in HS1 (D_2). The degree of deuterium incorporation decreases as the number of carbon atoms in alkane increases. This suggests that the shorter the alkane chain, the greater the probability of alkane existing as an alkyl chain or an alkylene bridge of aromatics.

Structural Features of HS2 and HS3 Fractions

The FD/MS spectra of the HS2 and HS3 fractions give number-average molecular weights of *ca* 461 and *ca* 509 respectively. The presence of distinct peaks appearing at a regular interval of m/z 14 on FD/MS spectra of HS2 (H_2) suggests that various kinds of alkylated aromatic compounds are contained. These features are also observed in the FD/MS spectra of HS3 (H_2).

Figure 2-13 shows the mass spectra of specific products obtained from Curie-point pyrolysis of HS3 (H_2) and HS3 (D_2). The xylene spectra of HS3 (H_2) and HS3 (D_2) are compared in Figure 2-13A. The similar comparison of dimethylphenol is shown in Figure 2-13B. In the case of xylene, its molecular ion from HS3 (D_2) is higher by 4 mass units than that from HS3 (H_2), while the $(\text{M} - \text{CH}_3)^+$ fragment ion from HS3 (D_2) is higher by 3 mass units than that from HS3 (H_2). Therefore one deuterium atom is believed to be incorporated in a methyl group of xylene from HS3 (D_2). Also in the case of

Table 2-12. Distribution of isotope in C_4^+ fragment of alkanes (mol ratio)

alkanes	C_4H_9^+	$\text{C}_4\text{H}_8\text{D}^+$	$\text{C}_4\text{H}_7\text{D}_2^+$
C12	65	22	13
C13	68	20	12
C14	61	22	17
C15	70	20	10
C16	58	27	15
C17	70	20	10
C18	73	19	8
C19	72	20	8
C20	77	18	5
C21	72	21	7
C22	81	15	4
C23	75	19	6
C24	79	17	4
C25	78	17	5
C26	79	16	5
C27	78	17	5
C28	80	16	4
C29	80	16	4

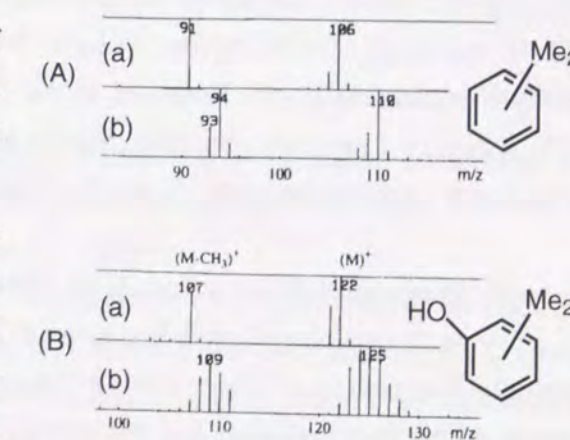


Figure 2-13. (A) Mass spectra of xylene from the Curie-point pyrolysis of HS3 fraction from the liquefaction product under H_2 (a) and D_2 (b). (B) Mass spectra of dimethylphenol from the Curie-point pyrolysis of HS3 fraction from the liquefaction product under H_2 (a) and D_2 (b).

Table 2-13. Average distribution of proton and deuterium in HS2 and HS3 fractions.

	atmosphere	Har	H α	H β	H γ
HS2	H ₂	30	39	24	7
	D ₂	37	44	16	3
HS3	H ₂	23	34	30	13
	D ₂	32	41	22	5

dimethylphenol, the molecular ion from HS3 (D₂) is higher by 3 mass units compared with that from HS3 (H₂). On the other hand, the (M - CH₃)⁺ fragment ion is higher by 2 mass units than that from HS3 (H₂). Therefore one deuterium atom is surely incorporated in each methyl group of dimethylphenol.

The average proton distributions in HS2 (H₂) and HS3 (H₂) and deuterium distributions in HS2 (D₂) and HS3 (D₂) were estimated according to their ¹H and ²H NMR spectra respectively. These results are listed in Table 2-13. From Table 2-13, it is clear that deuterium atoms are preferentially incorporated into aromatic nuclei and aliphatic carbons adjacent to aromatic compounds. These findings were also observed in the aromatic compounds of HS1 fraction. As for the preferential incorporation of deuterium atoms at α -carbon sites of aromatic compounds, I have obtained additional information; Figure 2-14 shows the region attributed to α -methyl groups in ¹³C-NMR spectra of HS2 (H₂) and HS2 (D₂). Peaks observed at 21.3, 19.9 and 19.5 ppm are indicative of α -methyl of aromatic compounds like the methyl of α -methyl-naphthalene (21.6), the methyl of toluene (21.4), the methyl of *m*-xylene (21.3), the methyl of *o*-xylene (19.7) and the methyl of α -methylphenanthrene (19.9). However, in the ¹³C-NMR spectra of HS2 (D₂), two broad peaks centered at 21.4 and 19.7 ppm are observed. Such a broadening of α -methyl peaks is considered due to the presence of coupling between ¹³C and D which is inserted into α -methyl groups.

Possible Mechanism of Deuterium Atom Uptake of Aromatic and Aliphatic Compounds

Nomura *et al.* have published several papers on coal liquefaction in the presence of massive amounts of molten salts. Their results indicated molten salts act as a dispersant of intermediate species from coal organic materials and the catalytic material. They proposed that both ionic and radical mechanism contribute to liquefaction in Lewis acid type molten salt like SnCl₂/KCl and ZnCl₂/KCl. The findings in this study that deuterium atoms are incorporated into aromatic and aliphatic compounds can be explained in this context.

Scheme 2-1 shows the possible ionic reactions for incorporation of D atoms; reaction a) indicates that D⁺ attacks the *ipso*-position of aromatic compounds, resulting in the formation of deuterium substituted aromatics and deuterium substituted methyl group linking aromatic compounds. From the

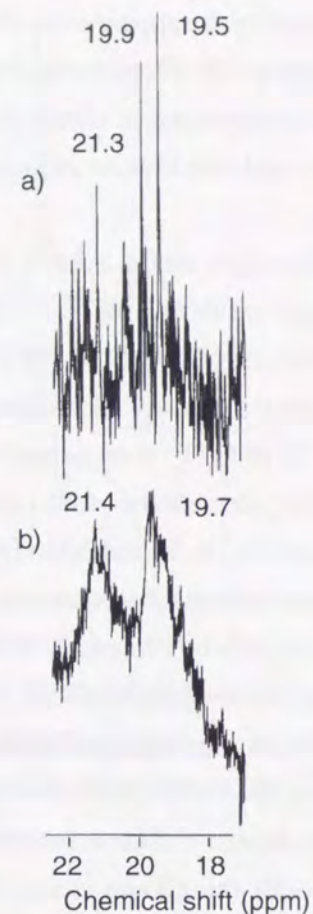
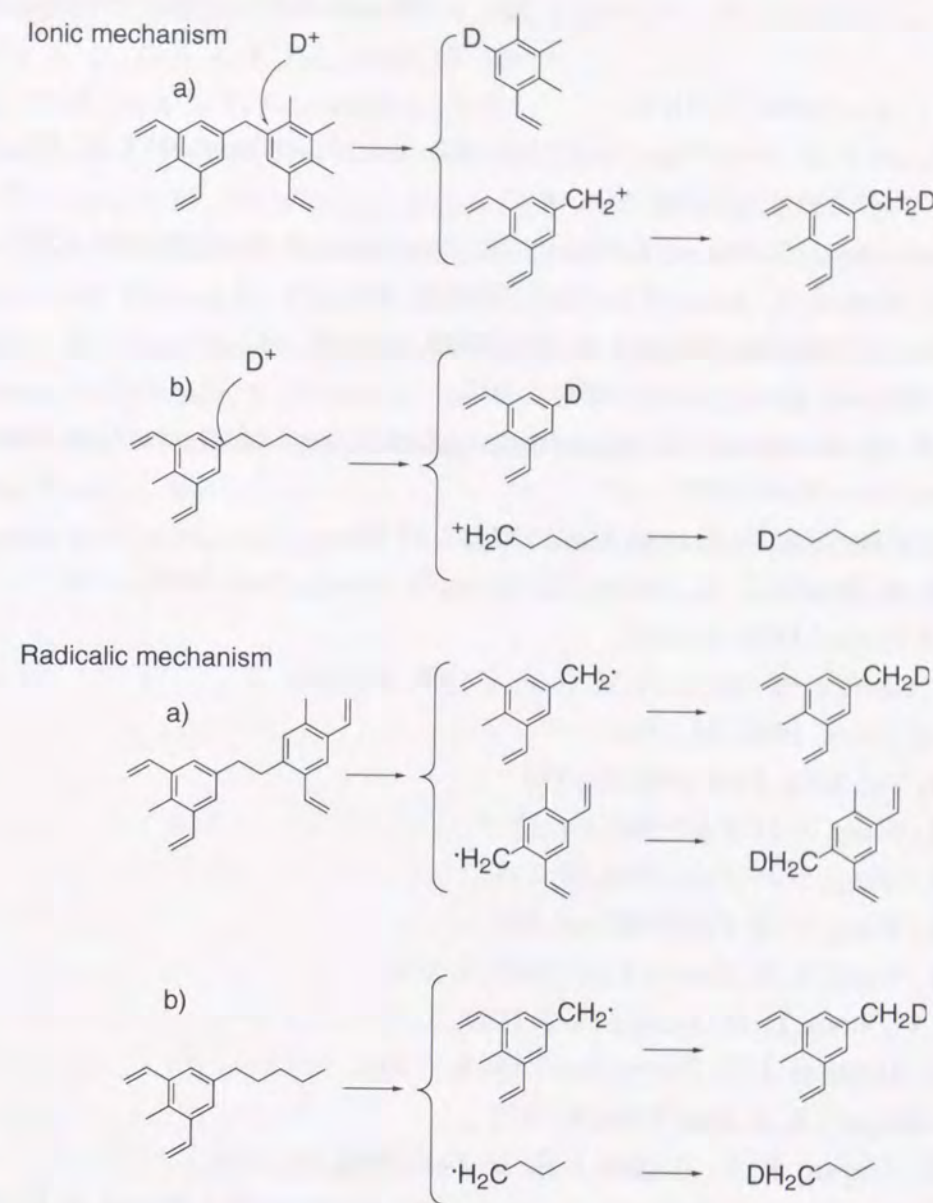


Figure 2-14. ¹³C NMR spectra of HS2 fraction from the liquefaction product under H₂ (a) and D₂ (b).

Scheme 2-1.



previous results,⁴³ I have shown that the methylene bridges connecting two aromatic compounds is very common in coal organic materials. Reaction *b* also explains the way that deuterium substituted aromatic and deuterium substituted aliphatic compounds are formed.

Scheme 2-1 also indicates the radical mechanism of incorporation of deuterium atoms. In reaction *a*) homolytic fission of 1,2-diarylethane yields two benzyl radicals. These radicals abstract D atom from D₂ dissolved in melts. In reaction *b*) alkyl substituted aromatics yields benzyl type radical and alkyl radical. These two radicals abstract D atom in the way similar to reaction *a* in Scheme 2-1. The alkyl radical undergoes the disproportionation reaction to yield olefin and alkane. Olefin then takes up D₂ to form two deuterium atoms containing alkane by addition reaction.

2-4 References

- 1 Gorbaty, M. L.; Larsen, J. W.; Wender, I. Eds. "Coal Science", Chapter 4, Academic Press 1982.
- 2 Gorbaty, M. L. *Fuel* **1994**, 73, 1819.
- 3 Kovac, J.; Larsen, J. W. *Prep. Pap.- Am. Chem. Soc. Div. Fuel Chem.* **1977**, 22, 181
- 4 Nishioka, M. *Fuel*, **1993** 72, 1719.
- 5 Iino, M.; Takanohashi, T.; Obara, S.; Tsueta, H.; Sanokawa, Y. *Fuel* **1989**, 68, 1588.
- 6 Larsen, J. W.; Yurum, Y.; Sams, T. L. *Fuel* **1983**, 62, 476.
- 7 Ouchi, K.; Itoh, S.; Makabe, M.; Itoh, H. *Fuel* **1989**, 68, 735.
- 8 Huffman, G. P. et al., *Energy Fuels* **1992**, 6, 293.
- 9 Silverstein, R. M.; Bassler, G. C. Spectrometric Identification of Organic Compounds, John Wiley & Sons, New York 1967.
- 10 Cody, G. D.; Winans, R. E.; *Energy Fuels* **1994**, 8, 1370.
- 11 Buchanan, D. H.; Warfer, L. C.; Bailey, S.; Lucas, D. *Energy Fuels* **1988**, 2, 32.
- 12 Hombach, H.-P. *Fuel* **1981**, 60, 663.
- 13 Olson, E. S.; Diehl, J. W.; Froelich, M. L. *Fuel* **1987**, 66, 992.
- 14 Mori, S. *Anal. Chem.* **1983**, 55, 2414.
- 15 Stock, L. M.; Tse, K.-T. *Fuel* **1983**, 62, 974.
- 16 Stock, L. M.; Wang, S.-H. *Fuel* **1985**, 64, 1713.
- 17 Stock, L. M.; Wang, S.-H. *Fuel* **1986**, 65, 1552.
- 18 Stock, L. M.; Wang, S.-H. *Fuel* **1987**, 66, 921.
- 19 Stock, L. M.; Wang, S.-H. *Energy Fuels* **1989**, 3, 533.
- 20 Muntean, J. V.; Stock, L. M. *Energy Fuels* **1991**, 5, 767.
- 21 Stock, L. M.; Muntean, J. V. *Energy Fuels* **1993**, 7, 704.
- 22 Mallya, N.; Zingaro, R. A. *Fuel* **1984**, 63, 423.
- 23 Ilsley, W. H.; Zingaro, R. A.; Zoeller, J. H., Jr. *Fuel* **1986**, 65, 1216.
- 24 Standen, G.; Boucher, R. J.; Eglinton, G.; Hansen, G.; Eglinton, T. I.; Larter, S. R. *Fuel* **1992**, 71, 31.
- 25 Boucher, R. J.; Standen, G.; Eglinton, G.; *Fuel*, **1991**, 70, 695.
- 26 Blanc, P.; Valisolalao, J.; Albrecht, P.; Kohut, J. P.; Muller, J. F.; Duchene, J. M. *Energy Fuels* **1991**, 5, 875.
- 27 Mojelsky, T. W.; Ignasiak, T. M.; Frakman, Z.; McIntyre, D. D.; Lown, E. M.; Montgomery, D. S.; Strausz, O. P. *Energy Fuels* **1992**, 6, 83.
- 28 Strausz, O. P.; Mojelsky, T. W.; Lown, E. M. *Fuel* **1992**, 71, 1355.
- 29 Zielke, C. W.; Struck, R. T.; Evans, J. M.; Costanza, C. P.; Gorin, E. *Ind Eng. Chem. Process Des. Dev.* **1966**, 5, 158.
- 30 Struck, R. T.; Clark, W. E.; Dudt, P. J.; Rosenhoover, W. A.; Zielke, C. W.; Gorin, E. *Ind. Eng. Chem. Process Des. Dev.* **1969**, 8, 546.
- 31 Zielke, C. W.; Klunder, E. B.; Maskew, J. T.; Struck, R. T. *Ind. Eng. Chem. Process Des. Dev.* **1980**, 19, 85.
- 32 Berg, L.; Malsam, J. S. US Patent **1973**, 3,746,250.
- 33 Mobley, D. P.; Bell, A. T. *Fuel* **1979**, 58, 661.
- 34 Taylor, N. D.; Bell, A. T. *Fuel* **1980**, 59, 499.
- 35 Salim, S. S.; Bell, A. T. *Fuel* **1982**, 61, 745.
- 36 Frederick, T. J.; Bell, A. T. *J. Catal.* **1984**, 87, 226.
- 37 Ida, T.; Nomura, M.; Nakatsuji, Y.; Kikkawa, S. *Fuel* **1979**, 58, 361.
- 38 Nomura, M.; Miyake, M.; Sakashita, H.; Kikkawa, S. *Fuel* **1982**, 61, 18.
- 39 Nomura, M.; Kimura, K.; Kikkawa, S. *Fuel* **1982**, 61, 1119.
- 40 Nomura, M.; Sakashita, H.; Miyake, M.; Kikkawa, S. *Fuel* **1983**, 62, 73.
- 41 Nomura, M.; Yoshida, T.; Morita, Z. *Ind. Eng. Chem. Product Res. Dev.* **1984**, 23, 215.
- 42 Nomura, M.; Kawakami, H.; Kawakami, Y. Advances in Coal Chemistry, 1988, University of patras, Patras, p. 287.
- 43 Nomura, M.; Yhuzu, S.; Fujimoto, T.; Ida, T.; Miyake, M. *Fuel* **1990**, 69, 972.

Chapter 3. Construction of Chemical Structure Model for Chinese Bituminous Zao Zhuang Coal

3.1. Introduction

Due to the complicity of coal organic materials, a number of model structures published so far have been based on the concept of average molecular structure.¹⁻⁴ Based on these models, Spiro figured out the pathway that coke was produced during carbonization.⁵ Shinn proposed a model structure of Illinois No. 6 coal based on relatively detailed information about its average structural parameters.⁴ Liquefaction process has been explained at the level of molecule by several researchers with referring to his model; however, it is true for the most of chemists, who engage in pyrolytic study of coal, that these average structures could not explain the distribution of products obtained from pyrolytic data of coal organic materials and their extracts. The reason is that these model structures are constructed only based on average structural parameters: In more true sense, these average model structures of coal can not reflect any substantial aspects of real coal structure.

Through extensive studies on pyrolysis of coal, its extract, and coal model compounds, I have begun to try construction of coal model structure based on the pyrolytic data coupled with a nondestructive analytical method like solid state ¹³C NMR.⁶ However, pyrolysis accompanies formation of a considerable amount of coke. If one can not analyze the constituents of coke, he can evaluate coal organic materials only by referring to its pyrogram. In the previous paper,⁶ by assuming that volatile fraction from the pyrolysis of coal represents whole coal, we have constructed a model structure for Akabira coal, of course, by referring to the distribution of different kinds of carbon containing in coal organic materials deduced from ¹³C NMR. We are beginning to feel that we have to examine above assumption, because we have encountered the example where we could construct no reasonable model for a Japanese caking coal (Miike coal) according to our proposed method.^{7,8}

In a preliminary study, I have investigated the chemical structure of Chinese bituminous Zao Zhuang coal by means of Curie-point pyrolysis and solid state ¹³C NMR, having found a kind of disagreement between pyrolytic and NMR data.⁹ This means that volatile components from the pyrolysis can not reflect the constituents of the whole coal. Therefore, we applied ether bond cleavage reaction with SiCl₄-NaI reagent for the coal in order to get more volatile products by pyrolysis. The aim of this study is to construct a chemical structure model for this coal on the basis of the pyrolytic data of chemically transformed fractions by the above reaction along with the data from CP/MAS ¹³C NMR and CP/MAS/DD ¹³C NMR analyses.

3.2. EXPERIMENTAL

Samples, Reagents, and Instruments

All the reagents were commercially available and used without further purification. Solvents (methylene dichloride and acetonitrile) for the ether bond cleavage reaction were purified by conventional distillation methods. CP/MAS ¹³C NMR measurements of Zao Zhuang coal were conducted with JEOL GSH20MU (50 MHz) with high speed MAS (12 kHz). Curve fitting was carried

out by using commercial program on an NEC PC-9801 personal computer. FT/IR spectra were recorded on a JEOL JIR-AQ-20M spectrophotometer.

Preparation of Solvent Refined Coal (SRC) from Zao Zhuang Coal

Pulverized coal (under 100 mesh, 5 g) was placed with 10 mL of tetralin in a 50 mL stainless steel autoclave (SUS316), then nitrogen being charged up to 20 kg/cm². This autoclave was heated up to 440 °C at a heating rate of 8K/s, being kept at this temperature for 5 min. After the end of the reaction, the apparatus was cooled to room temperature. The gaseous products were collected, aliquot of which was submitted to Shimadzu GC-3BT and GC-8A gas chromatographs. After that, the products remained in the autoclave was recovered by washing the inside of the autoclave with pyridine, then the product being separated into hexane soluble (HS), hexane insoluble/benzene soluble (HI/BS), benzene insoluble/pyridine soluble (BI/PS), and pyridine insoluble (PI) by Soxhlet extraction. These yields were 11, 7, 51, and 18 %, respectively.

Pyrolysis of Coal Extracts

About 1 mg of extract was placed on a pyrofoil. This sample was heated up to 670 °C within 0.3 s under a nitrogen stream, being kept for 2.7 s at this temperature, using a Curie-point pyrolyzer of Japan Analytical Industries. A volatile fraction evolved was inserted into a Shimadzu GC-14BPFsc gas chromatograph connected to the pyrolyzer, where many different kinds of constituents

of extract were eluted. On the basis of measurement of their mass spectra, each constituent was identified. Details concerning the procedure and the apparatus were described in the former section.¹⁰ Pyrolytic results of SRC fractions were cited in Table 3-1.

Table 3-1. Yield of volatile, tar, and coke fractions from pyrolysis of SRC of Zao Zhuang coal.

sample	volatile	tar	coke
SRC-HS	36	47	17
SRC-HI/BS	36	16	48
SRC-BI/PS	23	20	57
Residue(PI)	11	0	89

Pretreatment of Coal with SiCl₄-NaI

Reaction of Zao Zhuang coal with SiCl₄-NaI reagents was conducted according to the following procedure: SiCl₄ (10 mL) was added gradually to a CH₂Cl₂-MeCN (80 mL, 1:1, v/v) solution containing pulverized coal (3.6 g; 100 mesh under dried at 100 °C under 2 mmHg for 10 h) and NaI (6.6 g), the reaction mixture being refluxed (40 °C) for 15 h. After the reaction, water (25 mL) was added to the reaction mixture to hydrolyze the resulting silyl ethers. The resulting mixture was filtered, a precipitate being washed with CH₂Cl₂ and water. The filtrate was extracted twice with CH₂Cl₂ (100 mL), then the precipitate was extracted with CH₂Cl₂ and pyridine, successively, by using a Soxhlet apparatus. Two CH₂Cl₂ soluble fractions were combined, the solvent being removed by a rotary evaporator. Methylene chloride soluble (MS), pyridine soluble (PS), and pyridine insoluble fractions (PI) were submitted to Curie-point pyrolytic analysis. As a blank experiments, extraction of non-treated coal with methylene dichloride followed by pyridine was carried out.

3.3. RESULTS AND DISCUSSION

An Attempt to Construct Unit Chemical Structure of Zao Zhuang Coal

At first, Nomura's method to evaluate unit chemical structure was applied to Zao Zhuang coal.⁶ Zao Zhuang coal showed following elemental analysis (wt%, daf basis): C 86.9, H 5.1, N 1.5, S 1.6, O 4.9 (difference); number of OH per 100 carbon is 1.4. According to an arbitrary assumption with its molecular weight being 5,000, Zao Zhuang coal has following molecular formula such as $C_{362}H_{253}N_5S_2O_{15}$ with 4 OH groups in it. On the other hand ^{13}C NMR suggests that carbon aromaticity is 0.77 so that number of aromatic and aliphatic carbons should be 287 and 75, respectively. As for nitrogen and sulfur atom containing compounds, five nitrogen atoms are assumed to exist as quinoline, 2-methylquinoline, indole, 2-methylindole, and carbazole, sulfur-atoms being to exist as thiophene and 2-methylthiophene by referring to the literature. These hetero compounds contain 54 aromatic carbons and 3 aliphatic carbons. So that we have to think about only 233 (287-54) of aromatic carbons and 72 (75 - 3) aliphatic carbons. Figure 3-1 shows the distribution of aromatic compounds derived from the results of pyrolytic analysis: Here, as Nomura *et al.* had point out in their paper,⁶ volatile portion of HS, HI/BS, BI/PS, and PI are

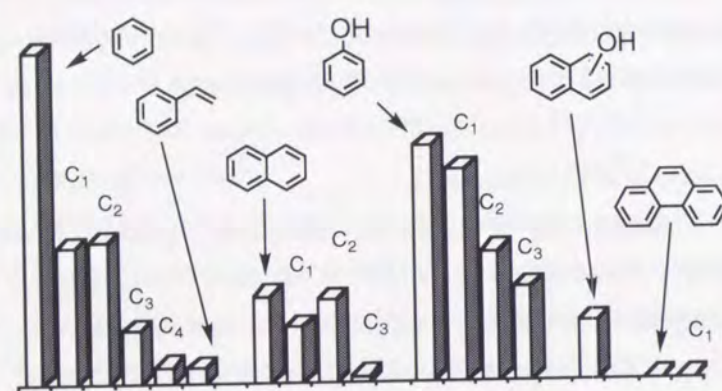
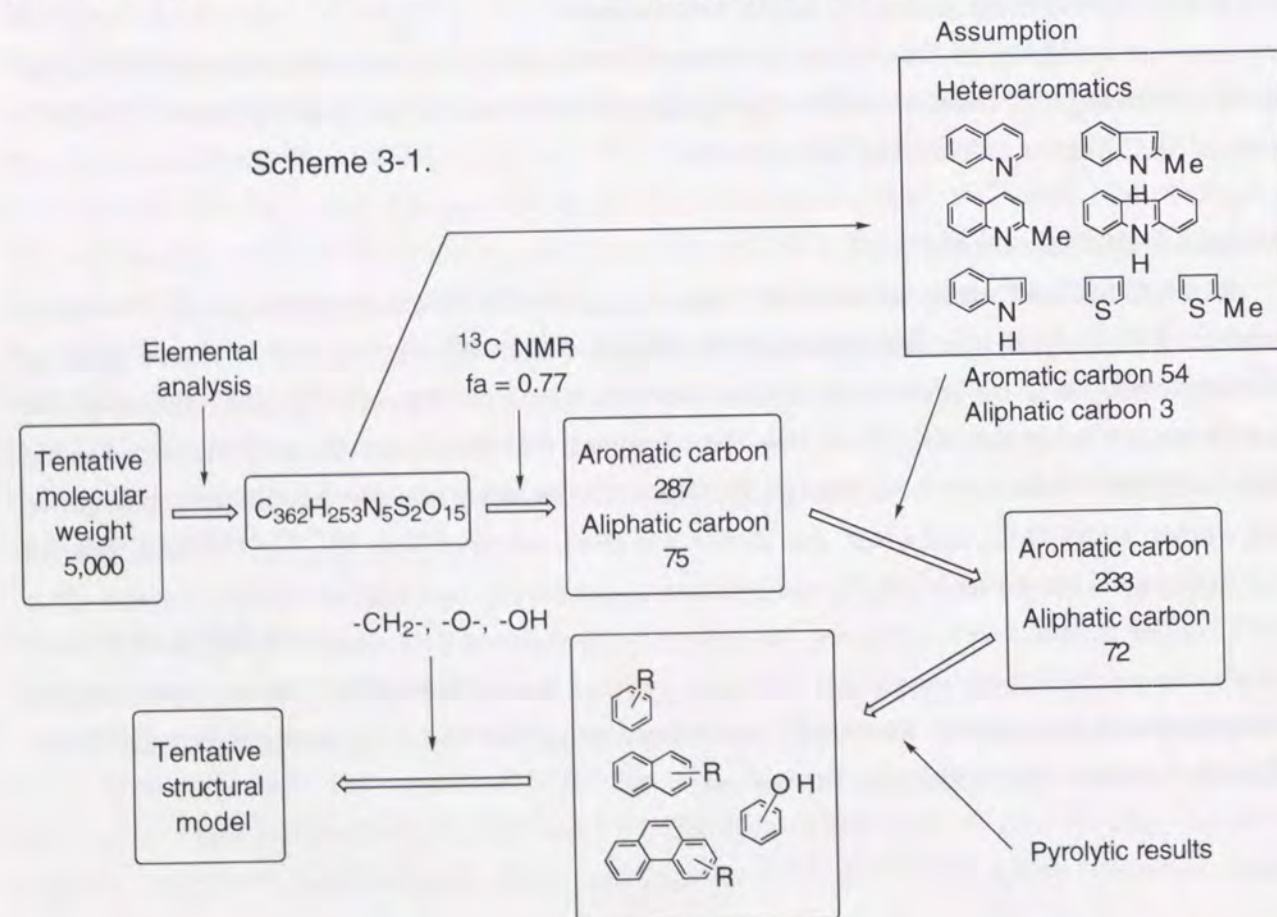


Figure 3-1. Distribution of aromatic compounds from pyrolysis of SRC fraction.



assumed to represent whole constituents of each extract. According to the carbon distribution deduced from CP/MAS ^{13}C NMR, we constructed several possible structures. However, the resulting structures have very higher H/C ratio compared with the value of original coal (0.76). This fact strongly suggests that sizes of aromatic compounds in above structure are relatively small. For example, if the distribution of aromatic compounds deduced from pyrolytic data did not reflect the real aromatic features of original coal (more high condensed aromatics), resulting H/C ratio should increase, because aromatic compounds with smaller degree of condensation shows higher H/C ratio. These trial in constructing unit chemical structure of Zao Zhuang coal resulted in poor conclusion. A problem is the assumption that the volatile portion can reflect the whole constituents of extract. Here we have to notice that SRC fractions of Zao Zhuang coal accompany a lot of coke upon their pyrolysis (Table 1). Amounts of coke increase as SRC fractions become heavy. So increasing the amount of volatile upon the pyrolysis is a key issue to overcome above problem. This consideration leads to the following experiment such as application of pretreatment of coal before extraction.

Ether Bonds Cleavage Reaction of Coal Causing Increased Amounts of Volatile in Pyrolysis

The presence of ether bonds in coal organic materials (COM) is well proved so that the cleavage of ether bonds of COM by chemical reaction may improve the amount of volatile from extract when being pyrolyzed. $SiCl_4$ -NaI reagents can cleave alkyl-aryl ether bond according to the following equation. Three fractions, methylene chloride soluble (MS-1), pyridine soluble (PS-1), and pyridine insoluble (PI-1), were obtained from the pretreated Zao Zhuang coal, their yields and elemental analyses being compared with those of three fractions obtained from non-treated Zao Zhuang coal (Table 3-2). It is interesting to note that each yield of three fractions changed slightly after the pretreatment of coal. The ratio of H/C of each corresponding fraction with or without pretreatment is very similar except that of MS fraction. Figure 3-2 shows the yield of volatile, tar, and coke fractions from Curie-point pyrolysis of three fractions with and

Table 3-2. The yield of MS, PS, and PI fractions from Zao Zhuang coal along with their elemental analyses

sample	yield (wt%, daf)	elemental analysis (wt%, daf)					H/C
		C	H	N	S	O ^a	
virgin coal	-	85.8	5.1	1.3	1.3	6.5	0.71
MS	10	85.8	6.1	1.2	2.3	4.6	0.85
PS	20	83.7	5.4	2.2	1.8	6.9	0.77
PI	70	87.9	4.9	1.6	1.9	3.7	0.65
MS-1	11	76.3	6.0	0.8	16.9 ^b		0.94
PS-1	23	72.9	4.6	2.0	20.5 ^b		0.75
PI-1	66	78.6	4.4	1.7	15.3 ^b		0.67

^a By difference. ^b This fraction contained a considerable amount of iodine so that contents of sulfur could not be determined.

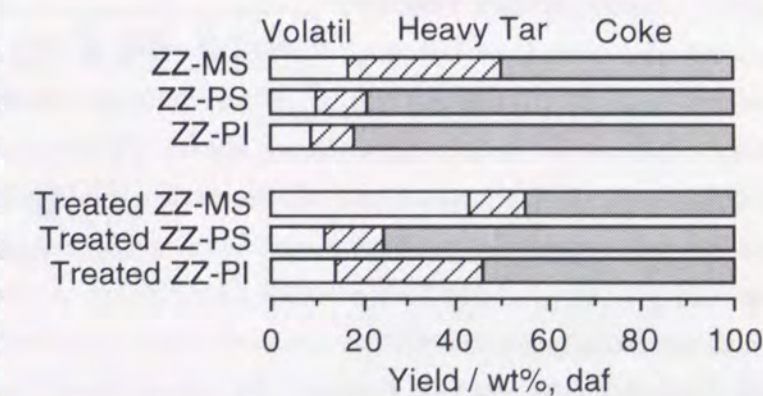


Figure 3-2. Yield of volatile, tar, and coke fractions from Curie-point pyrolysis of each extract

without pretreatment. From this figure, it is clear that volatile of MS with pretreatment increased remarkably compared with that of MS from original coal. The relatively high H/C ratio of MS from treated coal may be correlated with above observation. Distribution of aromatic compounds in each pyrogram of three fractions were, at first, calculated, then resulting distributions being summed up by considering each weight of fraction (Figure 3-3). Here, there is assumption that volatile can represent residual part of each fraction. Apparently, polyaromatic compounds in volatile fraction increased when ether bond cleavage reaction was applied on Zao Zhuang coal. The possible reasons for the increasing amount of volatile caused by this pretreatment are discussed here. First possibility is a depolymerization of coal by SiCl_4 -NaI in treated coal extract. On the other hand, contamination of the extract with iodine was confirmed by its elemental analysis, this causing us to consider another reason. The role of iodine is now considered in the way that iodine interacts strongly with aromatic π -electron clouds of aromatic in COM and assists the separation of π - π interaction observed between aromatic planes: This leads to the increasing amount of volatile and increasing amount of highly condensed aromatic compounds.

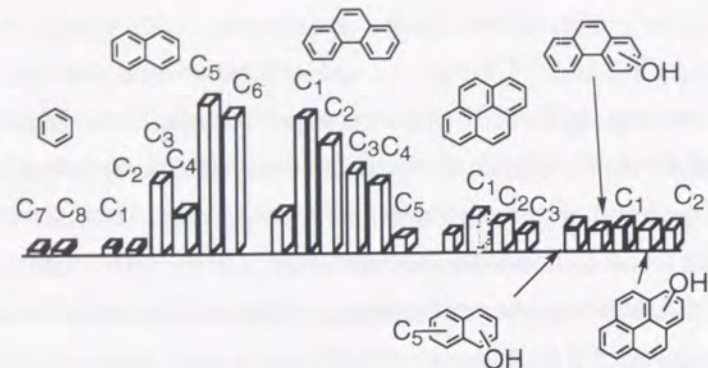


Figure 3-3. Distribution of aromatic compounds estimated from the pyrolytic data of extracts after ether bond cleavage reaction

Treatment of PS and PI Fractions with SiCl_4 -NaI Reagent

Ether bond cleavage reaction of PS and PI fractions obtained from extraction of the treated Zao Zhuang coal was also carried out: the reaction afforded methylene chloride soluble fractions from PS and PI and pyridine soluble fraction from PI (Scheme 3-2). Total amount of methylene chloride soluble fractions and pyridine soluble fractions reached to 21 and 26%, respectively. These results seem to suggest that SiCl_4 -NaI reagent could react on the surface or their layer of the coal particle. The reason is that if SiCl_4 -

Scheme 3-2.

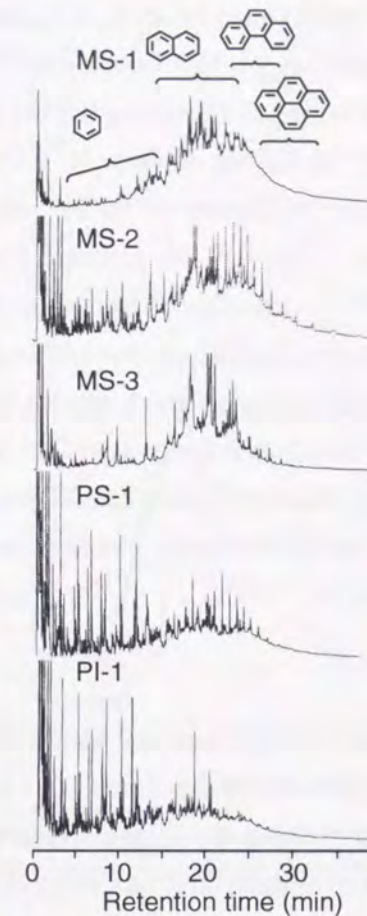
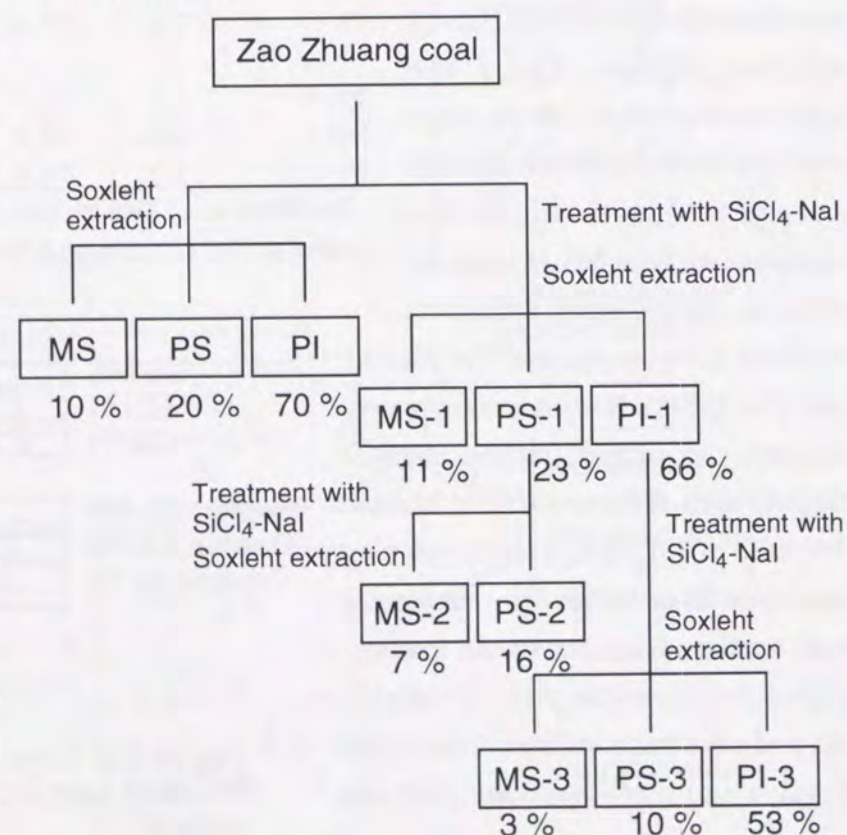


Figure 3-4. Curie-point pyrograms for Zao Zhuang coal extract at 670 °C for 3 s.

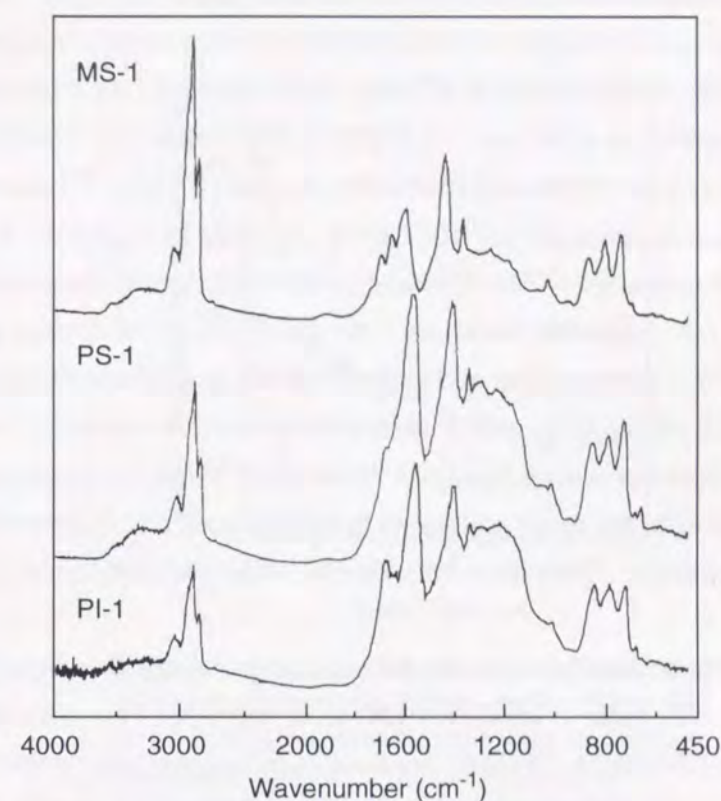


Figure 3-5. IR spectra for MS, PS, and PI fractions from SiCl_4 -NaI treated Zao Zhuang coal.

NaI reagent reacts with coal organic material in a homogeneous way, solvent extraction can not give further crops as described

above.

Figure 3-4 shows the pyrograms for MS-1, PS-1, PI-1, MS-2, and MS-3 (Scheme 3-2), this indicating that each MS fraction was very similar to each other and much amount of three-ring compounds was found in the pyrograms. FT-IR spectra of MS-1, PS-1, and PI-1 were shown in Figure 3-5, these spectra also being similar to each other. These results seem to suggest that constituents of these fractions were similar each other.

Can Volatile Fraction Represent Whole Constituents of Coal ?

This is one of the most problematic points of this study. When we constructed the chemical structural model of Akabira coal, we assumed that a volatile fraction represents constituents of starting material. In a previous section,¹⁰ I investigated pyrolytic behavior of 14 coal model compounds, in which the results indicated that although pyrolysis proceeds in a complicated fashion accompanying several secondary reactions and formation of tar and coke fraction, the pyrolytic products obtained could reflect the chemical structure of original model compounds: I can easily evaluate chemical features of starting materials quantitatively based on pyrolysis products. Nomura *et al.* had confirmed that the volatile fractions from pyrolysis of synthetic polymers such as phenol resin and naphthalene-formaldehyde oligomers can tell us the chemical structure of original polymers,¹¹ so that I could conclude

volatile fraction could represent the structure of the original compounds. On the other hand, I confirmed that volatile fraction from pyrolysis of some coals correspond well with the results of solid state ^{13}C NMR, while pyrolysis of other coals afforded less condensed aromatic ring compounds than that supposed by solid state ^{13}C NMR.^{7,8} The former coal includes Japanese bituminous Akabira (C 82%) and US subbituminous Illinois No. 6 coals (C 78%).^{7,8} Japanese bituminous Miike coal (C 83%)^{7,8} was found to belong to the latter group, this coal being known as caking coal. Iino *et al.* had reported that heat treatment of Zao Zhuang coal at relatively low temperature (< 300°C) resulted in the formation of solvent insoluble materials.¹² As described in the former section, pyrolysis of the extracts of coal without pretreatment and solvent soluble fractions obtained from liquefaction gave much amount of coke, respectively, where there observed much amount of benzene and naphthalene derivatives in the volatile fraction on pyrolysis. However, I found that pyrolysis of extracts from pretreated Zao Zhuang coal afforded much amount of three-ring aromatic compounds. Consequently, we would like to notice here that we have to be very careful when handling the results of pyrolysis.

Carbon Distributions and Average Ring Sizes of Zao Zhuang Coal

In order to obtain insight into distribution of carbon functionalities, I have measured solid state ^{13}C -NMR with CP/MAS method in recent studies. Several authors, however, had pointed out that from CP/MAS ^{13}C NMR quantitative information is hardly obtained and SPE (single pulse excitation) is better.¹³ Therefore, we decided to use SPE/MAS method. First, I have examined an effect of a pulse delay (PD, the time for data acquisition) time on carbon aromaticity (*fa*) with 512 scans. The value of *fa* remarkably increased from 0.71 to 0.83 by increase of the PD time from 10 sec to 100 sec. At more than 100 sec of PD, *fa* was no longer changed (e.g. at 500 sec of PD, *fa*=0.82). Consequently, I found that quantitative spectrum could be obtained with more than 100 sec of PD.

Table 3-3 shows the distribution of carbon functionalities of Zao Zhuang coal, where the spectrum was separated into 9 Gaussian curves, terminal methyl, α -methyl, methylene in alkyl side chains, ring-joining methylene like methylene carbon in diphenylmethane, methyl or methylene carbon attached to oxygen atoms, aromatic carbon at ortho-position to substituted hydroxyl or ether group, aromatic carbon bearing hydrogen, aromatic carbon bearing alkyl groups, and aromatic carbon bearing hydroxy or alkoxy groups. However, resolution of peak for aromatic carbons was not so good, so that we decided to measure dipolar dephasing (DD) NMR method to get further information for distribution of aromatic carbons. It should be noted that I employed here CP/MAS/DD method. The resulting spectra and the decay of magnetization were shown in Figures 3-6 and 3-7. The decay of magnetization was divided into two decays according to the following equation.

Table 3-3. Distribution of carbons in Zao Zhuang coal (%)

method and sample	Bridge-			Ar-H	CH ₃ O	CH ₂ '	α-CH ₃	t-CH ₃
	Ar-O	Ar-R	head					
SPE/MAS and curve fitting								
original coal	5	18		59	2	8	5	3
PS-1	7	10		60	1	16	4	2
PI-1	13	13		48	8	13	3	2
CP/DD/MAS								
original coal	4	14	24	40				

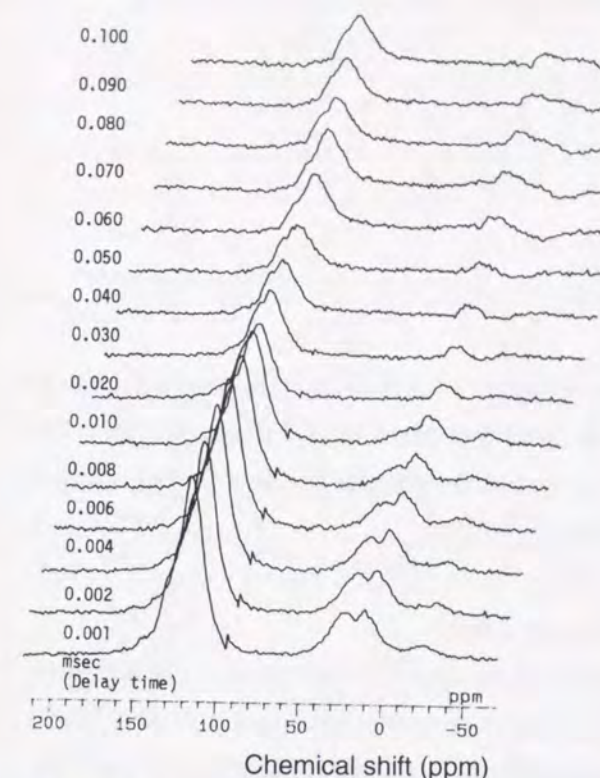


Figure 3-6. Stack plot of dipolar dephasing NMR of Zao Zhuang coal.

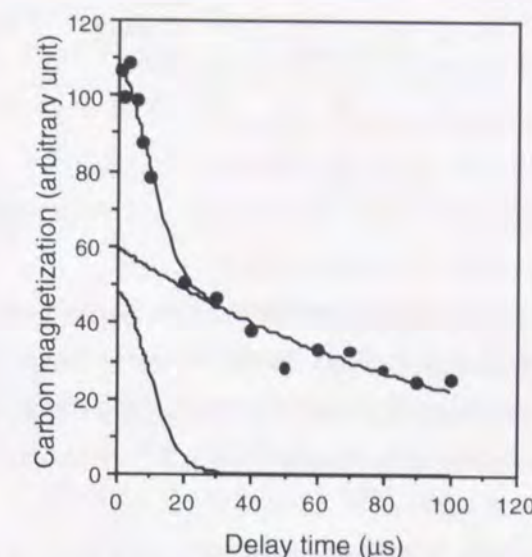


Figure 3-7. Decay of carbon magnetization of aromatic carbon. Filled circle and solid lines indicated measured value of carbon magnetization and simulated curve according to the eq. 1, respectively.

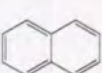
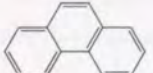

$$M(t) = M_{OL} \exp(-t/T_L) + M_{OG} \exp[-0.5(t/T_G)^2]$$

where, M_{OL} =53.0, T_L =124.7, M_{OG} =55.1, T_G =9.6. From Figure 3-7, relative contents of tertiary aromatic carbons and quaternary aromatic carbons were calculated to be 40 and 42 % of total carbons in COM, respectively. At delay time of 20 μs , the peak of aromatic carbons, in which tertiary aromatic carbons had almost decayed, could be separated into three peaks, bridgehead and internal carbons (24%), aromatic carbons bearing alkyl groups (14%), and aromatic carbons bearing oxygen (4%). The latter two values agreed completely with the value obtained by CP/MAS ^{13}C NMR and curve fitting method (Table 3-3).

Pugmire *et al.*^{14,15} had reported that an average ring size could be calculated based on the data of DD NMR. Stock *et al.* had employed Pugmire's method when they construct structural model for Argonne Pocahontas No. 3 coal. Thus, I tried to calculate the value according to their method. They used the parameter, χ_b , which could be calculated according to the following equation: χ_b = bridgehead carbons / total aromatic carbons. I could estimate relative amount of bridgehead carbons and total aromatic carbons as 24 and 82% of total carbons in COM, so χ_b could be calculated to be 0.29. The value of 0.29 corresponds tricyclic aromatic compounds such as anthracene or phenanthrene, because these compounds have the value of 0.286 (=4/14). This result agrees well with the average ring size of the extract from Zao Zhuang coal reported by Iino *et al.* and the results of pyrolysis/GC of MS-1 fraction, suggesting that pyrolysate from MS-1 fraction could represent whole constituents of the fraction.

In this study, I employed CP/MAS/DD method, however this method has a possibility to

Table 3-4. Structural parameters for the coal and some aromatic hydrocarbons

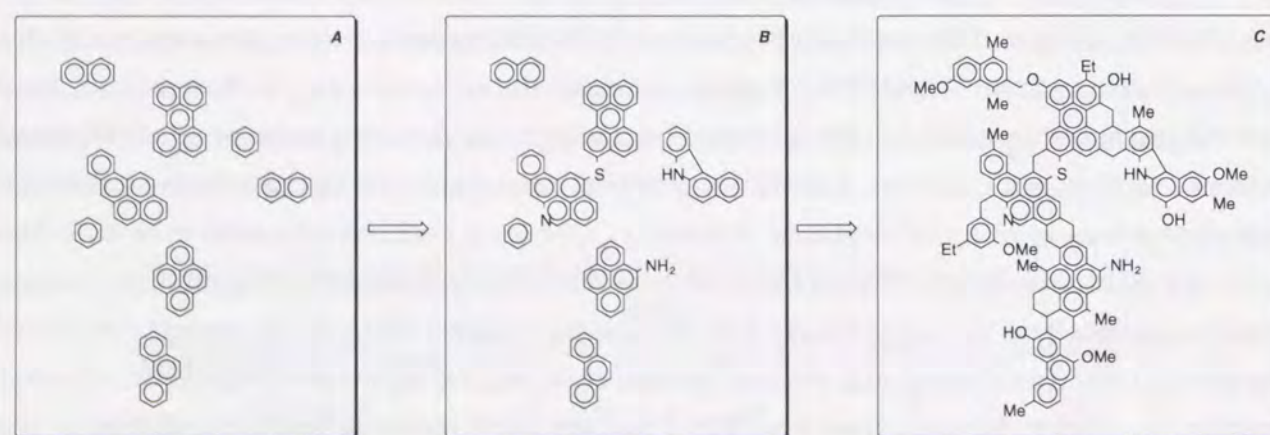
parameter	Zao Zhuang coal			
χ_b	0.30	0.20	0.29	0.31
aromatic carbons per cluster	15	10	14	16

underestimate internal carbons. Some authors recommended a use of SPE/MAS/DD method instead of CP/MAS/DD method. However these technique could not be applied in this paper, because the method requires very long time for measurement (in this case, one or two weeks). In a further study, I will discuss the data obtained from SPE/MAS/DD method.

Construction of a Chemical Structural Model for Zao Zhuang Coal

Based on the above results, I tried to construct a chemical structural model for Zao Zhuang coal. In this case, I assumed the following items; 1) molecular weight of model assumed is 10,000, 2) PI model was composed of two small molecules, 3) average ring size is 3 or 4 and distribution of aromatic rings in three fractions was similar to each other, and 4) major alkyl side chains are methyl and ethyl groups. As to first assumption, *real* molecular weight of coal molecules could not be measured, so I have to assume the molecular weight of coal molecules, as Shinn had assumed.⁴ As to the second item, some researchers had proposed that this coal has association structure, so we employed this assumption. Third item was derived from the experimental results described in the present paper. As to the last item, I had carried out ruthenium ion catalyzed oxidation of the coal, this indicating that concentration of longer alkyl side chains than C_3 is very low (see also section 2.3.2).

Based on the results of extraction and elemental analysis, tentative molecular formula of methylene chloride soluble (MS), pyridine soluble (PS), and pyridine insoluble fractions (PI) were $C_{71}H_{61}NSO_3$, $C_{139}H_{107}N_3SO_9$, and $C_{512}H_{340}N_8S_4O_{16}$, respectively. Outline for construction of the model for PI fraction is shown in Scheme 3-3. At first, a set of polycyclic aromatic hydrocarbons was selected based on the



Scheme 3-3. Construction of PI molecules based on the elemental analysis, pyrolytic results, and carbon distribution from ^{13}C NMR

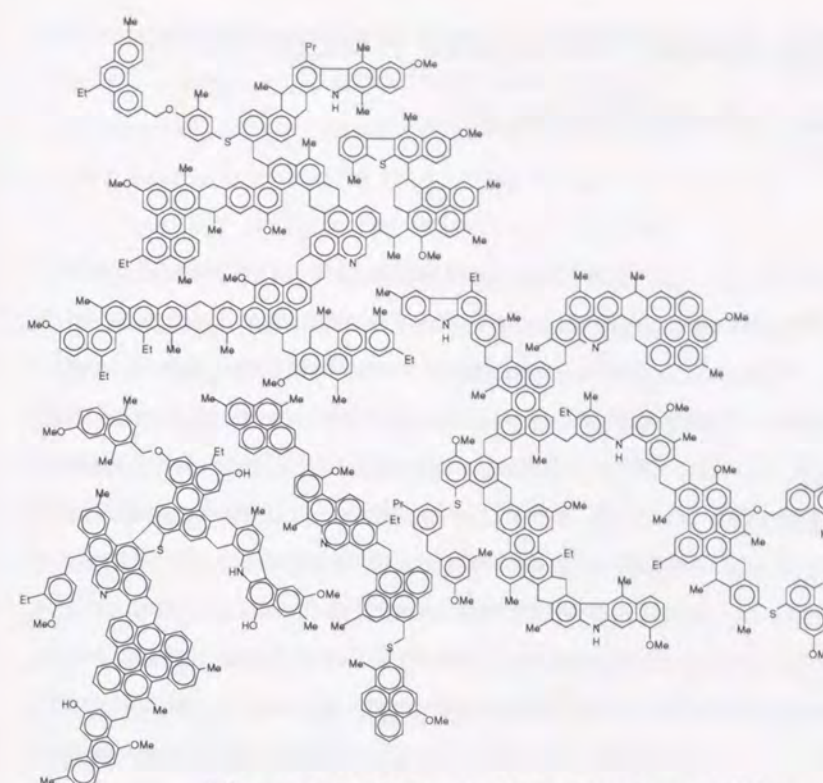


Figure 3-8. Chemical structural model for Chinese bituminous Zao Zhuang coal

data of DD NMR and pyrolysis GC/MS analyses (Scheme 3-3A). Then, heteroatoms (sulfur and nitrogen) were added (Scheme 3-3B). Since, no information was available for their functionality and distribution, I employed the data for a coal with similar carbon content reported so far. At last, aliphatic- and oxygen-containing functional groups were added based on the SPE/MAS NMR (Scheme 3-3C). According to this method, the models for MS and PS fraction were also constructed. The resulting model for the coal has the molecular formula, $C_{705}H_{575}N_{10}S_6O_{29}$ (MW 9831), the elemental analysis and carbon

distribution of which agree well with those of the virgin coal. However, atomic ratio of hydrogen to carbon of the model was 0.815, which was 0.1 higher than that of the real coal. The difference between two values might be derived from the assumptions employed in this study.

3.4. References

- Given, P. H. *Fuel* **1960**, 39, 147.
- Wiser, W. H. *NATO ASI Ser. C* **1984**, 124, 325.
- Solomon, P. R. *New Approaches in Coal Chemistry, Am. Chem. Soc. Symp. Ser. 169*, **1981**, 61.
- Shinn, J. H. *Fuel* **1984**, 63, 1187.
- Spiro, C. L. *Fuel*, **1981**, 60, 1121.
- Nomura, M.; Matsubayashi, K.; Ida, T.; Murata, S. *Fuel Process. Technol.* **1992**, 31, 169.
- Hama, H.; Matsubayashi, K.; Murata, S.; Nomura, M. *J. Jpn. Inst. Energy* **1993**, 72, 467.
- Hama, H.; Murata, S.; Nomura, M.; *J. Jpn. Inst. Energy* **1994**, 73, 177.
- Nomura, M.; Murata, S.; Hama, H.; Yamamoto, A. *Unpublished results*.
- See section 1.3.2.
- Nomura, M.; Matsubayashi, K. *Unpublished results*.
- Takanohashi, T.; Iino, M.; Nakamura, K. *Energy Fuels*, **1994**, 8, 395.
- Franz, J. A.; Garcia, R.; Linehan, J. C.; Love, G. D.; Snape, C. E. *Energy Fuels* **1992**, 6, 598.
- Solum, M. S.; Pugmire, R. J.; Grant, D. M. *Energy Fuels* **1989**, 3, 187.
- Fletcher, T. H.; Bai, S.; Pugmire, R. J.; Solum, M. S.; Wood, S. Grant, D. M.; *Energy Fuels* **1993**, 7, 734.

Chapter 4. Computer-Aided Molecular Design Study of Coal Model Molecules

4.1. Introduction

CAMD (Computer Aided Molecular Design) has been applied to drug design and protein modeling. Recently, this technique has begun to be applied to the area of fuel science, being involved in the work on coal molecular models,¹⁻⁴ kerogen macromolecules,^{5,6} and catalyst systems⁷ using commercial CAMD softwares. Carlson *et al.* had proposed the most probable conformation of each coal model molecule previously reported by Given,⁸ Wiser,⁹ Solomon,¹⁰ or Shinn.¹¹ They also discussed its physical density, potential energy, hydrogen bonding, and so on based on their own calculations. Among the parameters obtained by using CAMD software, physical density is considered to be one of the most significant parameters which may be compared with experimentally observed value. In this chapter, a new method was proposed for calculation of physical density of coal model molecules by using a commercial CAMD software, Polygraf and it was applied to three types of coal model molecules, (1) simple models containing polycyclic aromatic hydrocarbons with polymethylene bridges, (2) four Japanese coal models which represent their elemental analyses, carbon aromaticity, and oxygen-functional groups, and (3) relatively large model for Japanese bituminous Akabira coal proposed by Nomura *et al.*¹² The results are briefly described.

4.2. Method

CAMD studies were carried out using PolyGraf (version 3.0, Molecular Simulations inc.) and TITAN 750V graphic work station (Kubota Computer Inc.). Polygraf allows the construction of a relatively large molecular structures (up to 20,000 atoms) and the subsequent manipulation of these structures using molecular mechanics and dynamics techniques to determine the most probable structure. Polygraf supports several force fields (AMBER, MM2, and DREIDING¹³). The current study used DREIDING's force field. Polygraf also allows the use of periodic boundary conditions. In these conditions, the molecules are placed in an unit cell which is surrounded by the identical cells three-dimensionally. In this approach, the polymeric molecule can extend to multiple cell. If the segment exits from the one surface of the cell, the same segment enters from the opposite surface. The current limit for the number of the atoms in the periodic boundary conditions is 1,000 atoms. The draw back to this approach is that the molecules in the unit cell and all in the neighboring cells are identical. One can overcome this problem by generating various amorphous structures, then performing simulations, and calculating the average values of the properties. All the interactions among the atoms, both bonded and nonbonded within the unit cell as well as the interactions of the atoms in the neighboring cells are calculated. Using the periodic boundary conditions seems to be the reasonable way to simulate bulk properties, such as density and plastic constants of the materials.

Scheme 4-1 shows the procedure to estimate the density of model molecules. After inputting the model molecule (Figure 4-1a, the automatically generated polymer molecule having the anthracene skeleton linked by trimethylene as a monomer unit), we carried out the calculation of molecular

mechanics and charge modification to optimize the potential energy of the model molecule until rms (root mean square) became less than 0.1. Then the model was submitted to molecular dynamics calculation for 100 psec to search more stable conformation. The conformation having the lowest potential energy was extracted as the best conformer (Figure 4-1b). In this procedure hydrogen atoms attached to a carbon atom were treated as included in each carbon group such as methine, methylene or methyl groups according to DREIDING's method. When the periodic boundary conditions are applied for calculation, this model molecule is enclosed in a cell (Figure 4-1c). The density of the system is calculated from both the volume of this cell and the weight of all the atoms in the cell. When the model molecule was enclosed into the cell, potential energy of the system increased because the repulsive forces is caused by the contact of atoms among cells. Then, molecular mechanics calculation was carried out to obtain more stable conformation by considering the effect of surrounding molecules in the periodic boundary

Scheme 4-1. Method to estimate the physical density of the model

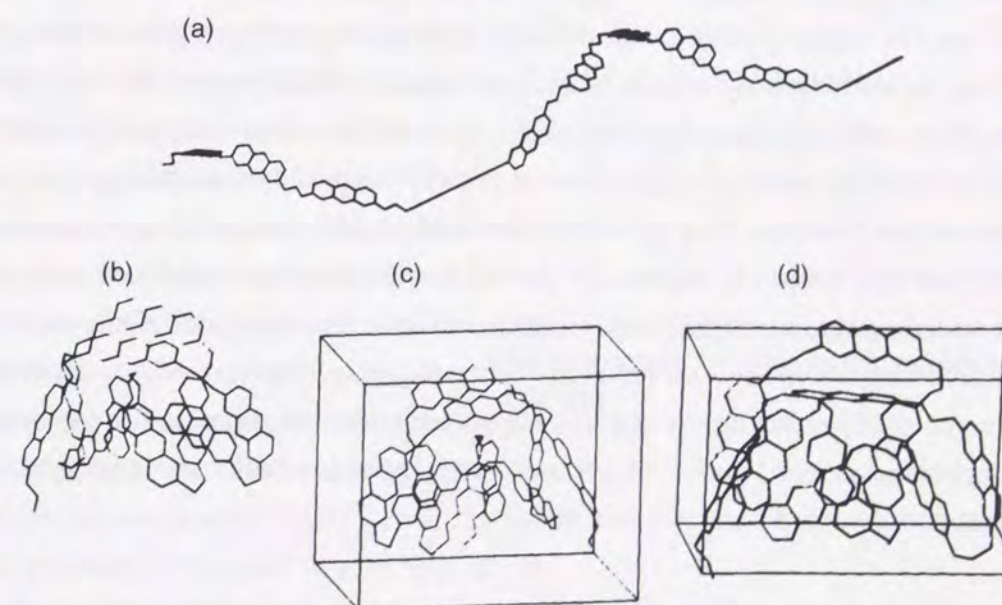
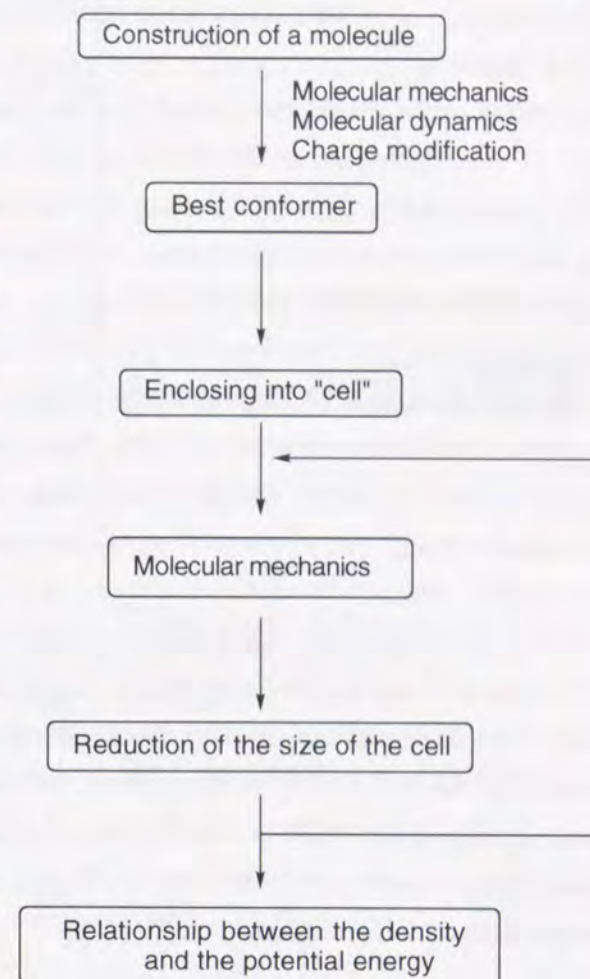


Figure 4-1. (a) The coal model molecule, (b) the most probable conformation of the model after 100 ps molecular dynamics calculation, (c) the model after enclosing into the cell, and (d) the model having the most probable physical density.

conditions until rms became less than 1.0. In the molecular mechanics calculation, the inter- and the intramolecular potential energy were optimized toward lower potential energy by changing conformation of the model molecule. Here, the size of the cell was decreased so that both the density and the potential energy of the system increased. Then, molecular mechanics calculation was carried out in order to reduce the potential energy of the system until rms became less than 1.0. This sequence was repeated for about 10 times. In each iteration, the size of the cell decreased within 5 - 10 %. Through the cycles of this sequence, the potential energy of the system decreased with accompanying the increase of the density. Then the potential energy turned to increase *via* a certain minimum point, where its model structure corresponds to the one of Figure 4-1d. We have defined the density of the energy minimum as the true density of the system, that is, the true density of the model molecule based on the consideration of both micropores and closed pores, and intermolecular interaction.

4.3. Results and Discussion

4.3.1. Estimation of Physical Density of Coal Model Molecules

Generally, two densities of coals can be defined. True density is the weight of a unit volume of the pore free solid, as would be measured by helium pycnometry. While particle density is the weight of a unit volume of the solid including pores and cracks, as would be measured by mercury porosimetry. The calculation with which Carlson *et al.* obtained physical density of coal model is carried out for an isolated single molecule, therefore this calculated value could not be comparable to the measured true density because even true density is believed to include both micropores and closed pores and to be affected by a certain interaction within coal molecules. Many evidences that there are significant porosity closed to helium size in coals are reported.¹⁴ Therefore true "true density" can not be measured by helium pycnometry. Then we report here the improved method to estimate the physical density including micropores and closed pores, which could be comparable with true density measured by helium pycnometry.

Estimation of the physical density of styrene oligomer

In order to evaluate the reasonability of the method described above, we carried out the calculation of the density of styrene undecamer ($C_{88}H_{90}$) by using this method. Figure 4-2 shows the relationship

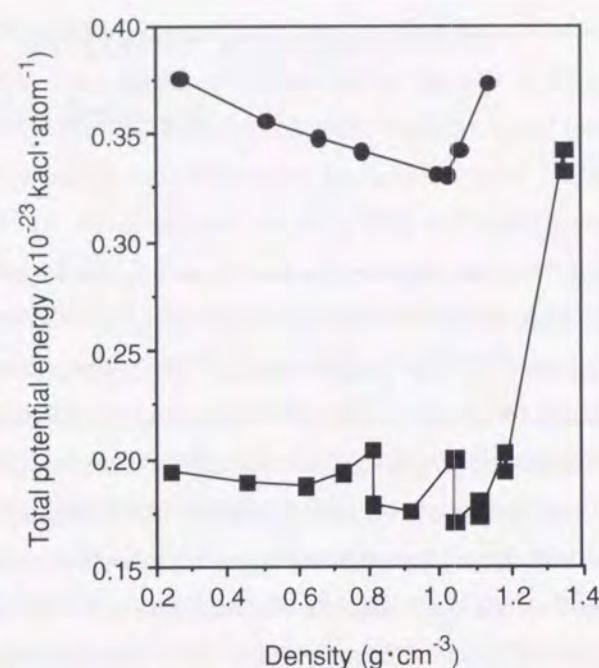


Figure 4-2. Relationship between the density of the styrene oligomer and its total potential energy normalized to each atom, treating hydrogen atoms as including in each carbon group (●) and treating hydrogen atoms as separate from carbon atoms (■).

between the density and the total potential energy of the styrene normalized to each atom (Figure 4-2, ●). From this figure, the density of the styrene oligomer was found to be 1.02 g/cm³. Generally polystyrene is known to be composed of the crystal and the amorphous parts, the experimentally measured values of the density of two parts being reported to be 1.12 g/cm³ and 1.04 - 1.065 g/cm³, respectively. The method proposed in this paper seems to simulate the density of the amorphous part of polystyrene to a reliable extent.

In order to check the reliability of treating hydrogen atoms as included in each carbon group, separate calculation was carried out using the method of treating hydrogen atoms as separate from carbon atoms (Figure 4-2, ■). In the Figure 4-2, several marks are not on the smooth line. This is due to the fact that a steric hindrance caused by employing the model molecule holding hydrogen atoms in CAMD calculation makes its potential energy to fall into its local minimum. Where an increase of total potential energy was observed as stated above, molecular dynamics calculation was carried out in order to search a more stable conformer: In this molecular dynamics calculation, model molecule can change toward a more stable state. The density of styrene oligomer was found to be 1.04 g/cm³, the value of which agrees well with the value obtained in the calculation treating hydrogen atoms as included in each carbon group (1.02 g/cm³). We have concluded the method with the treatment of hydrogen atoms as included in each carbon group can simulate the density of polymeric molecules to a reliable extent.

As for the potential energy, treatment of hydrogen atoms as separate from carbon atoms was found to afford about half of the energy as calculated by the treatment of hydrogen atoms as included in each carbon group. By examining each energy term (refer to the following section) included in both

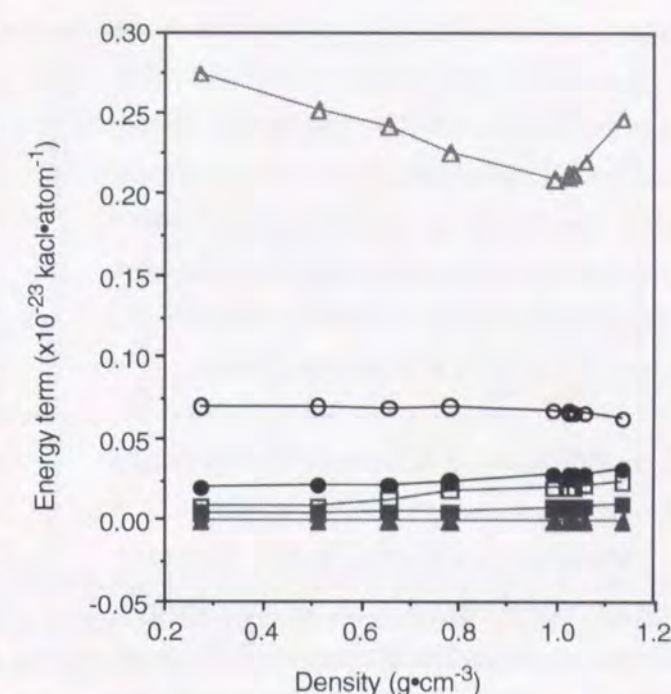


Figure 4-3. Relationship between the density and the various energy terms of styrene oligomer normalized to each atom; stretch (○), bend (●), torsion (□), inversion (■), van der Waals (△), and electrostatic energy (▲).

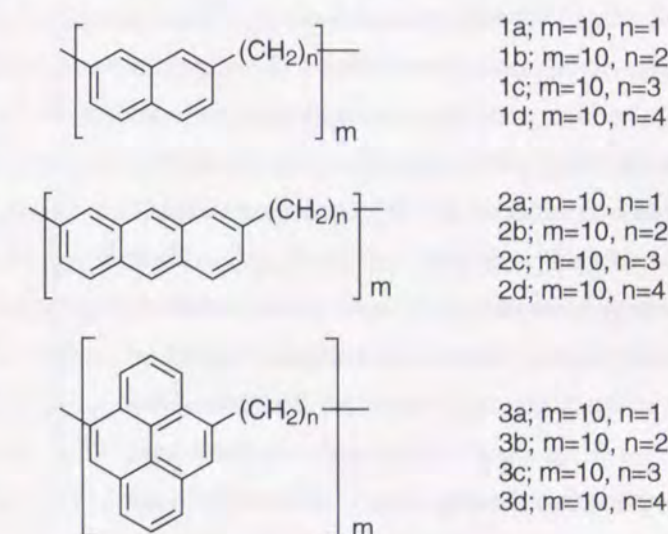


Figure 4-4. Coal model molecules composed of polyaromatic hydrocarbons and polymethylene bridges.

methods, we found that big difference of the energies is due to the difference of each E_v value. This is probably caused by the van der Waals interaction of hydrogen atoms in the treatment of hydrogen atoms as separated from carbon atoms. This method is time consuming, therefore we employed here the treatment of hydrogen atoms as included in each carbon group.

Relationship between the energy and the density of styrene oligomer

When the size of the cell was decreased, the total potential energy of the styrene oligomer decreased until the density reached 1.02 g/cm^3 , then turning to increase beyond this point. Figure 4-3 shows the various energy terms of the styrene oligomer in the calculation with the treatment of hydrogen atoms as included in each carbon group. DREIDING's force field can calculate the total potential energy (E) as a sum of bonded interactions (E_s =stretch, E_b =bend, E_t =torsion, and E_i =inversion) and nonbonded interaction (E_v =van der Waals, E_e =electrostatic, and E_h =hydrogen bonds): $E = (E_s + E_b + E_t + E_i) + (E_v + E_e + E_h)$. Each energy term except E_v term (van der Waals energy) was almost unchanged. However, E_v term decreased until the density of the system reached 1.02 g/cm^3 and increased beyond this density. The profile of E_v term represents that of total potential energy. In DREIDING's force field, E_v energy term is calculated using Lenard-Jones 12-6 potential.

$$E_v = D_0 [(R_0/R)^{12} - 2(R_0/R)^6] \times S$$

D_0 : van der Waals bond strength

R_0 : equilibrium bond length

S : switching term to cut off van der Waals calculations beyond a certain atom - atom distance

According to this equation, E_v term works as attractive force until a distance between two atoms reached equilibrium length and changes to repulsive force when the distance between two atoms

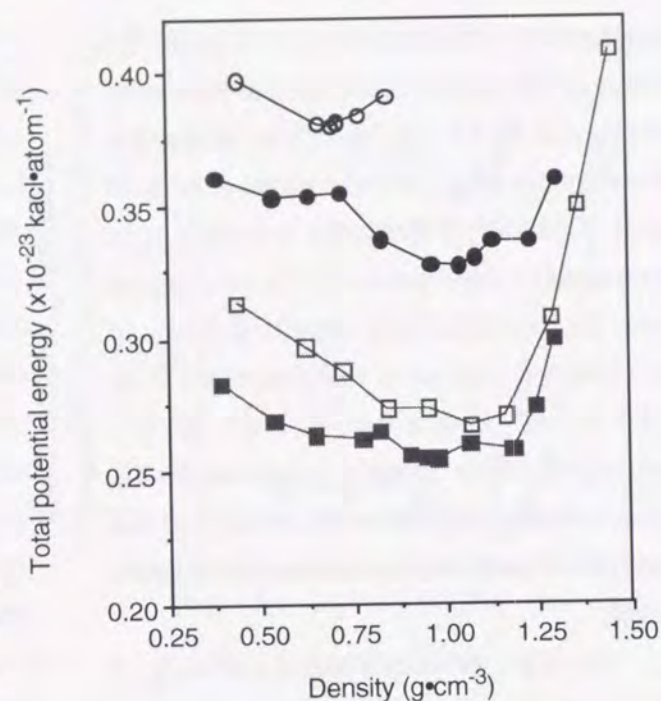


Figure 4-5. Relationships between the density of the coal model molecules and its total potential energy normalized to each atom; **2a** (○), **2b** (●), **2c** (□), **2d** (■).

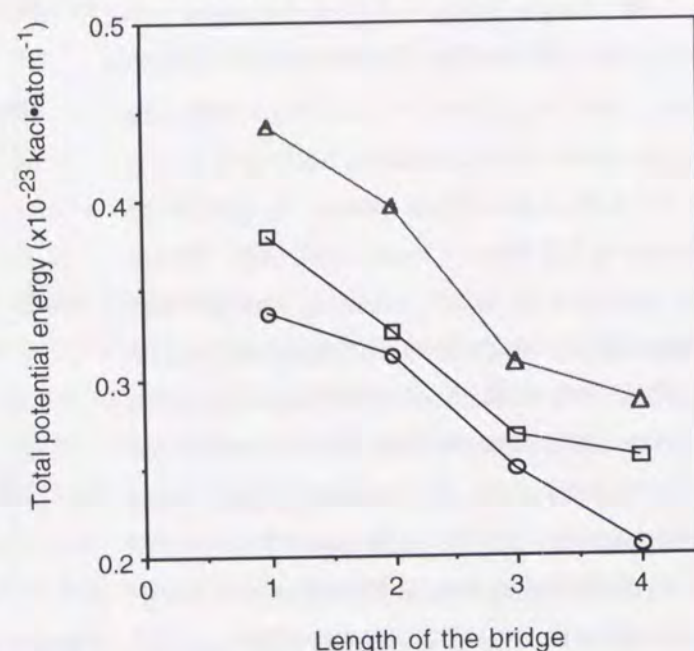


Figure 4-6. Relationships between the length of the bridges and the total potential energy normalized to each atom of the model molecules; naphthalene (**1a-d**, ○), anthracene (**2a-d**, □), and pyrene (**3a-d**, △).

becomes less than equilibrium length. Thus E_v term is one of the most significant factor affecting the decrease of total potential energy against increase of the density in non-polar molecules such as polystyrene.

Evaluation of the density - structure correlation of the simplified coal models

Generally, chemical structure of coals is thought to be composed of aromatic, hydro-aromatic, and heteroaromatic moieties linked by aliphatic and ether chain. We adopted the polymers of polyaromatic hydrocarbon (naphthalene, anthracene, and pyrene) linked by polymethylene chain (mono, di, tri, and tetramethylene) as simplified coal models (Figure 4-4) and studied the density - structure relationship. At first, we applied the above method to evaluation of the physical density of polymer being composed of anthracene molecules linked with polymethylene chains ranging from mono- to tetramethylene (**2a-d**). Figure 4-5 shows function of change of polymethylene chain against the total potential energy and the density of these model molecules. The calculated density of the anthracene molecules linked by monomethylene (**2a**) was 0.70 g/cm^3 , this being rather lower than the values of the other three ($0.98 - 1.07 \text{ g/cm}^3$). This suggests that in these models the higher density needs the longer chain ($n=2, 3$, and 4).

The order of each total potential energy obeyed the following sequence; (**2d**) < (**2c**) < (**2b**) < (**2a**). This result shows that the longer the chain becomes, the more stable a model molecule is. In the case of naphthalene- (**1a-d**) and pyrene-based polymers (**3a-d**), similar trend of the order of potential energy was observed as shown in Figure 4-6. Here it should be noted that the order of potential energy followed the sequence: naphthalene- < anthracene- < pyrene-based polymers.

Figure 4-7 shows the correlation between length of the bridges with changing size of aromatics in model molecule. The values of the density of (**1a-d**) were slightly increased with the increase of chain length. The density of anthracene-based molecules (**2a-d**) increased during the increase of chain length from 1 to 2. The density of pyrene-based polymers (**3a-d**) increased markedly during the increase of chain length from 2 to 3. This suggests that the more condensed an aromatic moiety is, the longer the chain needed for the higher density is.

Calculated values of the physical density of these models with both methylene bridge and aromatic moiety being changed fall in the following region from 0.63 to 1.09 g/cm^3 . These values were found to be rather lower than the measured values of the actual coals ($1.25 - 1.60 \text{ g/cm}^3$). This is partly due to both the lack of other functionalities in coals such as hydroxyl groups, ether bonds, or heteroaromatic moieties and assumption of only linear structure as whole coal models. Further study on the application

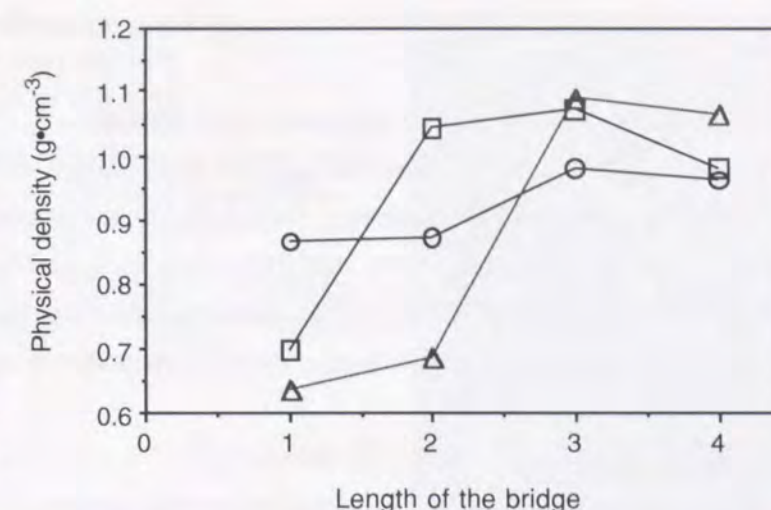


Figure 4-7. Relationships between the calculated density and length of the bridges of the model molecules; naphthalene (**1a-d**, ○), anthracene (**2a-d**, □), and pyrene (**3a-d**, △).

of this method to our coal model published recently¹² is described in the following section.

4.3.2. Density Simulation for Four Japanese Coal Models

The purpose of this study is to investigate the applicability of the above method to models more closely related to existing coals. A series of models for Japanese coals [Tempoku, Taiheiyo, Akabira, and Yubari coals; carbon content (wt%, daf) 71.5, 77.9, 81.2, and 86.7 and physical density (g•cm⁻³) 1.37, 1.27, 1.28, and 1.24, respectively] which were proposed previously by Iwata *et al.*^{15,16} was chosen (Figure 4-8) and simulation of their physical densities was attempted by my CAMD method.

Optimization of the Structure of the Coal Models

The model molecules for the four Japanese coals proposed by Iwata *et al.*^{15,16} are oligomers composed of the unit structures shown in Figure 4-8. They were constructed on the basis of ¹H-NMR, elemental analysis, and hydroxyl group analysis of their liquefied products. In this study, each model molecule is assumed to have a molecular weight of approximately 2,500 (Table 4-1). Thus, the models for Tempoku, Taiheiyo, Akabira, and Yubari coals used for the calculation are heptamer, heptamer, hexamer, and tetramer of the given unit structures, respectively. The carbon contents of the models are 71.5, 77.9, 81.2, and 86.7 wt%, respectively and are consistent with those observed for the four coals.^{15,16}

Table 4-2 summarizes the results for the energy calculations without periodic boundary conditions. Figure 4-9 shows the most stable conformational structure for the Tempoku coal model as a representative one. The calculation for each model molecule was carried out by considering that it is isolated in a vacuum as is usual in CAMD. The DREIDING force field method employed calculates the energy, *E*, as a linear combination of covalently-bonded interactions (*E_s*=stretch, *E_b*=bend, *E_t*=torsion, and *E_i*=inversion energies) and non-covalently bonded interactions (*E_v*=van der Waals, *E_e*=electrostatic, and *E_h*=hydrogen bond energies), *i. e.*, $E = E_s + E_b + E_t + E_i + E_v + E_e + E_h$. Each energy value obtained is also given in Table 4-2. In order to obtain the normalized potential energy for each model molecule, the total energy was divided by the total number of atoms. The total potential energy per atom (Kcal/g atom) was found to increase as the rank of the coals becomes higher. The major factors affecting the total potential energy appear to be the electrostatic and hydrogen bonding energies, *E_e* and *E_h*. As the rank of the coals (*i. e.*,

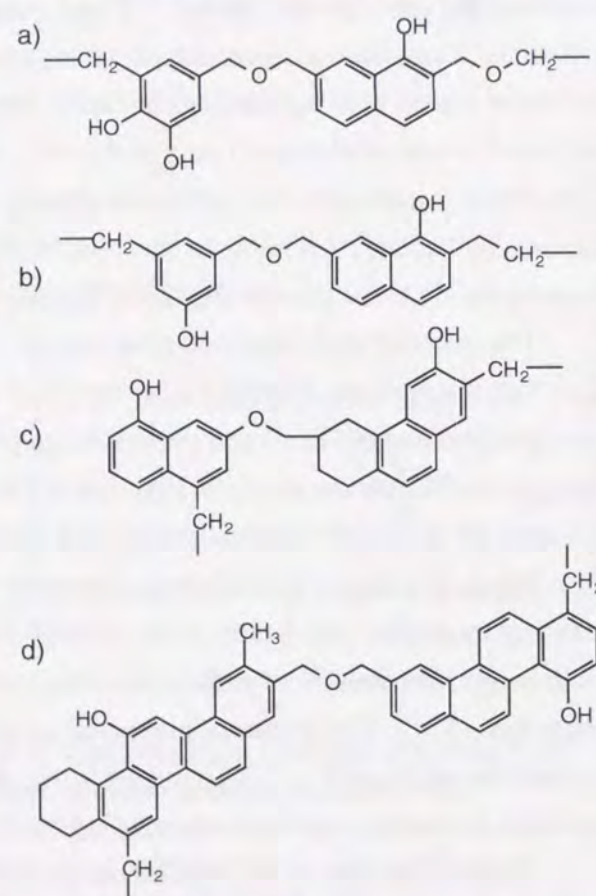


Figure 4-8. Structures of the coal models proposed by Iwata *et al.*^{15,16} for (a) Tempoku, (b) Taiheiyo, (c) Akabira, and (d) Yubari coals.

Table 4-1. Degree of oligomerization, molecular formula, molecular weight, carbon content, and number of hydroxyl groups of the coal model molecules

	Tempoku	Taiheiyo	Akabira	Yubari
deg of oligomerzn	7	7	6	4
mol formula	C ₁₄₇ H ₁₄₂ O ₃₅	C ₁₄₇ H ₁₄₂ O ₂₁	C ₁₆₂ H ₁₄₆ O ₁₈	C ₁₈₀₇ H ₁₄₂ O ₁₂
mol wt	2469	2245	2381	2497
carbon content (%)	71.5	78.7	81.7	86.6
no. of OH	21	14	12	8

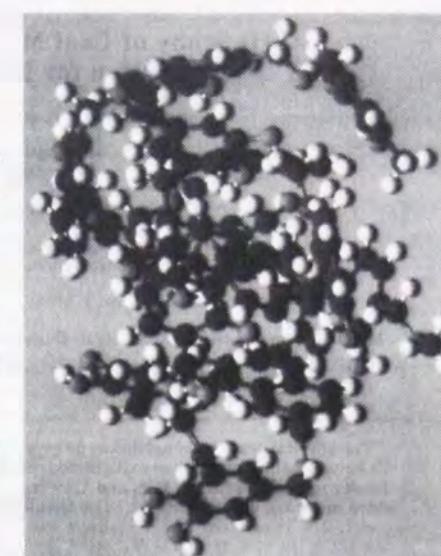


Figure 4-9. The most stable conformational structure of the Tempoku coal model.

the carbon contents) decreases, these energies tend to large negative values. This may be due to the fact that the lower rank coals have relatively larger numbers of hydroxyl groups and ether oxygen atoms per molecule.

According to the suggestion of the one reviewer, we have examined the relationship between total potential energy and the heat of combustion of these coals. Sugimura *et al.*¹⁷ and Krevelen *et al.*¹⁸ had reported that as coal rank increases, the heat of combustion, at first, increases, reaches the maximum value at 90% of carbon, and then, turns to decrease. Direct comparison of the value of the heat of combustion with the potential energy calculated in this paper could not be undertaken, however, it is interesting to note that the tendency of these two values are quite similar.

Estimation of Physical Density of the Coal Models

Figure 4-10 shows the relationships between the total potential energy and the physical density of the coal models calculated under the periodic boundary conditions by inputting the structural and energy data obtained for each single oligomeric model molecule. As is seen, there is a minimum potential energy for each model which corresponds to the optimized density. The physical densities for the models thus obtained are recorded in Table 4-3 along with the corresponding values previously

Table 4-2. Potential energy of the coal model molecules

	Tempoku	Taiheiyo	Akabira	Akabira ^a	Yubari
total potential energy (kcal/mol)	206.4	204.7	371.1	384.7	583.5
covalently bonded energy	164.0	131.8	169.8	179.0	242.0
stretch	53.8	49.7	67.3	56.7	101.4
bend	64.4	42.7	52.5	80.0	73.2
torsion	44.8	37.9	49.0	41.6	65.1
inversion	1.0	1.5	1.0	0.7	2.3
non-covalently bonded energy	42.4	72.9	201.3	205.7	341.5
van der Waals	311.3	260.6	337.5	282.3	407.4
electrostatic	-160.0	-138.3	-103.3	-60.1	-49.2
hydrogen bond	-108.9	-49.4	32.9	-16.5	-16.7
total potential energy per each atom (kcal/g•atom)	0.6	0.7	1.1	1.2	1.8

^a Modified structure of Akabira coal.

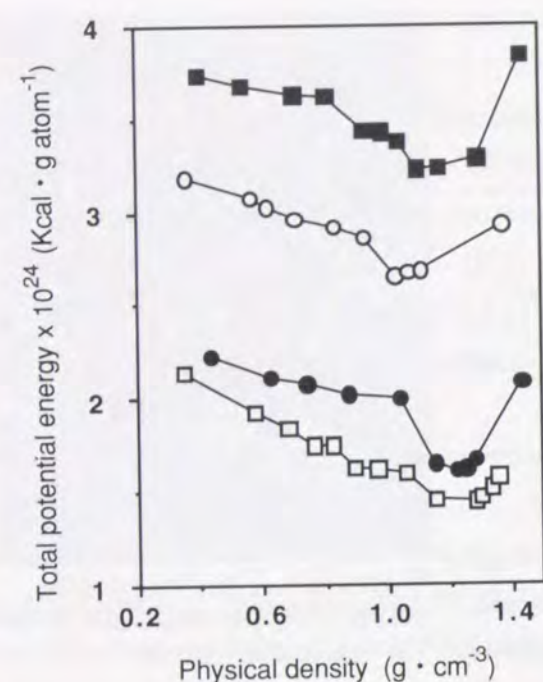


Figure 4-10. Relationships between the total potential energy and the physical density of the coal models for Tempoku (□), Taiheiyō (●), Akabira (○), and Yubari (■) coals.

is consistent with the general observation that the density of coals decreases as the coal rank increases up to carbon contents of 85–87%.¹⁹ The results for the calculations appear to be well in harmony with the trend except the Akabira coal model (Figure 4-11).

In the section 4.3.1, I demonstrated that the simulated physical density of polymeric hydrocarbons composed of polyaromatics and polymethylene chains markedly depends on the length of the chains and the number of the aromatic rings: these functions may greatly affect the flexibility of the polymeric molecules and thus affect the density by influencing the ability of the molecules to pack efficiently to minimize the density.

Each of the coal models used has two aromatic moieties whose ring numbers depend on the rank of the original coals and which are connected by a $-\text{CH}_2\text{OCH}_2-$ chain, except for the Akabira coal model (Figure 4-8). The Akabira coal model has a shorter chain $[-\text{CH}_2\text{O}-]$. We considered that the shortness of the chain could be a major reason for the disagreement of the calculated model density with carbon content-density correlation. Consequently, a modification of the Akabira coal model was made as illustrated in Figure 4-12 (refer to Table 4-2 as for energy terms of the revised Akabira coal). The modified model has a $-\text{CH}_2\text{OCH}_2-$ chains, as have the other models, while

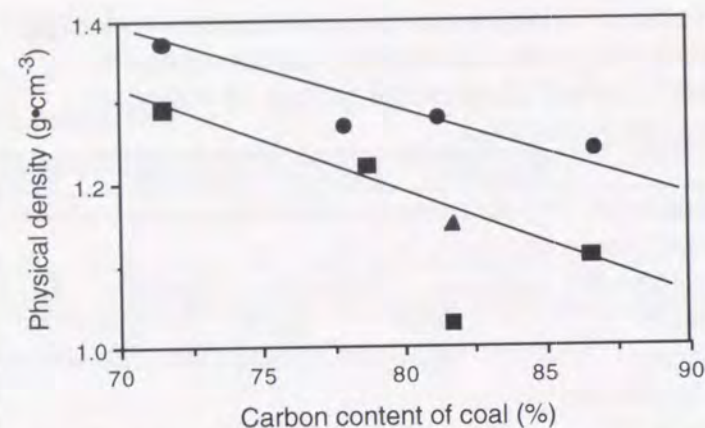


Figure 4-11. Relationship between the carbon content and the physical density; observed values (●), calculated values of the models (■), and calculated value of the modified Akabira coal model (▲).

measured experimentally for the original coals using sink-float method. The observed densities of the coal specimens follows the sequence Tempoku > Taiheiyō ≈ Akabira > Yubari, increasing as the carbon content decreases. This

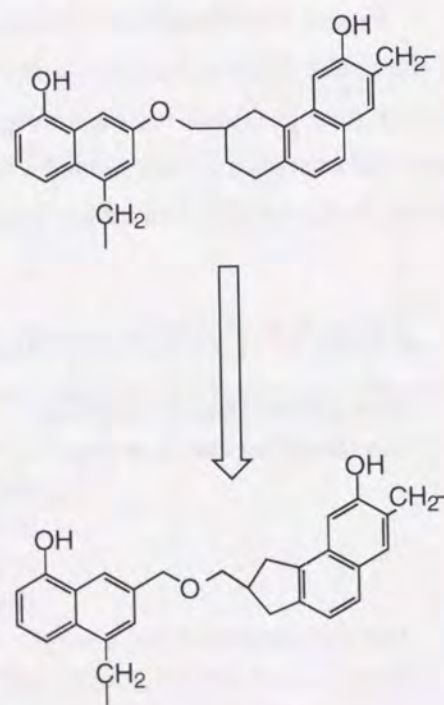


Figure 4-12. Modification of the Akabira coal model.

carbon content, molecular weight, and aromaticity are unchanged. Using the revised structure, a calculated density of 1.15 was obtained. The value is between those for Taiheiyō and Yubari coal models, which suggests that the change of the bridge structure may be appropriate. The change in density appears to be attributable to the increased flexibility of the modified model molecule.

In connection with the above argument, it should be pointed out that the Tempoku model is very similar to the Taiheiyō model, while there is a considerable difference in the two calculated densities. It may be reasonable to consider that the origin derives mainly from the difference in the linkages connecting the unit structures. The former model has a $-\text{CH}_2\text{CH}_2\text{OCH}_2-$ group and the latter has a shorter linkage of $-(\text{CH}_2)_3-$. Therefore, the Tempoku coal oligomer model is expected to be more flexible than the Taiheiyō coal model, giving the higher calculated density.

In summary, the density-carbon content correlation for the four Japanese coals could be successfully simulated by using the CAMD method we previously proposed. While the coal models employed in this study, which were suggested by Iwata *et al.*, are rather simple, they appear to represent the characteristics of the original coals reasonably, at least for the simulation of the coal density, although the Akabira coal model had to be somewhat modified. This also suggests that, in constructing coal models, it is important to build up the linkage connecting aromatic moieties carefully. The calculated densities were low by 0.05–0.13 compared with the corresponding original coals. The measured density of coals is known to vary in a range of about 0.1 depending on the method of the measurement and because of their inhomogeneous natures.^{17,18,20} Nevertheless this procedure is considered to be very useful as an evaluation method for the adequateness of coal models constructed.

4.3.3. Density Simulation for Model Structures of Bituminous Akabira Coal

Recently, an effective strategy for the construction of coal models consisting of a combination of CP/MAS ^{13}C NMR and flash or Curie-point pyrolysis/GC-MS analyses has been proposed by Hatcher *et al.* and Nomura *et al.*,¹² independently. The latter has constructed a unit structural model of bituminous Akabira coal having a formula of $\text{C}_{390}\text{H}_{362}\text{N}_6\text{O}_{38}$ by using the method.

On the other hand, the technique of computer-aided molecular design (CAMD) has appeared to be a useful tool in constructing coal model molecules and simulating their physical properties, as well as drug design and protein modeling in biological chemistry. One of the significant parameters for representing the nature of coals is the physical density. I have proposed a method to estimate the density for coal model molecules using CAMD software in which intermolecular interaction and void volume can be taken into consideration. With the method, I calculated the density of simple coal model molecules which are composed of polyaromatic hydrocarbons and polymethylene chains and four Japanese coal model structures with different carbon contents, each of which is an oligomer of a rather low molecular weight aromatic unit structure involving oxygen as heteroatom. In the latter, the correlation between the carbon contents and the physical densities for the original coals could be

Table 4-3. Physical density of the coal models

coal	physical density (g/cm^3)	
	calculated	measured
Tempoku	1.29	1.37
Taiheiyō	1.22	1.27
Akabira	1.03	1.28
Akabira ^a	1.15	
Yubari	1.11	1.24

^a Modified structure of Akabira coal.

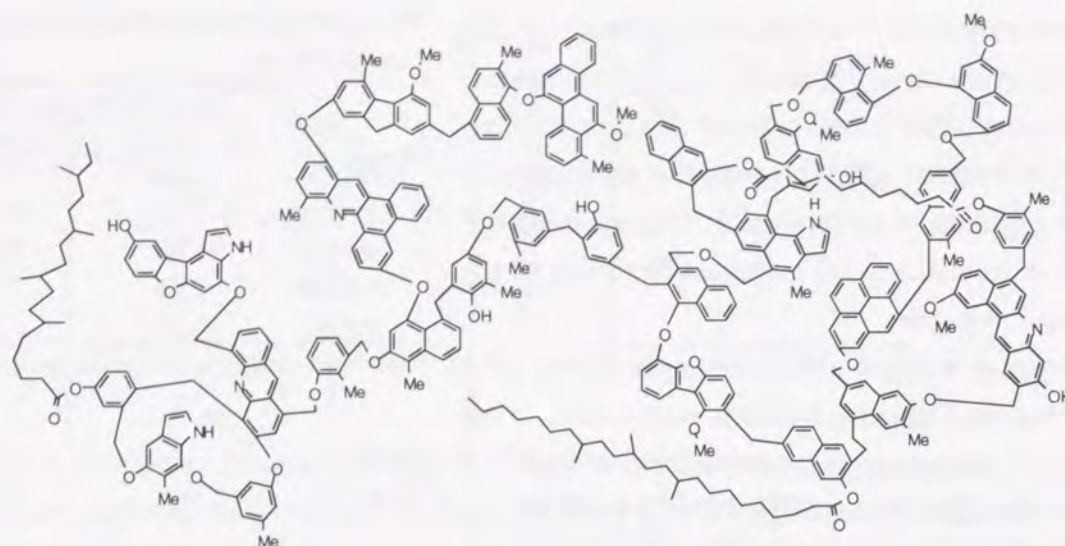


Figure 4-13. Proposed model structure for Akabira coal (model O)

Table 4-4. Carbon distribution (%) of models O and A-D^{a,b}

model	t-CH ₃	α-CH ₃	CH ₂	CH ₂ '	OCH ₃	ArH	ArC	ArO	COOR
O ^c	2.3	3.8	14.9	3.3	1.5	47.7	12.8	12.6	1.0
A	2.3	3.8	12.6	5.4	1.5	47.7	18.2	7.2	1.0
B	2.3	4.4	14.9	2.8	1.5	48.5	12.3	12.3	1.0
C	2.3	5.1	14.6	2.3	1.5	49.0	11.8	12.3	1.0
D	2.3	5.1	12.3	4.6	1.5	47.7	18.2	7.2	1.0

^a t-CH₃: terminal methyl. α-CH₃: methyl attached to aromatic ring. CH₂ and CH₂': methylene bridge connecting aromatic moieties. ArH, ArC, and ArO: aromatic carbons bearing hydrogen, aliphatic carbon, and oxygen, respectively. ^b Internal carbons and methine carbons are counted as in ArH and CH₂, respectively.

^c Reference 14.

reasonably reproduced.

In light of these results and as part of my studies on coal structure, I have attempted to calculate the physical density of the Akabira coal model (Model O) mentioned above, which is a considerably large molecule compared with those treated previously, together with the corresponding four modified models (Model A-D). The modifications have been systematically made in the linkages which connect aromatic moieties in the model, since the flexibility of model molecules depending on their structures has been found to markedly affect the density. Careful examination of the results may be expected to afford more precise model structures of the coal.

Description of Akabira Coal Models

The model structure of Akabira coal (model O) is shown in Figure 4-13. This, with a molecular formula of C₃₉₀H₃₆₂N₆O₃₈ (MW 5784), was constructed on the basis of the combined data of Curie point pyrolysis GC-MS of its SRC (94% yield based on the original coal) and CP/MAS ¹³C NMR of the original coal. In the present study, the following four modified models A-D were also subjected to the density simulation as well as model O. The modifications were made by considering the facts that

the pyrolysis/¹³C NMR technique can give little information regarding the mode of chemical bonds connecting aromatic moieties, while the length of the bonds appears to be an important factor determining the physical density, and there is a considerable difference between model O and the previous simple coal models that model O is a macromolecule involving branched and cross-linked structures, whereas the previous ones are linear oligomers.

Figure 4-14A represents model A. In this modification, the linkages connecting aromatic moieties were lengthened to some extent, by which the molecule may become more flexible. Thus, 30 methylene groups were added to 24 short linkages in model O, while two long alkyl chains and one long aliphatic bridge were shortened by the same number of the carbons; 6 Ar-O-Ar' and 9 Ar-CH₂O-Ar' chains were transformed into 15 Ar-CH₂OCH₂-Ar', and 9 Ar-CH₂-Ar' bridges to Ar-CH₂CH₂-Ar'. Model B was obtained by breaking one aromatic ether bond and two methylene bridges (Figure 4-14B). As a result, the cyclic structures due to the cross-linked bonds in model O disappeared, giving a chain structure having a number of branched moieties. The modification of model O to C was made by a combination of the two procedures applied to models A and B (Figure 4-14C). Model D was obtained by cutting four methylene bridges and two ether bonds in model O (Figure 4-14D). By this modification, four medium-sized molecular fragments

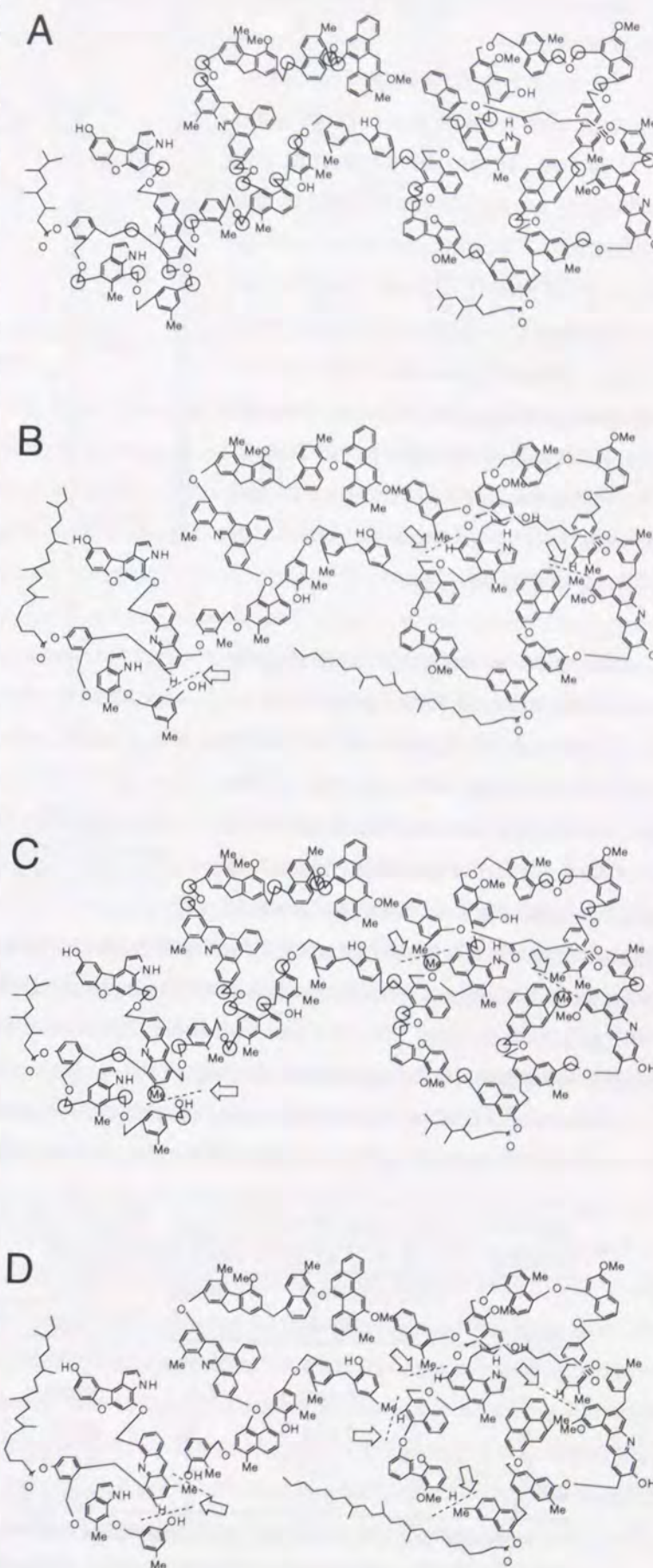


Figure 4-14. Modified structures for Akabira coal model

were formed, the cyclic structures having disappeared.

The carbon distribution of model A-D together with those of model O are listed in Table 4-4. It can be seen that the distributions are only little affected by the modifications. The quotient of aromatic to total carbons ($f_a=0.73$) and the average size of aromatic moieties (2.3 rings) have not been changed, since the modifications were made only in the linkages and the aliphatic chains. Although the numbers of ArH, ArC, and ArO carbons are not constant, the total of these three kinds of carbons is identical.

Influence of the Structural Changes of the Model Molecules on Physical Density

Figure 4-15 depicts relationship between the total potential energy and the physical density for models O and A-D calculated with the periodic boundary conditions. All the curves are not smooth, suggesting that each model has some metastable conformers. This can be due to the fact that steric hindrance in the large molecules makes barriers for the single bonds to rotate, yielding local minimums of the potential energy. It is obvious that there is a minimum total potential energy for each model which corresponds to the optimized density.

Table 4-5 summarizes the calculated data of density and volume at each minimum total energy. The order of the density (g/cm^3) calculated for these model molecules followed the sequence O (1.03)

Table 4-5. Total potential energy, density, and volume of models O and A-D at their best conformers

model	total potential energy (kcal/mol)	density (g/cm^3)	volume (\AA^3)		
			cell ^a	molecule ^b	void ^c
O	1074.1	1.0	9281.9	6807.0	2474.9(167.1)
A	1090.5	1.1	8629.1	6727.0	1920.1(91.8)
B	1011.5	1.1	8470.8	6721.5	1749.3(26.0)
C	1020.5	1.2	8414.5	6734.1	1680.4(8.6)
D	925.4	1.2	8314.5	6791.9	1522.6(7.3)

^a Volume per unit cell. ^b Volume per model molecule. ^c Void volume per unit cell. The value in parentheses indicates void volume to which helium can be accessible which was obtained by the sample probe method.

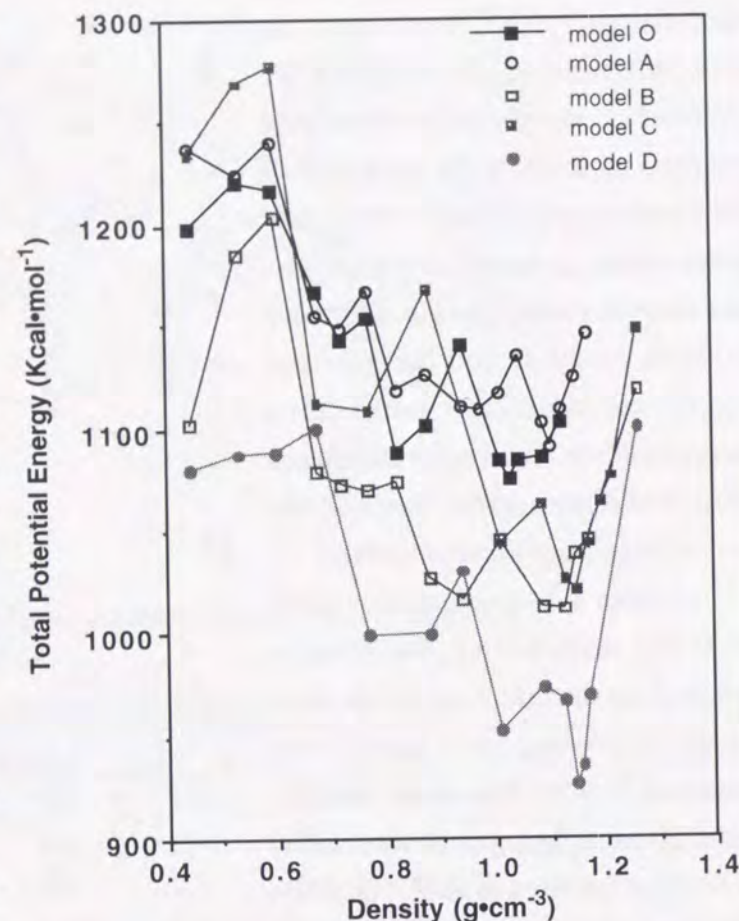


Figure 4-15. Relationship between the total potential energy and calculated density for model O and A-D.

Table 4-6. Potential energy of models O and A-D at their best conformers

model	O	A	B	C	D
covalently bonded energy (kcal/mol)	619.1	619.0	592.9	581.3	558.3
stretch	146.3	153.5	143.8	157.5	131.6
bend	259.0	283.4	270.9	268.4	250.5
torsion	206.8	176.5	170.9	149.1	170.6
inversion	7.0	5.6	7.3	6.3	5.6
non-covalently bonded energy (kcal/mol)	454.9	471.5	418.6	439.3	367.0
van der Waals	513.3	522.2	470.6	486.2	458.6
electrostatic	-45.0	-27.1	-45.3	-27.5	-61.8
hydrogen bonding	-13.4	-23.6	-6.7	-19.4	-29.8

< A (1.10) < B (1.13) < C (1.15) = D (1.15). One of the predominant factors affecting the density may be the flexibility of the model structure. Thus, an increase of $0.07 \text{ g}/\text{cm}^3$ in the density by the modification of O to A appears to be due to the increment of the flexibility as expected. This also parallels the previous results that in the oligomer-type models, the molecules having longer linkages connecting aromatic fragments have larger densities than those with shorter ones. The transformation of model O to B increased the density by $0.10 \text{ g}/\text{cm}^3$. Comparison of these two density values obtained suggests that cutting some linkages at the cyclized parts in the model O to give the corresponding linear polymer with some branches more effectively relaxes the molecules than prolonging many linkages connecting aromatic moieties accompanied by shortening terminal aliphatic chains. It can be considered that model C is derived from both models A and B via the same modification procedures applied to O to B and O to A, respectively. The changes in the density were 0.05 (A to C) and 0.02 (B to C) g/cm^3 . This seems to confirm the different effectiveness for relaxing the model molecules between the two procedures. The fact that the density of model D is as high as model C indicates that the fragmentation to four molecules accompanied by the disappearance of the cyclic structures effectively increases the flexibility as expected. It should be noted that the present software employed for the calculation can treat model D as a cluster molecule.

The volume of the unit cell which contains one optimized model molecule in the calculation under periodic boundary conditions decreased, as the density increased (Table 4-5). This is a matter of course, since the density was calculated by dividing the molecular weight of the model molecule by the cell volume. By contrast, the volumes of the model molecules themselves were almost invariant irrespective of the change of the model structure. This can be due to the fact that they are estimated by van der Waals radii of the constituent atoms, the molecular formula of the models being essentially identical. With these values the void volumes of the cells can be calculated to be 18-26% of those. However, the volumes seem to involve those to which gases such as helium cannot enter because of their narrowness of the pores. Consequently, the volumes to which helium can be accessible were calculated by the sample probe method using a van der Waals radius of the gas of 1.4\AA . Thus, they were estimated to be only 0.1 - 1.8% of the unit cells. This clearly indicates that the present method calculates the true density of the single molecular assembly of each model. It may be conceptually considered that micropores to which helium can enter also yield between the plural assemblies.

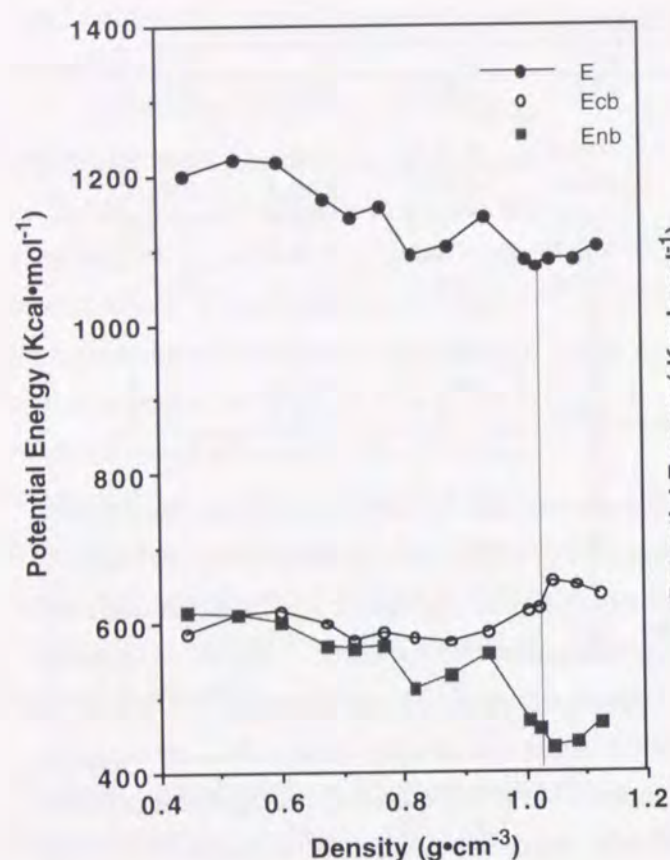


Figure 4-16. Relationship between the density and the total, covalently bonded, and non-covalently bonded interaction energies for model O.

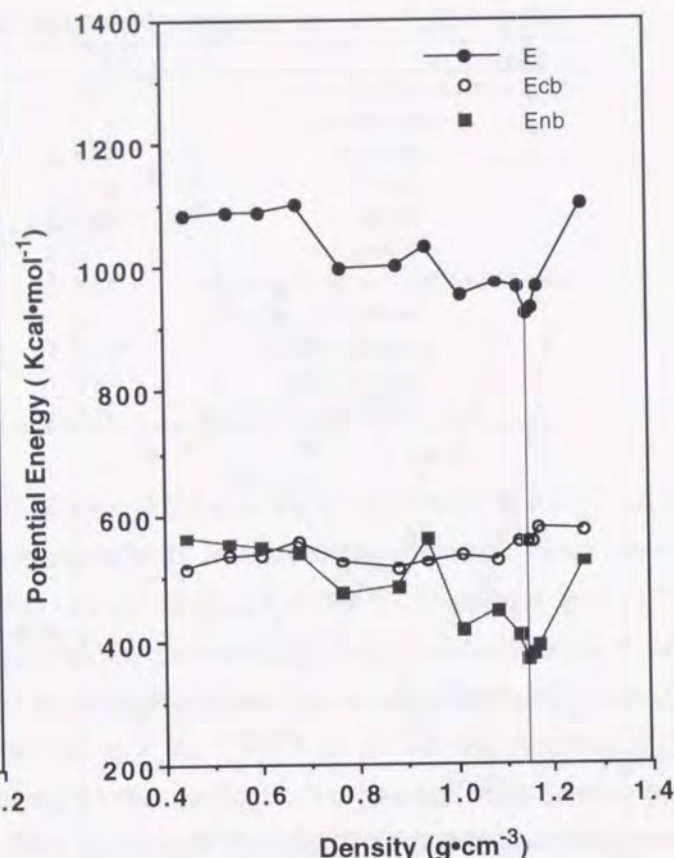


Figure 4-16. Relationship between the density and the total, covalently bonded, and non-covalently bonded interaction energies for model D.

Relationship between the Potential Energy and the Model Structure

The total potential energy indicated in Table 4-5 and Figure 4-15 is calculated as the linear combination of covalently bonded interaction energies and non-covalently bonded interaction energies. Each of these energy values at the optimized density with the minimum total potential energy for each model is given in Table 4-6. The total potential energy for the models followed the sequence $A > O \gg C > B \gg D$. This indicates that the transformation of O to A and B to C by the elongation of the linkages causes a little increase in two of non-covalently bonded interaction energies E_v and E_e . By contrast, the hydrogen bonding energy E_h is decreased by this transformation. This may be a possible reason why it affords a higher density, despite the increment of the total potential energy. On the other hand, the transformation of O to B, A to C, and O to D by breaking the cross-linked bonds decreases both E_{cb} and E_{nb} . This is mainly due to the decrease of E_l and E_v . Thus, the latter transformation may allow it to be more easily packed into smaller volumes than the starting models and give relatively higher densities, compared with the former.

It is worth noting that the optimization of the model systems depends mainly on that of E_{nb} . However, the density at the optimized E is not always the same as that at the lowest E_{nb} . The densities at the minimum E_{nb} for models O and A-D are 1.05, 1.10, 1.13, 1.17, and 1.15, respectively. The densities determined by E are identical to those by E_{nb} for models B and D, whereas in the case of

models O, A, and C, their densities based on E are different from those based on E_{nb} . This appears to be due to the considerable increase of E_{cb} around the optimized density, as the model molecules become to be packed closely. Figures 4-16 and -17 which show the relationships between E, E_{cb} , and E_{nb} and the density for models O and D, respectively, are representative.

Correlation of the Model Molecules with the Original Akabira Coal

Akabira coal has a measured physical density of 1.28 g/cm³ by helium pycnometry. The same value was also obtained by using sink-float method.

The previous simulation study using the oligomer-type coal models has suggested that the CAMD method employed tends to under estimate the density around a value of 0.1 compared with that for the existing coal, although the observed density of coals is known to vary in the same range depending on the method of the measurement and because of their inhomogeneous natures. One of the possible reasons for this may be that native coals consist of a large number of molecules having various molecular weights to form relatively more compact masses. Nevertheless, this calculation procedure has appeared to be useful as an evaluation method for the adequateness of coal models constructed: the discrepancy is not large, and it is capable of reproducing the relationship between the carbon content and the density of the existing coals.

With the above in mind, the density value of Akabira coal seems to be reproduced by models B, C, and D which have no cyclic linkage structures owing to the cross-linked bonds, whereas model molecules O and A are considered to be too rigid to form compact conformers. Since the method apparently calculates the true density as discussed above, the reason for the underestimation is still difficult to be unambiguously rationalized.

Iino *et al.*²¹ have reported that a solvent system of carbon disulfide / 1-methylpyrrolidin-2-one can solubilize coals up to 70%, the solubility being remarkably affected by their carbon contents. The solubility of Akabira coal to the solvent system was determined to be as high as 22.6%. Thus, the molecules constructing model D or further fragmented ones may also be the representatives of the extractable materials, although a reliable evaluation of the molecular weight distribution of the extract is needed to obtain further plausible model structures. Our previous Curie-point pyrolysis/ GC-MS analysis of the SRC of Akabira coal has indicated that its hexane-soluble and hexane-insoluble/benzene-soluble fractions are composed of similar aromatic constituents, while molecular weight distributions between the two fractions are different. These results suggest that the representative structural model for Akabira coal may preferentially be the mixture of B, C, and D.

In summary, the present results of the density simulation for the five kinds of macromolecular type Akabira coal models suggest that the cyclic linkage structures exist, if any, to a lesser extent, although they may be formed by inter- and intramolecular non-covalently bonded interactions. The interactions could be one of the major origins for the formation of the considerable amount of coke in the pyrolysis. While the density of Akabira coal appears to be reasonably simulated by the modification of model O which was previously proposed, the distribution of the chemical bonds connecting aromatic moieties has not yet been well characterized. I am continuing experimental efforts to obtain the information about the bonds by chemical transformation of coals.

4.4. References

- 1 Carlson, G. A. *Prep. Pap.-Am. Chem. Soc., Div. Fuel Chem.* **1991**, 36, 398.
- 2 Carlson, G. A.; Granoff, B. *Coal Science II*; Schobert, H. H., Bartle, K. D.; Lynch, L. J. Eds. ACS Symp. Ser. 461; American Chemical Society: Washington, DC, 1991, p.159.
- 3 Carlson, G. A. *1991 Int. Conf. Coal Sci. Proc.* **1991**, 24.
- 4 Carlson, G. A. *Energy Fuels* **1992**, 6, 771.
- 5 Faulon, J. L.; Vandenbroucke, M.; Drappier, J. M.; Behar, F.; Romero, M. *Adv. Org. Geochem.*, **1989**, 16, 981.
- 6 Faulon, J.-L., Hatcher, P. G., Wenzel, K. A. *Prep. Pap.-Am. Chem. Soc., Div. Fuel Chem.* **1992**, 37, 900.
- 7 Freeman, C.; Catlow, R. *Chem. Ind.* **1990**, 3, 796.
- 8 Given, P. H. *Fuel* **1960**, 39, 147.
- 9 Weiser, W. H. *NATO ASI Ser. C* **1984**, 124, 325.
- 10 Solomon, P. R., *New Approaches in Coal Chemistry*, ACS Symp. Ser. 169; 1981; 61.
- 11 Shinn, J. H. *Fuel* **1984**, 63, 1187.
- 12 Nomura, M.; Matsubayashi, K.; Ida, T.; Murata, S. *Fuel Process. Technol.* **1992**, 31, 169.
- 13 Mayo, S. L.; Olafson, B. D.; Goddard III, W. A. *J. Phys. Chem.* **1990**, 94, 8897.
- 14 Mahajan, O. P., *Coal Structure* (Meyers, R. A Ed.); Academic Press: New York, **1982**: pp 54-60.
- 15 Iwata, K.; Itoh, H.; Ouchi, K. *Fuel, Process. Technol.*, **1980**, 3, 221.
- 16 Iwata, K. Dr. thesis, "Studies on average chemical structure of coal", Hokkaido University, 1983.
- 17 Sugimura, H.; Osawa, Y.; Hatami, M.; Sato, S.; Honda, H. *Nenryo Kyokaishi*, **1966**, 45, 199.
- 18 Bangham, D. H.; van Krevelen, D. W. *Fuel* **1954**, 33, 348.
- 19 Meyers, R. A. *Coal Structure*; Academic Press: New York, **1982**: pp 54-60.
- 20 When this study was submitted to publication in the Journal of Energy and Fuels, one of reviewers pointed out the fact that these calculations systematically underestimate the coal density deserve another comments. As for this reason, it may be considered that native coals are more strained and more compacted due to their coalification process.
- 21 Iino, M.; Takanohashi, T.; Ohsuga, H.; Toda, K. *Fuel* **1988**, 67, 1639.

Conclusion

This thesis deals with construction and evaluation of chemical structure models of coal using methodology of organic chemistry and computer simulation. The results obtained through this work are summarized as follows.

In chapter 1, pyrolysis of two classes of coal model compounds were investigated to obtain fundamental information of the pyrolytic behavior of coal. In the Curie-point pyrolysis of the one class involving 14 aromatic hydrocarbons, each of which consists of one or two identical aromatic skeleton(s) and a longer alkyl side chain or a longer alkylene bridge at 670 °C under N₂, alkanes and alkenes as well as aromatic fragments were appeared to be formed. One of the important parameters, molar ratio of alkanes to alkenes formed was found to vary depending on the aromatic skeletons and the bridge groups. Seven benzyl-substituted polycyclic aromatic hydrocarbons as the other class were also submitted to pyrolysis at 430 °C in the presence or absence of a hydrogen-donor solvent. The results indicated that reactivity and reaction mode of the compounds were remarkably affected by the mother aromatic skeletons and the position of the substituent. Based on these pyrolysis data and the results of molecular orbital calculations for possible intermediates, plausible mechanisms for the pyrolysis were proposed.

In chapter 2, I investigated coal chemical structure of coal by using three different methods. At first, a specific coal, US bituminous Illinois No. 6 coal, was treated with quinoline at 350 °C under nitrogen. By this procedure, a solvent soluble fraction was found to be obtained in 85 % yield. Then, molecular weight distribution of this fraction was measured, so that association nature of the components of the coal could be discussed. It was found that the constituents of the extract showed a strong tendency to associate even in polar solvents. Next, some coals were submitted to ruthenium ion-catalyzed oxidation reaction, which may give information about the distribution of alkyl side chain attached to aromatic rings in coal. The results suggested that methyl group was the major alkyl side chain attached to aromatic rings in coal and the concentration of those with more than three carbons was very low. Finally, Akabira coal was hydroliquefied using deuterium in the presence of tin(II) chloride and potassium chloride. This afforded more than 80 % of solvent soluble matter. Detailed analysis of the solvent soluble products by using ²H NMR and GC/MS brought about deduction of a part of the structure of the bonds connecting aromatic clusters in coal.

In chapter 3, construction of a structural model for Chinese bituminous Zao Zhuang coal using the pyrolysis / ¹³C NMR method was attempted. In this study, a new method, pretreatment

of coal with a mixture of silicon tetrachloride and sodium iodide, was employed to cleave relatively weak chemical bonds, especially ether linkages, in coal. This treatment was found to result in the increase of yield of volatile products in the Curie-point pyrolysis of coal. Another method specifically employed here was dipolar dephasing NMR (DD NMR) which may give precise information concerning average size of aromatic rings in coal. These devices appeared to enable to make more reliable models of coal.

In chapter 4, CAMD (computer-aided molecular design) technique was applied to coal model molecules. Among the parameters derived from CAMD study, physical density is considered to be one of the most important ones. Consequently, a new method for calculation of physical density of coal model molecules was developed. This method was also applied to three types of coal model molecules, (1) simple models containing polycyclic aromatic hydrocarbons with polymethylene bridges, (2) four Japanese coal models which represent their elemental analyses, carbon aromaticities, and oxygen-functional groups, and (3) a relatively large model for Japanese bituminous Akabira coal proposed by Nomura *et al.* It was demonstrated that evaluation of reasonableness of the models could be made by this new method.

